2010

Cosmogenic 21Ne and 3He dating and geochemistry of young basaltic lavas from southern Mendoza, Argentina

Venera R. Español
University of Wollongong

Cosmogenic 21Ne and 3He dating and geochemistry of young basaltic lavas from southern Mendoza, Argentina

Abstract

The Andino-Cuyana Basaltic Province (ACBP) located in the province of Mendoza, central western Argentina, constitutes an extensive volcanic area to the east of the Andes, with more than 800 volcanoes, and which has been divided in two volcanic fields, the Llancanelo Volcanic Field to the north (LLVF) and the Payunia Volcanic Field (PVF) to the south. The ACBP lacks detailed chronological and geochemical information. This study constitutes the first to compare the two volcanic fields and to use cosmogenic noble gas surface exposure and Ar-Ar dating.

Previous studies estimate that the lavas from the ACBP date from approximately the Plio-Pleistocene to Holocene. Currently no accurate dates have been provided; as young lavas are difficult to date by conventional methods. Using cosmogenic $^{21}Ne^*$ and $^{3}He^*$ surface exposure dating technique, it was found that the basalts from the PVF range from 31.1±4.3 ka from Los Volcanes area, to <7 ka in Santa Maria>Volcano, which is considered to represent one of the latest eruptions in the PVF. The single sample analysed by cosmogenic dating from the LLFV indicates an age of 54.9±5.1 ka which may represent one of the youngest eruptions within the LLVF. In addition, ages indicated by Ar-Ar from the LLVF show that the volcanoes on the edge of Llancanelo Lake range from 1.69±0.29 Ma, in Cerro Coral to 0.395±0.068 Ma, in Cerro Trapal. The data provided here also confirm field observations that the LLVF is older than the PVF.

Chemical analysis of the basaltic rocks indicates that they are olivine-rich alkaline basalts, with some differences between the two volcanic fields. The geochemical information shows that the LLVF tends to have much more influence from the subducting slab than the PVF. Nevertheless, the basaltic bombs from PVF tend to have a chemical composition strongly influenced by fluid from the subducting Nazca plate. The PVF trachyte flow sampled is typical of a more evolved intermediate rock with low Sr and Sr/Nd values indicating plagioclase fractionation. Sample LL1, from Cerro Coral, constitutes the oldest dated sample within the LLVF and it also shows the strongest geochemical association with the volcanic arc. The subducting Nazca plate has a great influence on the geochemical processes that formed the ACBP, and the magmas produced.

Degree Type

Thesis

Degree Name

Bachelor of Science (Honours)

Department

School of Earth & Environmental Sciences

Advisor(s)

Allan Chivas

Keywords

Cosmogenic 21Ne and 3He, geochemistry, southern Mendoza, basalts, payunia

2010

Cosmogenic 21Ne and 3He dating and geochemistry of young basaltic lavas from southern Mendoza, Argentina

Venera Ruth Español

Cosmogenic ^{21}Ne and ^{3}He dating and geochemistry of young basaltic lavas from southern Mendoza, Argentina

Venera Ruth Españon

This thesis is presented as part of the requirements for the award of the Honours Degree Bachelor of Science of the University of Wollongong

School of Earth and Environmental Science
Faculty of Science

October, 2010

The information in this thesis is entirely the result of investigations conducted by the author, unless otherwise acknowledge, and has not been submitted in part, or otherwise, for any other degree or qualification.

Venera Ruth Espanon

ABSTRACT

The Andino-Cuyana Basaltic Province (ACBP) located in the province of Mendoza, central western Argentina, constitutes an extensive volcanic area to the east of the Andes, with more than 800 volcanoes, and which has been divided in two volcanic fields, the Llancanelo Volcanic Field to the north (LLVF) and the Payunia Volcanic Field (PVF) to the south. The ACBP lacks detailed chronological and geochemical information. This study constitutes the first to compare the two volcanic fields and to use cosmogenic noble gas surface exposure and Ar-Ar dating.

Previous studies estimate that the lavas from the ACBP date from approximately the Plio-Pleistocene to Holocene. Currently no accurate dates have been provided; as young lavas are difficult to date by conventional methods. Using cosmogenic $^{21}Ne^*$ and $^{3}He^*$ surface exposure dating technique, it was found that the basalts from the PVF range from 31.1±4.3 ka from Los Volcanes area, to <7 ka in Santa Maria Volcano, which is considered to represent one of the latest eruptions in the PVF. The single sample analysed by cosmogenic dating from the LLFV indicates an age of 54.9±5.1 ka which may represent one of the youngest eruptions within the LLVF. In addition, ages indicated by Ar-Ar from the LLVF show that the volcanoes on the edge of Llancanelo Lake range from 1.69±0.29 Ma, in Cerro Coral to 0.395±0.068 Ma, in Cerro Trapal. The data provided here also confirm field observations that the LLVF is older than the PVF.

Chemical analysis of the basaltic rocks indicates that they are olivine-rich alkaline basalts, with some differences between the two volcanic fields. The geochemical information shows that the LLVF tends to have much more influence from the subducting slab than the PVF. Nevertheless, the basaltic bombs from PVF tend to have a chemical composition strongly influenced by fluid from the subducting Nazca plate. The PVF trachyte flow sampled is typical of a more evolved intermediate rock with low Sr and Sr/Nd values indicating plagioclase fractionation. Sample LL1, from Cerro Coral, constitutes the oldest dated sample within the LLVF and it also shows the strongest geochemical association with the volcanic arc. The subducting Nazca plate has a great influence on the geochemical processes that formed the ACBP, and the magmas produced.

ACKNOWLEDGEMENTS

I would like to thank all the people that generously assisted me and without whom my project would not be possible. Special thanks to my supervisors, Professor Allan R. Chivas and Dr. Masahiko Honda, for their patience with my many questions and for their support especially when I found myself lost with some of the problems encountered along the project. I would like to thank Associate Professor Brian Jones who was the first person to introduce me to research.

The field work team, Allan R. Chivas, Adriana García, Roberto Violante, Daniel Smith, Coco (Jorge Chielsa), Leandro Rojo, Sabina D'Ambrosio, and the National Park rangers, made the field work enjoyable, despite some problems encountered.

I thank the staff at the University of Wollongong who assisted me with sample preparation and answering questions, particularly José Abrantes, David Wheeler, Professor Paul Carr, Associate Professor Chris Ferguson and Dr Solomon Buckman. To all the people at the School of Earth and Environmental Sciences who were there all the time to share a "hi " or a conversation, when I was running through the corridors, thanks because all of you made my life at university even more enjoyable.

To the staff of Australian National University, especially Shane Paxton, who helped my project to survive when I thought that all my olivine samples were lost. To Igor Iatsevich, who helped with the analysis and sample preparation. To Dr Marc Norman who provided strontium and neodymium data and interpretation. Also I would like to thank Associate Professor David Phillips from the University of Melbourne, who provided the Ar-Ar data.

To all my fellow students with whom I shared long days in the Honours room, and with whom I shared many laughs and who were there to listen to my problems and to help as well. Thanks!

I would also like to thank my boyfriend, Jan-Hendrik May, for being there for me, to read and listen about cosmogenics and geochemistry, but especially to give me love and support always. I would like to give my thanks to my family, Oscar Español, Silvia Español and Daniel Español, who were a support to me and who always where there participating in everything along the way, and who trusted me since the moment I started university.

TABLE OF CONTENTS

ABSTRACT ..... **ii**
TABLE OF CONTENTS ..... **iv**
LIST OF FIGURES ..... **vi**
LIST OF TABLES ..... **vii**
Chapter 1 Introduction **1**
1.1 General information 1
1.2 Geographical setting 3
1.3 Geological Setting 4
1.3.1 Formation of the Andino-Cuyana Basaltic Province (ACBP) 7
Chapter 2 Background information **9**
2.1 Geochemistry of the Andino-Cuyana Basaltic Province 9
2.2 Previous dates from the Andino-Cuyana Basaltic Province 11
2.3 Dating Methods 14
2.3.1 K-Ar and Ar-Ar dating 14
2.3.2 ^{26}Al & ^{10}Be dating 15
2.3.3 ^{36}Cl dating 16
2.3.4 Thermoluminescence 17
2.4 Cosmogenic ^{3}He and ^{21}Ne 18
2.5 Previous work in cosmogenic ^{21}Ne and ^{3}He dating 19
2.6 Aims of this thesis 21
Chapter 3 Methods **23**
3.1 Field sampling 23
3.2 Petrologic analysis 25
3.3 Geochemical Analyses 26
3.3.1 Crushing 26
3.3.2 X-ray Fluorescence 26
3.3.3 Loss on Ignition 27
3.3.4 Sr and Nd isotope analysis 28
3.4 ^{21}Ne and ^{3}He Sample preparation 29
3.4.1 Crushing 29
3.4.2 Magnetic Separation 29

3.4.3 Density Separation....30
3.4.4 Isotopic Analysis....31
3.4.5 Vacuum crushing analysis....32
3.4.6 Sensitivity and mass discrimination....33
3.4.7 Interference correction....33
3.4.8 Blanks....34
3.5 Ar-Ar dating....34
3.5.1 Sample preparation....34
3.5.2 Ar-Ar analysis....35
Chapter 4 Results....36
4.1 Petrography....36
4.2 Geochemistry....43
4.2.1 Major Elements....43
4.2.2 Trace Elements....49
4.3 Cosmogenic ^{21}Ne and ^{3}He....56
4.4 Ar-Ar dating....66
Chapter 5 Discussion....68
5.1 Magmatic origin and evolution....68
5.2 Cosmogenic ^{21}Ne and ^{3}He....71
Chapter 6 Conclusions and Recomendations....74
6.1 Conclusions....74
6.2 Recommendations....75
6.2.1 Areas for further geochemical analysis....75
6.2.2 Areas for further cosmogenic ^{3}He and ^{21}Ne analysis....75
REFERENCES....77
Appendix A *Forsterite content calculation* $(Mg,Fe)_2SiO_4$ *(Sample LL3)*....81
Appendix B Production rate calculation....82
Appendix C Cosmogenic ^{21}Ne, ^{3}He and age calculation....84
Appendix D Estimated ^{3}He trapped in fluid inclusions calculated from ^{21}Ne....85
Appendix E Major-element analysis of olivine separates....86
Appendix F Ar-Ar age spectra....87

LIST OF FIGURES

Figure 1.1 Geographical setting....3
Figure 1.2: Geological boundaries of the Andino-Cuyana Basaltic Province....6
Figure 1.3: Map of Payunia Volcanic Field....7
Figure 1.4: Formation of the Andino-Cuyana Basaltic Province....8
Figure 2.1: Comparisons between Stern et al., (1990) and Germa et al., (2010)....10
Figure 2.2: Previous dates from Andino-Cuyana Basaltic Province....13
Figure 3.1: Sampling location....24
Figure 3.2: Field location and samples for Ne-21 and He-3....25
Figure 3.3: X-ray Fluorescence instrumentation....27
Figure 3.4: Frantz Isodynamic Magnetic Separator....30
Figure 3.5: VG5400 noble gas ultra-high vacuum system at RSES, ANU....33
Figure 4.1: Olivine phenocrysts from sample LL1....36
Figure 4.2: Alkali Basalt sample LL2....37
Figure 4.3: Inter-granular olivine basalt sample LL3....37
Figure 4.4: Inter-granular olivine basalt sample LL4....38
Figure 4.5: Hypocrystalline scoria sample LL5....38
Figure 4.6: Pampas Negras scoria sample PY-3....39
Figure 4.7: Plain polarized light basaltic bomb sample PY-4....40
Figure 4.8: Cross polarized light sample PY-5....40
Figure 4.9: Holocrystallyne porphyritic basalt sample PY-6....41
Figure 4.10: Alkali olivine basalt sample PY-7....42
Figure 4.11: Hypocrystaline alkaline basalt sample PY-8....42
Figure 4.12: Olivine basalt sample PY-9....43
Figure 4.13: Total alkali vs. silica diagram....44
Figure 4.14: Alkali vs. silica diagram....44
Figure 4.15: Diagrams of SiO_2 plotted against K_2O, Al_2O_3, ΣFeO, MgO, P_2O_5, Na_2O, CaO, TiO_2 for rocks of LLVF and PVF....47
Figure 4.16: Diagrams of MgO concentration vs Al_2O_3, CaO, MnO, K_2O, Ti_2O....48
Figure 4.17: Ni vs. MgO....49
Figure 4.18 Primitive mantle normalized trace element diagram....51
Figure 4.19: Primitive mantle normalized trace element diagram for LLVF and PVF....51
Figure 4.20: Sr – Nd isotopic ratios....56
Figure 4.21: Three-isotope plot for neon extracted from olivine separates....59

LIST OF TABLES

Table 2.1: Examples of different nuclear reaction.....18
Table 3.1: Examples of different nuclear reaction.....23
Table 4.1: Major element composition.. 46
Table 4.2: Trace elements composition. 52
Table 4.3: Isotope ratios and REE ratios of whole rocks.....55
Table 4.4: Elemental and isotopic noble gas composition of neon. 60
Table 4.5: Elemental and isotopic noble gas composition of helium 61
Table 4.6: Forsterite and cosmogenic ^{21}Ne and ^{3}He production rate 63
Table 4.7: Cosmogenic ^{21}Ne (^{21}Ne*) and ^{3}He (^{3}He*) concentrations 66
Table 4.8: Ar-Ar ages from Llancanelo Volcanic Field. 67

Chapter 1

Introduction

1.1 General information

The study of magmatic processes is fundamental to the understanding of tectonic processes that happened in the past and shaped the landscape to produce its current topography and geomorphology. The different processes that have occurred since the formation of the Earth are diverse, and have affected every part of the Earth at various scales. In this investigation, the analysis of only a small portion will be discussed; however, is important to understand that similar processes have been taking place in the past and are currently occurring in different geographical settings.

The study area is located in the south-western part of South America, an area heavily influenced by magmatic activity associated with the subduction zone located approximately 150 km off the Chilean coast. The collision between the Pacific oceanic crust and the South American continental crust has resulted in the formation of the Andes. The Andes extend from ~10°N in northern Colombia to ~66°S in Tierra del Fuego in southern Argentina. The average elevation along the Andes is 4000 m above sea level but at ~20°S the ranges have their widest extent (about 800 km) and highest elevation (over 6000 masl) (Lamb and Hoke, 1997). Nevertheless, the highest peak, 6960 m, corresponds to Cerro Aconcagua at 30°S. The southern part of the Andes is relatively low in elevation compared with the northern part, dropping sharply to 2000 m at about latitude 37°S, apparently coinciding with a much thinner and younger part of the continental crust (Clapperton, 1993). The segment of the Andes south of 30°S and north of 42°S is characterized by a particular steep subduction angle of the Nazca Plate which permits the generation and rise of magmas, so that chains of andesitic central volcanoes are aligned on major fracture systems propagated by crustal extension (Clapperton, 1993). The present study analyses a small portion of this tectonically complex area, which forms part of a major basaltic province.

The Andino-Cuyana Basaltic Province (ACBP) is situated in the province of Mendoza in central-western Argentina. The volcanic field constitutes an exceptional area in which more than 800 volcanoes are located within an area of 15,900 km^2 with very long basaltic lava flows up to 180 km long (Pasquare et al., 2008).

A basaltic province is an area in which basaltic rocks are concentrated at the Earth's crust, and according to its origin, form different provinces with distinctive petrographic and chemical characteristic. There are three main types of basaltic province; 1) mid-ocean ridge basalts, 2) oceanic island basalts, and 3) continental flow basalts. The ACBP can be related geochemically to oceanic island basalts; however each basaltic province is different to each other. Another basaltic province which may have experienced similar processes of formation is the early Miocene Columbia River Basaltic Plateau, which has an area of 16,400 km^2 and more than 300 basaltic flows.

The ACBP is a large area that is divided into two volcanic fields, Llancanelo to the north and Payunia to the south. The words Llancanelo and Payunia come from the local Mapuche language. The word Llancanelo derives from an aboriginal word Yanca meaning quartz, which was used to make arrow tips, and Nelo, meaning green-blue colour. It is believed to refer to the elongated triangular shape of the lake, which, if seen from above, looks like the arrow tips used for hunting (Mendoza on line, 2010).

The ACBP constitutes a back-arc basin east of main Andean chain, produced by induced hot asthenospheric upwelling, implying mantle plume-like dynamics beneath the Patagonian lithosphere and preferential melting of hydrated mantle (Germa et al., 2010). As a result, extension and fracturing occurs along the overriding plate, promoting the ascent of magma to the surface. Consequently, the magmas of the ACBP contain information associated with the chemical composition of the mantle, which could unravel critical information to interpret the complex tectonic setting that forms the Andes. In addition, to determining the chemical composition of the each of the lava flows, several methods can be used to numerically date the time since a particular eruption occurred.

1.2 Geographical setting

The study area is located between 35°30'S and 36°30'S and 69°45'W and 69°W, in the central-western part of Argentina and the northern part of Patagonia (Fig 1.1). Also it is situated about 100-200 km east of the main Andes Cordillera (Inbar and Risso, 2001a). The Andino-Cuyana Basaltic Province comprises an area of 15,900 km^2 and is divided into two volcanic provinces: the LLancanelo Volcanic Field (LLVF) to the north and the Payunia Volcanic Field (PVF) to the south. Together the volcanic fields comprise more than 800 volcanic cones, commonly claimed to be world's largest eruption field.

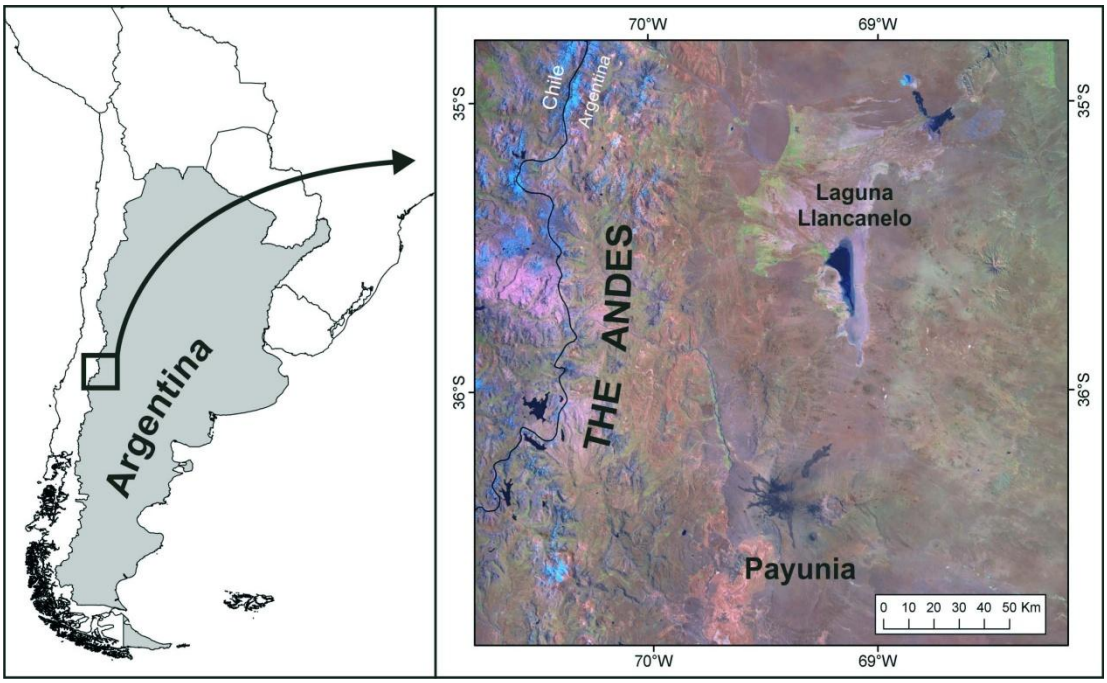

Figure 1.1 Geographical setting

In the area between 35° and 36°S, a topographic depression called the Huarpes Depression is situated between blocks with different elevations (Bermúdez and Delpino, 1989). The substrate that forms the depression can be related to the one that forms the Cordillera Principal in which the eastern-most basalt from LLVF is found. The elevation is greater along the PVF than in LLVF with a mean elevation of 2000 m however its highest peak is the Payún Liso volcano at ~4000 m (Germa et al., 2010). The LLVF has a mean elevation of 1500 m.

The northern part of the ACBP is an endoreheic basin flowing into Llancanelo lake, with water level fluctuating according to climatic change, while the southern area drains toward the Rio Grande (Inbar and Risso, 2001b).

The climate of the area plays an important role in the erosion rate of the volcanic rocks. The region has a semi-arid climate with annual precipitation around 200 mm (Inbar and Risso, 2001a). Winters are cold and summers are hot, with winds predominantly from the north-west and west (Inbar and Risso, 2001b). There is a marked difference with regard to vegetation and soil between the LLVF and the PVF, and the former volcanic field is older than the latter. Hence, as consequence of erosion, the soil evolution and cover in LLVF is greater than in PVF. Therefore more diverse and taller vegetation can be found in LLVF rather than in PVF where the vegetation cover is sparse and the mean vegetation height is 10 to 15 cm above the ground.

1.3 Geological Setting

The study area is part of the back-arc volcanism of the Andes. Payunia Volcanic Field (PVF) and Llancanelo Volcanic Field (LLVF) are located approximately 400 km east of the Chile-Peru trench in South America. In this subduction zone the denser oceanic Nazca Plate is subducting at an angle of 30°, under the less dense continental South American Plate. The current rate of collision between these two plates is 7-9 cm/yr; this subduction rate is greater than the long-term rate of subduction which has produced upper plate shortening and thrust belts within the Andes (Royden, 1993).

The basement of the LLVF is mainly composed of Cenozoic igneous and sedimentary rocks. In this volcanic field lava, flows are mainly of aa and pahoehoe type in the eastern part of the field and mainly of pahoehoe type with tumuli and lava tubes in the western part (Inbar and Risso, 2001b).

The Payunia Volcanic Field rests on Mesozoic sedimentary basement and younger Cenozoic piedmont deposits (Inbar and Risso, 2001b). This area constitutes the youngest volcanic field along the Patagonian Plateau. Furthermore eruption in the PVF took place from east to west. To the east of the Payún Matrú caldera the oldest very extensive pahoehoe lavas are found. However, to the east of the caldera the youngest aa flows are also observable. There are more than 500 volcanoes in this area, mainly strombolian and cinder cones, which are aligned in relation to a major east-west trending fault, the Carbonilla Fault.

The back-arc volcanism of the Andino-Cuyana Basaltic Field was caused by a steepening of the subducting slab, which introduced hot asthenospheric upwelling, associated with melting of hydrated mantle (Stern, 2004, Quidelleur et al., 2009, Germa et al., 2010, Violante et al., 2010). The steepening of the subducting slab has been evident for the last 5 Ma, after a period of shallow or near horizontal subduction during the Miocene. During the Miocene this basaltic province was exposed to a period of tectonic compression, and the generation of arc-like lavas migrated successively eastwards to approximately 500 km east of the present arc (Quidelleur et al., 2009). However, since the Pliocene, the area of the Andino-Cuyana Basaltic Province has experienced a period of tectonic extension that assisted upwelling of the magmas.

The geological boundaries of the Andino-Cuyana Basaltic Province are to the north the early Permian San Rafael block, the Mesozoic Neuquén basin to the south, Las Mantras block to the east, and the Cordillera Principal to the west (Fig 1.2).

The Andino-Cuyana Basaltic Province (ACBP) is mainly dominated by basaltic rocks and basaltic-andesitic rocks, with some trachytes, rhyolites and ignimbrite flows of various ages. The LLVF constitutes the oldest part of the ACBP; it is mainly composed of basaltic rock; however, some trachy-andesite flows occur around Cerro Nevado. Previous studies suggest that the general age of the LLVF is Pliocene.

The PVF is characterized by a large variety of emitted products with a very good relative timing constraint (Germa et al., 2010). Los Volcanes is the youngest basaltic field in the ACBP; it is principally composed of alkaline basalts, cinder, and scoria cones, aligned in an E-W direction along the Carbonilla Fault. The Guadaloso is the oldest basaltic field in the PVF (Payunia Volcanic Field). The El Rengo group, a basaltic field to the east of the Payún Matrú caldera is older than Los Volcanos, and it may be from the late Pleistocene (Fig 1.3). The Payún Matrú Caldera is mostly composed of ignimbrite, rhyolitic and trachyte flows.

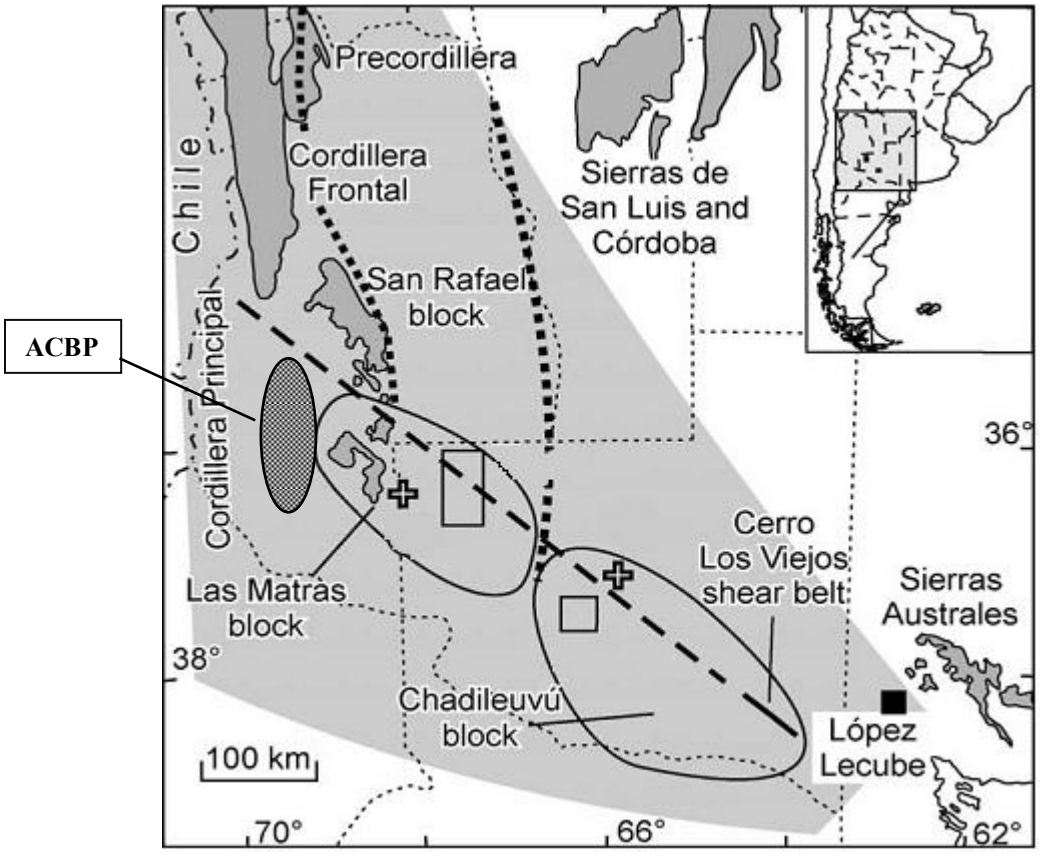

Figure 1.2: Geological boundaries of the Andino-Cuyana Basaltic Province, labelled ACBP (Llambías et al., 2003)

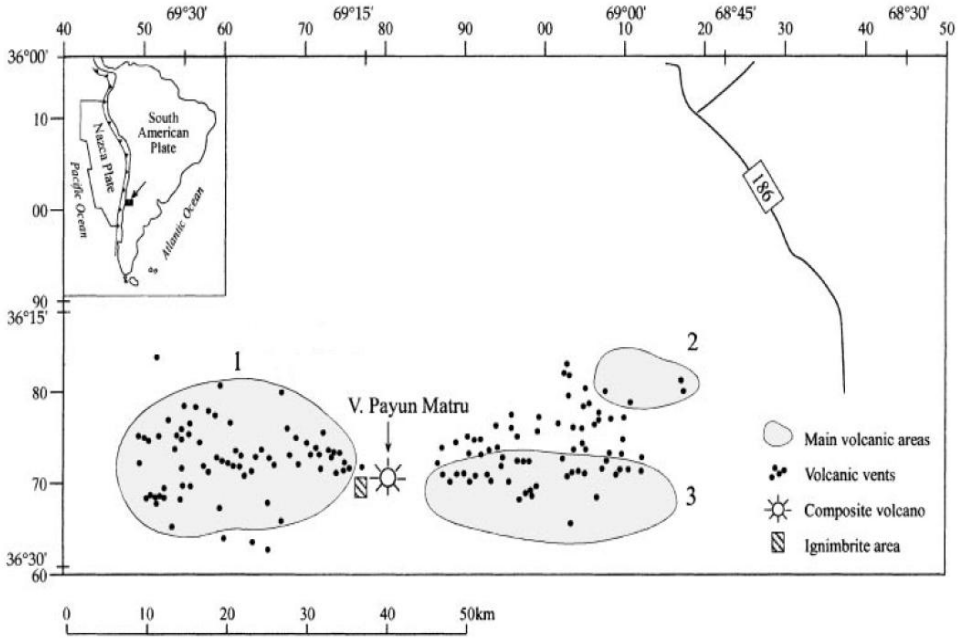

Figure 1.3:Map of the Payunia Volcanic Field. 1) Los Volcanes group, 2) Guadaloso, 3) El Rengo (Inbar and Risso, 2001a)

1.3.1 Formation of the Andino-Cuyana Basaltic Province (ACBP)

During the late Miocene the angle of the subducting slab was shallow (~ less than 10°) (Fig 1.4a) . Hence in this period there was not enough space between the oceanic subducting slab and the overriding continental crust for hot asthenosphere injection. The cessation of volcanism where subduction is flat is thought to be due to the virtual lack of asthenosphere between the subducted and the overriding plate (Van Der Pluijm and Marshak, 2004). Consequently, a period of compression occurred in the area that now comprises the ACBP, while the volcanic arc-lavas migrated eastwards. This resulted in extension in the eastern part, which facilitated the upwelling of hot andesitic to dacitic magmas at ~ 8 to 5 Ma forming the Chachaúen Volcanic Complex, which was erupted during the transient shallowing of the Andean subduction zone (Kay et al., 2004). This episode of shallowing of the subducting Nazca Plate is considered to have been initiated at the onset of contractional deformation in the early Miocene and to have peaked coincident with widespread deformation across the back-arc at the time of eruption of the Chachaúen Complex (Kay et al., 2004).

The Chachahúen Complex has geochemical characteristics and Sr isotope values similar to the transitional basalts described by Stern (1990). During the 5 Ma since the Miocene, the subducting slab increased its angle of subduction (Fig 1.4b), producing extension in the back-arc and forming the Andino-Cuyana Basaltic Province. The steepening of the Nazca Plate during the Pliocene and Pleistocene accords with preferential melting of hydrated mantle exposed to a thickening asthenospheric wedge (Kay et al., 2004).

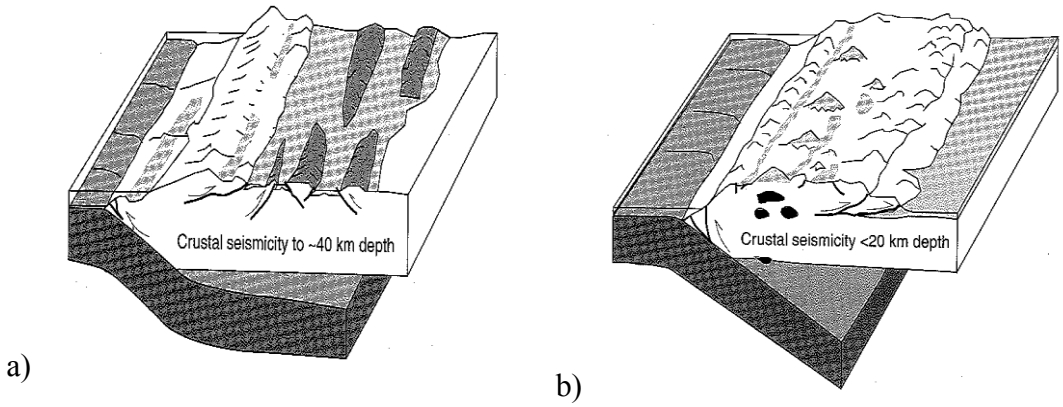

Figure 1.4 : Formation of the Andino-Cuyana Basaltic Province. a) Flat subduction during the Miocene. b) Steep subduction during the last 5 Ma. (Van Der Pluijm, B. & Marshak C., 2004)

Chapter 2

Background information

2.1 Geochemistry of the Andino-Cuyana Basaltic Province

The back-arc basalts from Patagonia in Argentina (Palaeocene–Holocene) constitutes one of the largest Cenozoic continental basaltic provinces on Earth (Bertotto et al., 2009). The Andino-Cuyana Basaltic Province (ACBP) is one of the youngest basaltic provinces along the Patagonian plateau and which has captivated the attention of scientists around the world. Several geochemical investigations have been made along the Patagonian plateau on broad and regional scales. In the case of the northern part of Patagonia, regional geochemical analyses of basalts are available for areas to the north, east and within the ACBP. In addition, broad-scale geochemical analyses by Stern et. al. (1990) has proposed a way of differentiating the basalts into "cratonic" and "transitional" along the Patagonian plateau, according to their isotopic, trace- and major-element compositions. Furthermore, in 2004 Stern produced a detailed study of the total volcanic activity of the Andes from north (5°N) to south (42°S) in which the volcanic centres were divided into Northern, Central, South and Austral Volcanic Zones. The area of the ACBP corresponds to the Southern Volcanic Zone (SVZ) of Stern, which has also been divided into northern, transitional, central and southern SVZ. According to this sub-division, the ACBP corresponds to the transitional SVZ, which follows the division criteria of cratonic and transitional basalts. According to Stern (2004), transitional basalts were erupted along the western edge of the outcrop belt of the Quaternary plateau lavas in areas that were the sites of earlier Cenozoic Andean orogenic arc volcanism. Transitional basalts can also be differentiated from cratonic basalts by their geochemical signatures as they possess a restricted isotopic composition, do not contain peridotite xenoliths and are intra-arc alkali basalts interspersed with central-vent arc stratovolcanoes (Stern et al., 1990).

Transitional basalts are widespread along the Patagonian plateau, and they all follow the same geochemical characteristics. In addition, the cratonic and transitional basalts of the Patagonian plateau are not quartz or nepheline normative (Stern et al., 1990); they tend to be more alkaline to strongly alkaline on a diagram of silica versus total alkalis. However, the cratonic basalts tend to be more strongly alkaline than transitional basalts.

Germa et al. (2010) also used the total alkali versus silica diagram, finding that the values from Stern et al. (1990) and Germa et al. (2010) are alike in relation to transitional basalts from the Patagonian plateau and from Payunia Volcanic Field (Fig. 2.1). In addition, the Quaternary Andean orogenic-arc high-Al basalts erupted between 36°S and 42°S are sub-alkaline and present lower Ni and MgO concentrations than the transitional basalts (Stern et al., 1990). The Patagonian alkali basalts are more enriched in high field strength elements (HFSE) than the Andean orogenic high-Al basalts. However, on a regional scale, Germa et al. (2010) suggested that the youngest part of the PVF (Los Volcanes), which constitutes the western part of PVF, is characterized by low abundances of high ionic potential elements or high field strength elements (HFSE) such as Ti, Nb, Zr, Ta, Hf, and Y. The Los Volcanes area shows enrichment of elements of low ionic potential such as Rb, Ba and Sr; these are characteristics of oceanic island basalts (OIB). This last statement is also reinforced by Bertotto et al. (2009) who suggested that basalts to the east of the PVF are in the range of ocean island basalts.

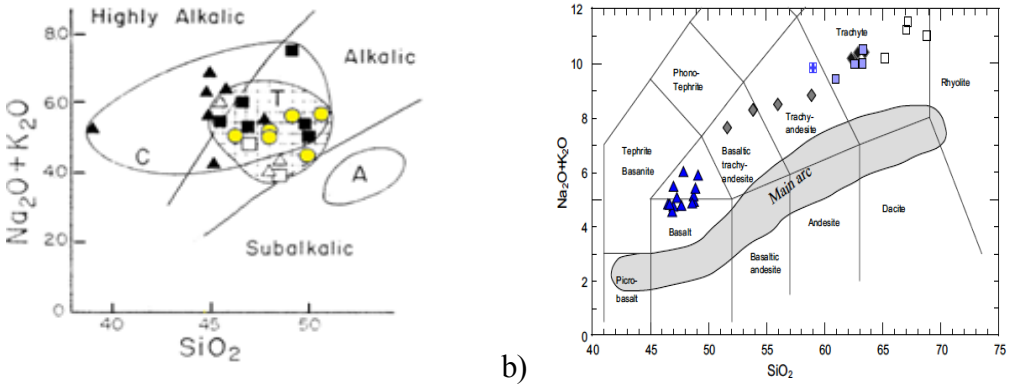

a) b)

Figure 2.1: Comparisons between Stern et al., (1990) and Germa et al., (2010). Yellow circles represents transitional basalts north of 39°S, blue triangles represent the basaltic flows from Payunia. Field C and T in a) correspond to cratonic and transitional basalts respectively. Field A in a) corresponds to the Andean volcanic arc. Note the similarity in the content of total alkali and silica in both graphs.

Furthermore, a detailed geochemical investigation by Pasquare et al. (2008) along the eastern part of the Payunia Volcanic Field, in the area called Pampas Onduladas, indicated that the magmatism of the Payunia Volcanic Complex mainly belongs to the Na-alkaline series and is prevailingly constituted by basaltic rocks ranging from hawaiites to slightly sub-alkaline basalts. In addition, Bertotto et al. (2009), Pasquare et al. (2008), and Stern et al. (1990) proposed that the negative anomalies of Nb and Ta suggest that the mantle source of the eastern part of Payunia parental magmas was probably affected by slab-derived metasomatism. The Th/Ta ratio, used in Patagonian basalts as an indication of subduction-enriched mantle source, is relatively high in the area east of PVF from 36°00'S to 36°30'S, while in the area east of PVF from 36°30'S to 37°30'S it is considerably lower (Bertotto et al., 2009). This indicates that one type of basalt has been enriched while the other not; however, the causes are not clearly established.

The geochemical analysis done by Bertotto et al. (2009) does not include the PVF; however, it provides important information on a regional scale. The magnesium numbers (Mg/Mg+Fe) presented by Bertotto et al. (2009) for the area east of Payunia Volcanic Field are strongly associated with the magnesium transitional values presented by Stern et al. (1990) from the Patagonian plateau. These similarities reinforce that the basalts east of PVF are transitional and follow the same geochemical composition as the transitional basalts along the entire Patagonian plateau.

2.2 Previous dates from the Andino-Cuyana Basaltic Province

The majority of the numerical dates from the ACBP have been obtained from the Payunia Volcanic Field, especially from the intermediate flows in the Mayún Matrú caldera. The preferred technique used to date the intermediate and the mafic flows has been K-Ar, however some dates have been obtained using thermo luminescence, and also some relative dates have been acquired using geomorphometric and geomorphologic analysis. Nevertheless, it is important to comprehend that the Llancanelo Volcanic Field is relatively older than Payunia Volcanic Field.

This is evident from the geological maps as the basalts forming the LLVF such as the Chapúa Formation are mainly composed of olivine basalts, of early Pleistocene age, whereas the majority of the basalts from the PVF date from the middle Holocene (Fig 2.2).

The morphometric and morphological analysis by Inbar and Risso (2001b), demonstrated that the youngest flows are found in the area of Los Volcanes (east of Payún Matrú caldera); the relative age suggested for this area is 0.001 to 0.01 Ma and the oldest flows are found along the eastern parts of the LLVF and PVF. Some of the radiometric dates from the LLVF suggest that the age of some of the basalts in this area are 0.5 ± 0.2 Ma, corresponding to the late Pleistocene Puente Formation (Bermúdez and Delpino, 1989). More specific ages obtained from the south-eastern part of the LLVF using K-Ar indicate that the oldest age from this area is 1.878 ± 0.028Ma, corresponding to the Nevado Formation (Quidelleur et al., 2009). In addition, specific dates from the western part of the LLVF, especially from Cerro Trapal, and from the eastern part, such as Cerro Coral, have not been previously made.

However, according to the geological map of the area, two volcanic cones corresponding to olivine basalt from the Chapúa Formation are approximately from the middle Pleistocene. Additionally, the basalts from the far western part of Llancanelo Lake correspond to olivine basalts from the early Holocene Cerro Campanário Formation. Furthermore, K-Ar dates are available for the San Rafael Block located north of the LLVF (35°S). These dates show that basalts within the San Rafael Block range from 1.78 ± 0.11 Ma to 0.106 ± 0.011 Ma (Folguera et al., 2009). This age range is similar to the Llancanelo Volcanic Field; therefore, suggesting that the two areas were formed during the same geo-tectonic stage.

In relation to Payunia Volcanic Field different dates have been obtained using K-Ar and thermoluminescence. The oldest K-Ar date from the PVF is from the Payún or Payún Liso Volcano which yields a mean age of 265 ± 5 ka, while the youngest age is less than 7 ka (Germa et al., 2010). The youngest ages from the Los Volcanes area are from basaltic flows dated at 26 ± 11 ka (Germa et al., 2010). Furthermore dates from the Payún Matrú caldera, show that it was active in the last 300 ka rather than in the Pliocene, and it has been suggested that the caldera-forming eruption occurred between 168 ± 3ka and 82 ± 1 ka (Germa et al., 2010).

In contrast, dates from thermoluminescence techniques show much younger ages, suggesting that the ignimbrites from the Payún Matrú caldera are 4860 ± 400 a (Duran and Mikkan, 2009). In addition, a K-Ar date from the eastern part of the PVF from the Pampas Onduladas flow yielded an age of 0.40 ± 0.1 Ma (Pasquare et al., 2008). While thermoluminescence dates from the same area shows an age of 6900 ± 600 a for the same area (Duran and Mikkan, 2009). The extremely young thermoluminescence ages are not supported by any other dates in the area, and their geographical coordinates and methodology are not provided.

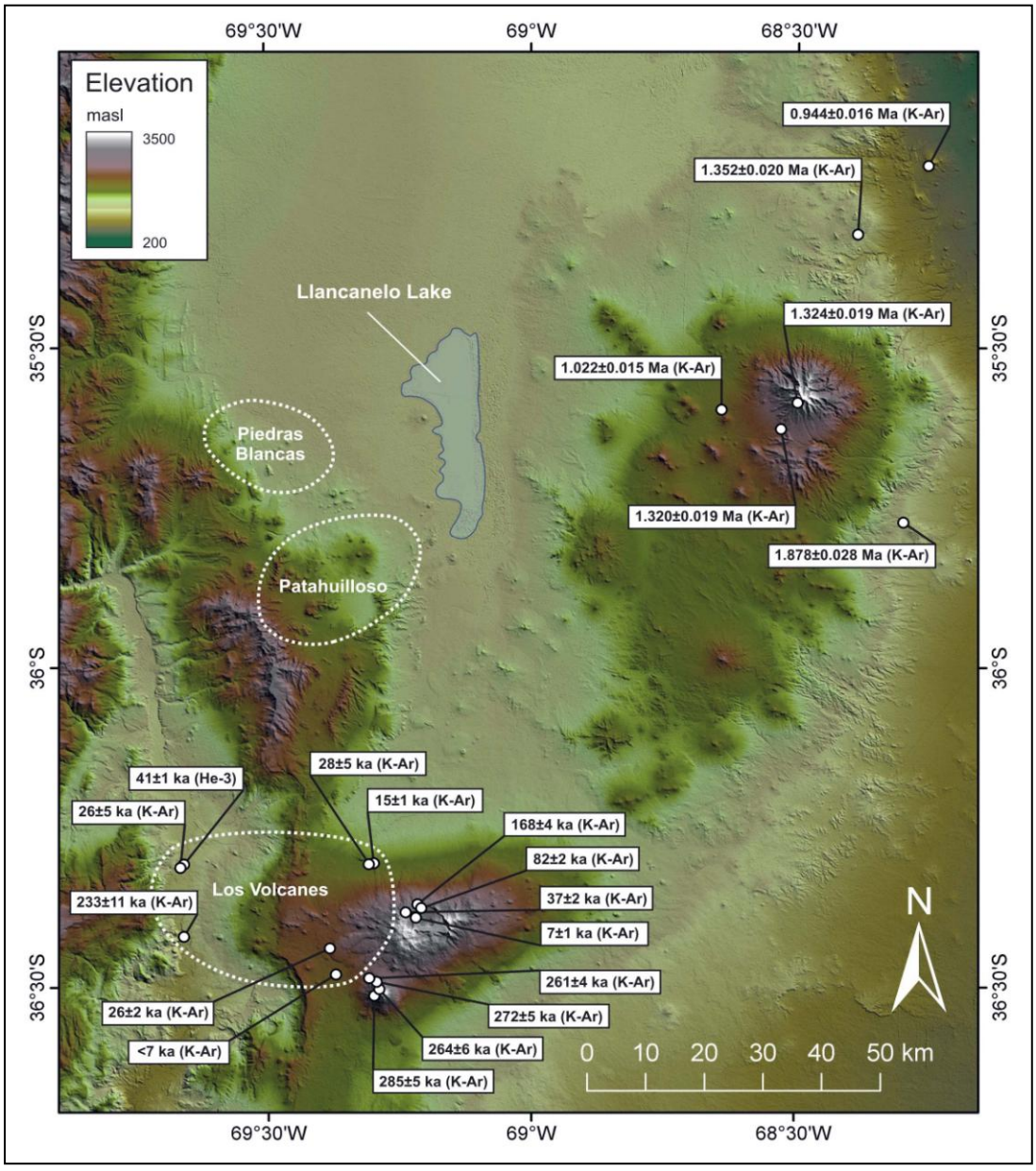

Figure 2.2: Previous dates from Andino-Cuyana Basaltic Province

In addition, a cosmogenic ^{3}He date has been obtained from one of the lava flows from the far west area of Los Volcanes along the Grande River on a primary lava flow surface (at ~36.31°S; 69.66°W). The cosmogenic age of this lava flow ranges from 37 ± 3 to 44 ± 2 ka (Marchetti et al., 2006). This is also in general accordance with the ages provided in the work done by Germa et al. (2010) as one of the K-Ar ages in the same area suggests that the basaltic flow is 26 ± 5 ka. Furthermore, a large ignimbrite emplacement and trachytic and trachyandesitic lava with sanidine, plagioclase and clinopyroxene phenocryst was sampled for cosmogenic ^{36}Cl close to Santa Maria volcano (Fujioka, 2006). The age of the flow according to ^{36}Cl is 15 ± 0.9 ka, which is in accordance with the K-Ar dates from Germa et al. (2010).

2.3 Dating Methods

2.3.1 K-Ar and Ar-Ar dating

Potassium is one of the most abundant elements on the Earth's surface. Nevertheless the radioactive isotope, ^{40}K, makes up only 0.012% of total potassium. In geological structures such as lava flows the content of ^{40}K and ^{40}Ar can be measured and from the concentration of ^{40}Ar the age of the lava since extrusion can be calculated. However the method involves some complications and assumptions.

Prior to and during the eruption of magma, the argon contained within the hot magma will have a strong tendency to partition into, and equilibrate with, the ambient gas phase which is likely to be atmospheric in composition at or near the Earth's surface (Rutter and Catto, 1996). If complete equilibration is achieved then all the radiogenic argon will be lost. Hence at the time of eruption the argon component in the magma will be the same as the atmospheric argon content. One of the main assumptions of K-Ar and Ar-Ar dating assumes that there would be no initial radiogenic ^{40}Ar inherited in the sample, and that all the radiogenic ^{40}Ar measured was generated by ^{40}K decay. When the magma cools the ^{40}K contained in the chemical lattice of some minerals within the rock will start to decay to ^{40}Ar. As a consequence, the amount of radiogenic ^{40}Ar in the rock is proportional to the initial content of K and to the time since eruption.

Corrections need to be made especially with respect to atmospheric ^{40}Ar; which is corrected using the air $^{40}Ar/^{36}Ar$ ratio of 295.5, and the remaining ^{40}Ar corresponds to ^{40}Ar produced by ^{40}K which is used to calculate a numerical age for the rock.

An important variant of the K-Ar method is Ar-Ar dating, which in principle is similar, however it is more accurate and the sample preparation is different. In the ^{39}Ar-^{40}Ar method, the sample is first irradiated with fast neutrons in a nuclear reactor, during which time a proportion of ^{39}K atoms is converted to ^{39}Ar atoms by (n,p) reaction (Rutter and Catto, 1996). This provides a major advance in the method as the argon isotopes are analysed together. When using K-Ar, the two required isotopes of potassium and argon are measured separately. These two methods have been widely used, as many rocks contain measurable amounts of potassium. However when the rock is very young, measurable amounts of radiogenic ^{40}Ar are hard to detect with high precision.

The younger age limit for whole-rock volcanic samples varies widely depending upon the actual atmospheric ^{40}Ar content and the K content of the sample, but is likely to be in the range of 20 ka to ~ 200 ka, for a precision of 10% or better in the measured age (Rutter and Catto, 1996). However, in particularly high-potassium samples, with low atmospheric argon, ages of <10 ka can be determined with acceptable precision (Rutter and Catto, 1996). The oldest limit of the method does not constitute a major problem as radioactive ^{40}K has a half-life of 1.25 Ga, hence the method can be used to date rocks as old as the age of the Earth. It is appropriate to consider that intermediate to felsic rocks tend to have high concentrations of potassium, while basaltic rocks generally have lower concentrations of potassium-bearing minerals.

2.3.2 ^{26}Al & ^{10}Be dating

This dating method combines two cosmogenic nuclides, ^{26}Al and ^{10}Be; these two isotopes are not stable and they are generated by cosmic rays at the Earth's surface. The basic principle of isotope production by reaction of cosmic rays with target elements at the Earth's surface is mainly the same as the production of ^{21}Ne and ^{3}He. ^{10}Be is derived from spallation of ^{16}O, whereas ^{26}Al is produced by spallation of ^{26}Si (Dickin, 2005). Spallation reactions are caused by fast neutrons, whose penetration decreases exponentially with depth.

Most of these spallation reactions occur in the top half metre of the rock surface. ^{26}Al can be used alone as a geochronometer in the measurement of rock exposure ages, however it is produced in very small quantities. By combining this cosmogenic isotope with ^{10}Be, which is also a cosmogenic isotope with a different half-life, the possible applications of the method increase and it also creates a more powerful and reliable dating method. The half-life of ^{26}Al is 0.705 Ma and of ^{10}Be 1.51 Ma (Dickin, 2005). The older limit for this method is approximately 3 Ma, as variations in erosional rates do not severely affect the value of the isotopic ratio in younger rocks (Rutter and Catto, 1996). The younger limit depends on the half-life of ^{26}Al and ^{10}Be; therefore samples younger than 0.5 Ma are not suitable, as they have not had adequate time to permit sufficient decay of the shorter lived ^{26}Al (Rutter and Catto, 1996).

This method is reliable and has been widely used especially in quartz-bearing rocks. Quartz, is resistant to chemical weathering, therefore it is resistant to contamination by atmospheric or "garden variety" ^{10}Be; this together with low ^{27}Al (atmospheric ^{27}Al) content makes quartz an excellent material for exposure dating (Dickin, 2005). However, in the case of mafic and ultramafic rocks it would not be appropriate as these rocks do not contain quartz.

2.3.3 ^{36}Cl dating

The use of cosmogenic ^{36}Cl to produce geochronological information was first proposed over 45 years ago, although it could not be widely applied because at that time there was no instrumentation with the appropriate analytical sensitivity to measure small amounts of chlorine. However, in 1979 with the development of accelerator mass spectrometry (AMS), very small amounts of ^{36}Cl were able to be detected (Rutter and Catto, 1996). The basic principle of production of ^{36}Cl is the same as ^{10}Be, ^{26}Al, ^{21}Ne and ^{3}He; however the target elements are K, Ca and Cl which offer a great advantage as it can be applied to a wide variety of rocks. Also atmospheric ^{36}Cl does not constitute a great problem unless absorbed in severely weathered material. ^{36}Cl is not a stable isotope; it has a half-life of 310 ka.

The production rate of ^{36}Cl in any particular rock at the Earth's surface depends on the geographical location as the cosmic ray influx would change according to latitude and altitude, and it also depends on the chemical composition of the rock. The older limit for this method is mainly based in the half-life of the cosmogenic isotope, which is one of the main limitations when unstable isotopes such as ^{36}Cl, ^{10}Be, ^{26}Al and ^{14}C, are compared with stable isotopes such as ^{21}Ne and ^{3}He which do not decay over time, therefore, theoretically they can be used to date rocks as old as the age of the Earth. Furthermore, the younger limit of the ^{36}Cl method can be as young as 20 years; however it mainly depends on the target mineral. In relation to basalts the method had been widely used, and also it fulfils the criteria for simple exposure history of complete shielding prior to sudden exposure (Tuniz et al., 1998).

2.3.4 Thermoluminescence

Thermoluminescence is the thermally stimulated emission of light following the previous absorption of energy from radiation (McKeever, 1985). Thermoluminescence in various minerals was first observed over a century ago; however, it was first suggested as a technique to determine the age of rocks in 1953 (McKeever, 1985). In the crystal lattice of minerals there are traps which are spaces in which electrons can accumulate. Once the mineral is heated in the laboratory, enough energy is provided for the electrons to escape from the crystal lattice of the mineral. The electrons lose energy when they escape from the lattice of the mineral emitting a photon of light. The amount of light produced is proportional to the number of trapped electrons that have been released which in turn is proportional to the radiation dose accumulated. The natural dose rate has to be determined, which is the dose accumulation per year that is mainly given by the radioactivity of uranium, thorium and potassium. Quartz and alkali feldspars are the commonly used minerals for thermoluminescence dating. Accordingly it is appropriate to suggest that the method may be suitable for intermediate and felsic rocks but not for mafic and ultramafic rocks, which contain low concentrations of alkali feldspar and quartz.

2.4 Cosmogenic ^{3}He and ^{21}Ne

Cosmic rays are highly energetic particles that arrive from space, and constantly bombard the Earth's surface. Cosmic rays are composed of particles, mainly neutrons and muons, which are generated by galactic cosmic rays. As these highly energetic particles reach the atmosphere they interact with the constituents of air. This attenuates the cosmic ray flux, and produces a shower of secondary protons, neutrons and other particles. The secondary particles generated can then react at the Earth's surface with atomic nuclei, due to spallation reactions, in which a few nucleons are sputtered off the target nucleus, to produce cosmogenic isotopes. These reactions are produced at the Earth's surface; however, the probability of producing a given daughter nuclide (e.g., ^{21}Ne) from a target nuclide (e.g., ^{28}Si) depends on nuclear excitation functions which are qualitatively based on the following principles (Niedermann, 2002):

- Neutrons may escape more easily from a nucleus than can protons
- Alpha particles are particularly stable, therefore show higher probability of nuclear reaction
- The mass between the target nucleus and the product is typically a few atomic mass units.

Target element	*Spallation*	*Thermal neutron capture*	*Negative muon capture*
Li		^{6}Li(n,α)^{3}H(β^{-})^{3}He	
O	^{16}O(n,2pn)^{14}C	^{17}O(n,α)^{14}C	^{16}O(μ^{-},pn)^{14}C
	^{18}O(n, αn)^{14}C		^{16}O(μ^{-},αpn)^{10}Be
	^{16}O(n,4p3n)^{10}Be		
Na	^{23}Na(n, pn) ^{22}Ne		^{23}Na(μ^{-},n) ^{22}Ne
	^{23}Na(n,p2n) ^{21}Ne		^{23}Na(μ^{-},2n) ^{21}Ne
	^{23}Na(n,p3n) ^{20}Ne		
Mg	^{25}Mg(n,α)^{22}Ne		^{24}Mg(μ^{-},pn)^{22}Ne
	^{24}Mg(n,α)^{21}Ne		^{24}Mg(μ^{-},p2n)^{21}Ne
	^{24}Mg(n,αn)^{20}Ne		
Al	^{27}Al(n,3p3n)^{22}Ne		^{27}Al(μ^{-},αn)^{22}Ne
	^{27}Al(n,3p4n)^{21}Ne		
	^{27}Al(n,2n)^{26}Al		

Si	$^{29}Si(n,2\alpha)^{22}Ne$		$^{28}Si(\mu^-,2n)^{26}Al$
	$^{28}Si(n,2\alpha)^{21}Ne$		$^{28}Si(\mu^-,\alpha pn)^{22}Ne$
	$^{28}Si(n,p2n)^{26}Al$		
		$^{35}Cl(n,\gamma)^{36}Cl^{\dagger}$	
K	$^{39}K(n,pn)^{38}Ar$	$^{39}K(n,\alpha)^{36}Cl^{\dagger}$	$^{39}K(\mu^-,n)^{38}Ar$
	$^{41}K(n,p3n)^{36}Cl^{\dagger}$		
Ca	$^{40}Ca(n,\alpha p)^{36}Cl^{\dagger}$		$^{40}Ca(\mu^-,\alpha)^{36}Cl^{\dagger}$
	$^{40}Ca(n,2p)^{38}Ar$		$^{40}Ca(\mu^-,pn)^{38}Ar$
Fe	$^{56}Fe(n,8p11n)^{38}Ar$		$^{54}Fe(\mu^-,n)^{53}Mn$
	$^{54}Fe(n,pn)^{53}Mn$		
	$^{56}Fe(n,p3n)^{53}Mn$		

Table 2.1: Examples of nuclear reaction. Types that produce nuclides which can be used in surface exposure studies (Niedermann, 2002)

The production of cosmogenic ^{3}He depends on several nuclear reactions in which the target elements are O, Si, and Al (Table 2.1). Hence the concentration and the production rate of ^{3}He will be different to ^{21}Ne. Cosmogenic ^{21}Ne and ^{3}He are stable isotopes that can be used to date geological events since first exposure on the land surface to cosmic rays. This method can be used to date young basaltic flows, as well as glacial events, meteorite impacts, or to date archaeological artefacts. The technique is mainly based on measuring the accumulation of cosmogenic ^{21}Ne and ^{3}He as it depends on the time since exposure to cosmic rays.

Consequently, the rock has to be exposed at the Earth's surface to produce cosmogenic isotopes; hence the amount of isotope generated is related to the age duration of exposure of the rock. A good target mineral is olivine (Mg_2SiO_4) as it promotes the production of the two isotopes, and also retains ^{21}Ne and ^{3}He in its chemical lattice.

2.5 Previous work in cosmogenic ^{21}Ne and ^{3}He dating

The production of noble gas isotopes by interaction of high-energy cosmic ray particles with rocks was first recognized half a century ago when Paneth showed that the high $^{3}He/^{4}He$ ratios in iron meteorites must be due to cosmic ray interactions and provide information about their ages (Niedermann, 2002).

Cosmogenic isotopes of noble gases have been used to study catastrophic floods, retreating ice sheets, eruption of volcanic lavas, deposition of alluvial surfaces, meteorite impacts and as an indicator of erosional denudation rates (Poreda and Cerling, 1992, Gillen, 2001, Niedermann, 2002, Gillen et al., 2010). The most used and extensively studied isotope for cosmogenic dating is ^{3}He, which has been used to date basalts between 1 and 200 ka. However, in 1979 Craig et. al. attributed the presence of excess ^{21}Ne (along with ^{3}He) in native metals from Greenland, to cosmic ray production (Niedermann, 2002). In 1987, Craig and Marti, detected ^{21}Ne along with ^{3}He produced by cosmic rays in olivine and clinopyroxene phenocrysts from Maui (Niedermann, 2002).

Conversely, since 1987 ^{21}Ne has not been widely used, except for the work by Poreda and Cerling (1992) on young basalts form Tabernacle Hill, Utah, and the work by Gillen et al. (2010) on young basaltic lava flows from the Newer Volcanic Province, western Victoria, Australia.

These two previous studies using ^{21}Ne yielded ages of 17 ± 0.2 ka for the basalts in Utah, and 36 ± 3 ka, 37 ± 5 ka, and 53 ± 5 ka for the basalts in western Victoria. Both results were validated using other dating methods such as ^{36}Cl, ^{3}He and ^{14}C, to demonstrate that the results were compatible.

The ^{21}Ne/^{3}He in olivine and pyroxene remains constant with latitude, elevation and time, up to 10 Ma (Fenton et al., 2009). However, in reality there are no ancient original exposure surfaces that have not been eroded through time. Therefore, and according to Poreda and Cerling (1992), cosmogenic ^{21}Ne and ^{3}He should be used to date young rocks.

In addition, the production rates of ^{21}Ne and ^{3}He play a major role in determining the age of the rock, as the amount of isotope in the rock is directly proportional to the time since exposure. The production rate depends on the latitude, altitude and the concentration of Mg as it is the target element for the production of ^{21}Ne, and the concentration of O, Si, and Al in the case of ^{3}He. Therefore, there is a compositional dependence of the cosmogenic ^{21}Ne/^{3}He production ratio on the Mg (Fo) content of olivine (Gillen et al., 2010). Several studies have made done in order to determine the production rates of different minerals.

Poreda and Cerling (1992) estimated that the production rate of ^{21}Ne for Tabernacle Hill is 135 atoms/g/a for Fo_{81} olivine at 1455m and 39°N or 45 ± 4 atoms/g/a at sea level and high latitude. However, they also calculated the production rate for plagioclase finding that it is 16.8 ± 1.7 atoms/g/a at sea level and 60° for an Ab_{36}. Another study by Fenton et al. (2009), suggested that the production rate of ^{21}Ne in clinopyroxene is ~25 ± 8 atoms/g/a, while the production rate of ^{21}Ne in olivine is 49 atoms/g/a for Fo_{81} for the Bar Ten Pleistocene flows in the United States. In the case of the Newer Volcanic Province in Western Victoria the production rate of ^{3}He and ^{21}Ne according to latitude, altitude and depth for olivine sample ranged from 90 to 35 atoms/g/a and 123 to 48 atoms/g/a, respectively (Gillen et al., 2010). Cosmogenic ^{21}Ne ages have not been previously produced from the Argentinian field area; however Marchetti et al. (2006) have produced a ^{3}He date from a basaltic flow from the western-most part of the Los Volcanes area that dammed the Rio Grande finding that the production rate of ^{3}He is 116 at/g/yr.

2.6 Aims of this thesis

The geochemical evolution of the back-Andean modern basaltic lava field will provide evidence on the formation of this unusual volcanic field. Furthermore the origin of these lavas will be investigated, in relation to which part of the Earth's mantle they are derived from. Currently, geochemical analyses have been made in the area on both a broad and regional scale, however not enough information has been provided from the Llancanelo Volcanic Field. This project will provide valuable information contributing to an improved understanding of the geochemistry and the geochronology of this important basaltic province in southern Mendoza, Argentina.

Previous studies estimate that the lavas from the ACBP date from approximately the Plio-Pleistocene to Holocene. Currently no accurate dates have been provided; this is due to the fact that young lavas are difficult to date by conventional methods. Cosmogenic ^{21}Ne and ^{3}He represent new numerical dating techniques that have been used in Australia to date the Newer Volcanic Province in western Victoria. These stable isotopes of neon and helium are used to assess the time since the lavas were extruded and exposed to the atmosphere.

The purpose of the project is to provide geochronological evidence using new dating methods in order to reconstruct the geological history, as well as to provide geochemical information about this young volcanic area. The research is mainly based on analysing young basaltic lavas, using ^{21}Ne and ^{3}He. However the dates will be validated using ^{39}Ar -^{40}Ar and previous dates from the area. The investigation is mainly based on analysing the amount of ^{21}Ne and ^{3}He present in olivine crystals which are directly associated with the crystallisation age of the rock. Additionally the Payunia and Llancanelo Volcanic Fields have not been accurately dated, therefore this new method can potentially provide accurate dates for lavas as young as 500 to 1000 years old. The investigation also provides geochemical information including major and trace elements analysis, as well as Sr and Nd isotopes. Some of the volcanoes lack general geochemical information, especially the ones around Llancanelo Lake. In relation to the Payunia Volcanic Field several investigations have been done, however the information obtained from this investigation will add to the knowledge of this back-arc province.

Methods

3.1 Field sampling

The Andino-Cuyana Basaltic Province constitutes an extensive area of well exposed, young basalt flows, with generally high olivine content. The ACBP is located in a rather dry area, thereby minimizing erosion and weathering processes. Consequently, rocks from the ACBP are well suited to geochemical and cosmogenic isotope studies. Field work in Mendoza, Argentina, took place from 7 to 17 February, 2010. During this time 14 samples were collected mainly from basaltic rocks from the Llancanelo and Payunia Volcanic Fields with only one intermediate sample corresponding to a trachyte flow from the PVF. The weight of the samples varies from 15 kg to ~1 kg, sufficient for extraction of olivine. The exposure surface and orientation of the rock were recorded for each cosmogenic dating sample.

From the total of 14 samples (Table 3.1 and Fig. 3.1 and 3.2), only five were selected as suitable for cosmogenic ^{21}Ne and ^{3}He dating (LL3, PY-4, PY-7, PY-8, and PY-9). Samples LL3, PY-8, and PY-9 are from the original ropy surface of the lava flow and which is one of the requirements for continuous cosmogenic exposure dating. Samples PY-4 and PY-7 are small basaltic bombs, which are assumed to be the original exposure surface since they were ejected from the volcano.

Sample name	Type of rock	Latitude S	Longitude W	Elevation (m)
LL1	basalt	35.64440°	69.09924°	1368
LL2	basalt	35.61320°	69.19963°	1510
LL3	basalt(top)	35.71184°	69.45692°	1449
LL4	basalt(bottom)	35.71184°	69.45692°	1446
LL5	basalt	35.80740°	69.05901°	1345
PY-1	scoria	36.34030°	69.46350°	2247
PY-2	scoria	36.34997°	69.44926°	2246
PY-3	scoria	36.35189°	69.43580°	2182
PY-4	basaltic bombs	36.39371°	69.39119°	2301
PY-5	trachyte	36.44312°	69.38201°	2217
PY-6	basaltic flow	36.44314°	69.38302°	2218
PY-7	basaltic bombs	36.30600°	69.31853°	1811
PY-8	basaltic flow	36.30600°	69.31853°	1811
PY-9	basaltic flow	36.31536°	69.36352°	1907

Table 3.1: Sample locations. (LL, refers to Llancanelo Volcanic Field, PY, refers to Payunia Volcanic Field)

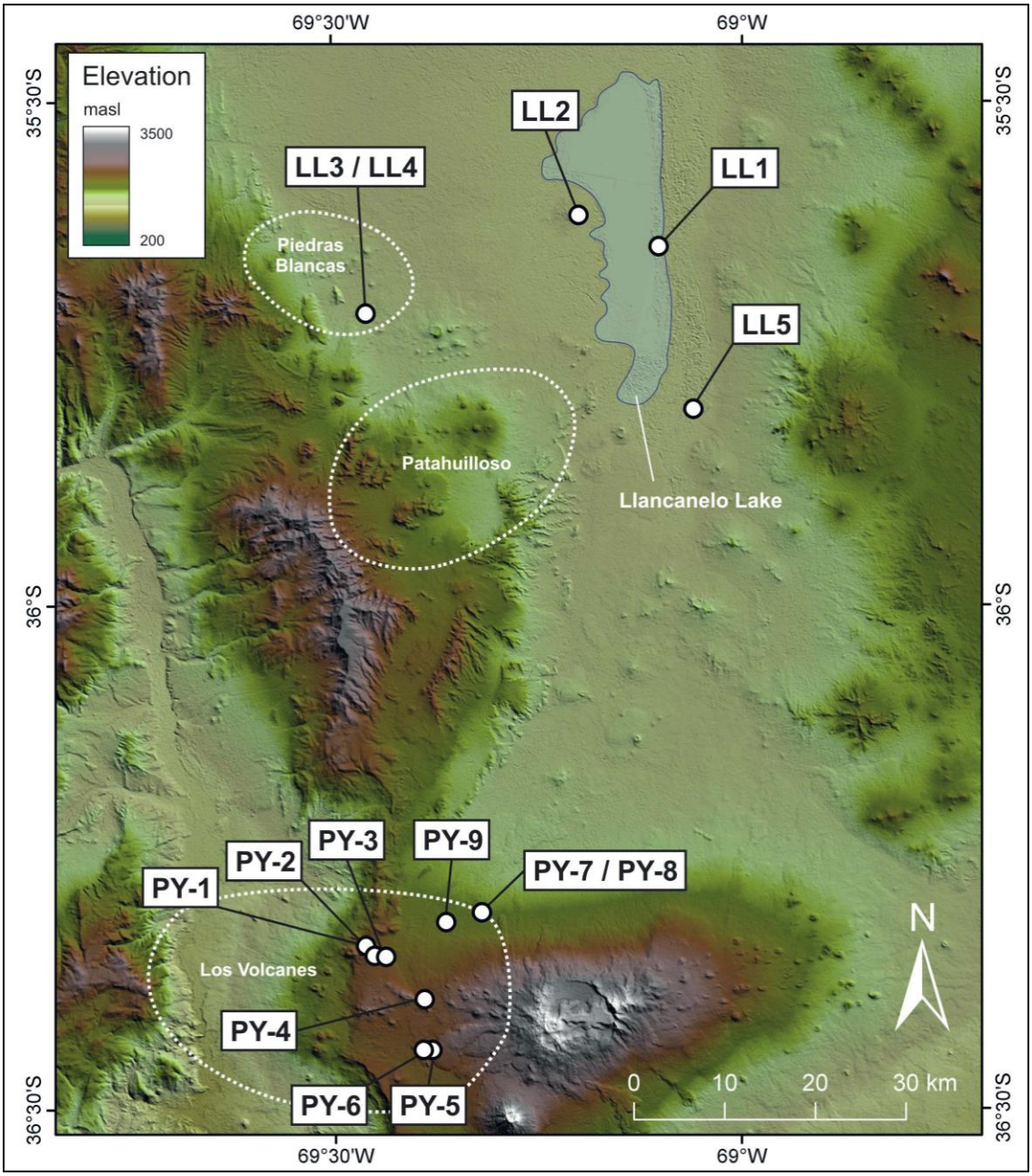

Figure 3.1: Sampling locations

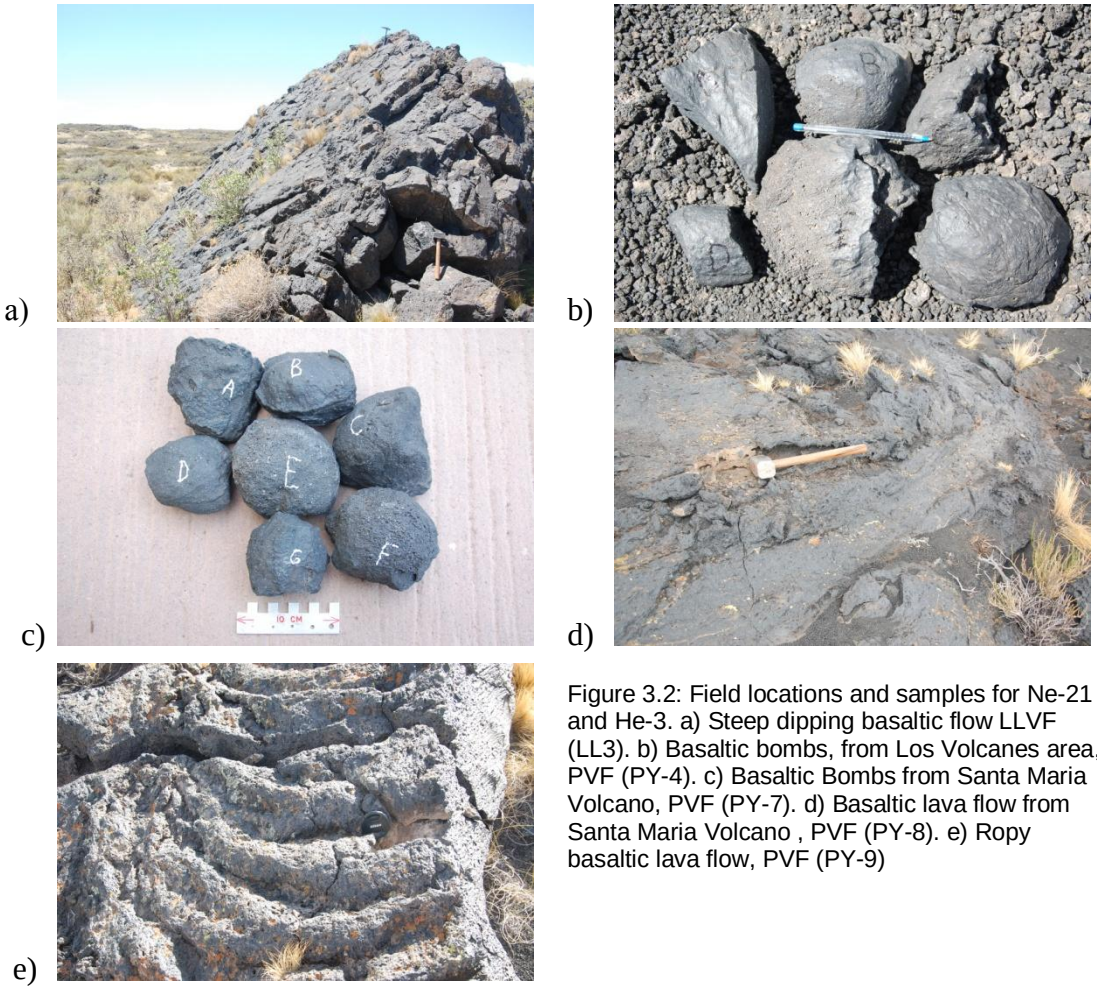

Figure 3.2: Field locations and samples for Ne-21 and He-3. a) Steep dipping basaltic flow LLVF (LL3). b) Basaltic bombs, from Los Volcanes area, PVF (PY-4). c) Basaltic Bombs from Santa Maria Volcano, PVF (PY-7). d) Basaltic lava flow from Santa Maria Volcano , PVF (PY-8). e) Ropy basaltic lava flow, PVF (PY-9)

3.2 Petrologic analysis

Thin sections of 13 samples (PY-2 was not suitable for thin section anlysis) were performed at the University of Wollongong to analyse and identify the different minerals composing the rocks. Each rock sample was sliced using a circular saw, then the sliced face was ground using 240 grit silicon carbide powders to eliminate any marks introduced by the cutting blade. Then a resin was prepared with blue dye to fill any porosity within the rock that could affect its further interpretation. This also helps to hold the fragile samples, such as the scoria samples. Then, the samples were ground using 240 grit silicon carbide powder to eliminate excess resin and mounted on the glass slide. The excess of rock is then sliced using a saw, ground using 240 grit, and finally ground using 600 grit silicon carbide power. The appropriate thickness of the slice is determined by the interference colour of plagioclase phenocrysts.

The thin sections were described using a Leica DM750P petrographic microscope, which has a Leica DFC295 camera connected to a computer for photographic documentation. The petrographic interpretation of thin sections was mainly based on MacKenzie and Guilford, 1980, MacKenzie et al., 1982 and Nesse, 1991.

3.3 Geochemical Analyses

3.3.1 Crushing

All the samples were crushed to a fine powder using a TEMA chromium steel rock crusher at the University of Wollongong. The resultant powder provides a homogeneous whole-rock sample suitable for XRF and other analysis.

3.3.2 X-ray Fluorescence

In order to determine major and trace elements present in mineral and rock samples, the essentially non-destructive x-ray fluorescence (XRF) method was utilised.
The major elements determined are; Si, Ti, Al, Fe, Mn, Mg, Ca, Na, K, and P, later expressed as oxides. Some of the more important trace elements determined are; Ba, Ce, Co, Cr, Cu, Ga, La, Nb, Ni, Rb, S, Sc, Sr, Rh, U, V, Y, Zr and Zn. The limit of detection for these is 1ppm.
The sample preparation and analysis of trace elements was performed before any other geochemical analysis as the procedure to prepare the samples for major-element analysis depends on the content of critical trace elements such as S, that may react with platinum crucibles.
The XRF trace element analysis was done by weighing approximately 5 g of powdered sample. Then 5 to 6 drops of an organic binder solution (PVC) were added to hold the sample together and it was pressed into aluminium cups, to obtain pellets, which were then dried in an oven at ~60°C for 12 hours. The samples were analysed by a Spectro Xepos XRF spectrometer (Fig. 3.3) at the University of Wollongong.
The sample preparation for major-element analysis was also performed at the University of Wollongong, using the same instrument. The sample preparation involved weighing approximately 2.4 g of 1222 flux (35.3% lithium tetraborate and 64.7% lithium metaborate) and 400 mg of each sample into Pt/Au crucibles.
The samples were then fused in a Sietronics OF 3077 furnace at 970°C by increasing the temperature from 600° by 70° every 10 min over an hour. Once the temperature

of 970° has been reached a pellet of NH_4I (ammonium iodide) was added to each of the crucibles to make the liquid less viscous. Then the liquid was poured, one by one onto a graphite disc and pressed to make a glass disc. Samples LL4 and LL5 were pre-treated with $LiNO_3$ as the samples contain high amounts of S.

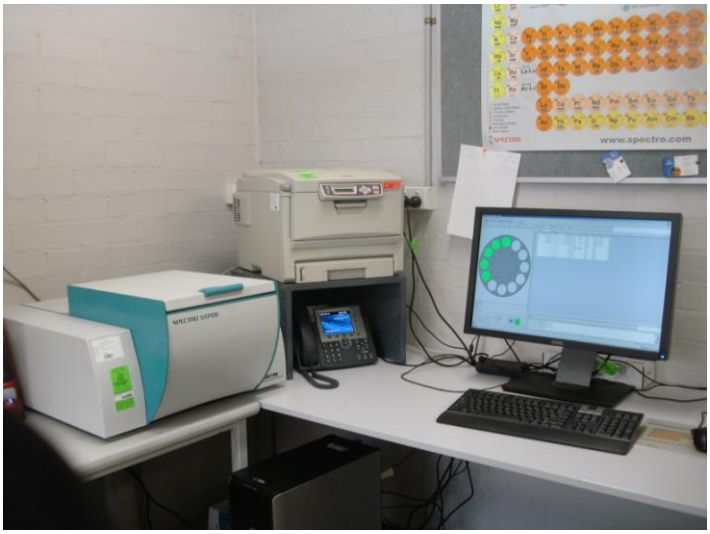

Figure 3.3: X-ray fluorescence spectrometer

3.3.3 Loss on Ignition

Loss on ignition (LOI) was conducted to quantify the amount of moisture or water in each sample. The method involves pre-heating ceramic crucibles to 1050°C for 2 hours and then weighing them precisely in an analytical balance. Then approximately 1 g of sample was added to each of the crucibles and the precise weight was recorded. The crucibles plus sample were then placed in the furnace at 1050°C for 2 hours. Finally the crucibles were weighted again. The difference between the initial weight and the final weight constitutes the loss on ignition value which is expressed as a percentage.

3.2.4 Sr and Nd isotope analysis

Strontium and neodymium isotopes were analysed on 3 whole rock samples (PY-5, PY-6 and PY-9), by Dr Marc Norman, Research School of Earth Sciences, Australian National University. Powdered samples were spiked with solutions enriched in ^{84}Sr, ^{85}Rb, ^{150}Nd, and ^{147}Sm for isotope dilution measurements and dissolved with HF–HCl in screw-cap teflon vials. Rb, Sr and a REE cut containing the Sm and Nd were separated from matrix elements by cation exchange chromatography using Biorad AG50W ion exchange resin. Nd and Sm were further purified using chromatography columns loaded with hexyl di-ethyl hydrogen phosphate (HDEHP)-coated Teflon powder. All chemical procedures were conducted in a dedicated positive-pressure laboratory equipped with HEPA-filtered clean-air stations using distilled reagents and 18 MΩ water.

Isotope ratios were measured by thermal ionization mass spectrometry using a Finnigan MAT-261 multicollector mass spectrometer operated in static mode with on-line corrections for potential Rb ($^{85}Rb/^{87}Rb$=2.5907) and Sm ($^{147}Sm/^{144}Sm$=4.7690; $^{147}Sm/^{150}Sm$=1.5087) interferences on the Sr and Nd isotopes, respectively. To correct for mass fractionation, Sr isotope ratios were normalized to $^{86}Sr/^{88}Sr$=0.1194, Nd ratios normalized to $^{146}Nd/^{144}Nd$=0.7219, and Sm isotope ratios were normalised to $^{149}Sm/^{152}Sm$ = 0.5168. As Rb has only two stable isotopes, an internal mass fractionation correction is not possible. Measured Rb ratios were corrected to a value of $^{85}Rb/^{87}Rb$ = 2.593 for the NIST 984 reference material run with the samples.

The weighted mean of $^{87}Sr/^{86}Sr$ measured by this mass spectrometer on the NIST 987 reference material during the past 12 months (since relocation of the mass spectrometer) is 0.710230±0.000005 (2SE, n=35). Measured $^{143}Nd/^{144}Nd$ ratios were corrected to a value of 0.511860 for the La Jolla standard, and Epsilon-Nd values (εNd(0), deviation from the Bulk Silicate Earth value in parts per 10,000), were calculated relative to $^{143}Nd/^{144}Nd$=0.512638.

3.4 ^{21}Ne and ^{3}He Sample preparation

Sample preparation for ^{21}Ne and ^{3}He analysis was done at the University of Wollongong, and included crushing, separation and washing.

3.4.1 Crushing

The three basaltic flow samples were sliced into 5 cm thick layers. The top 5cm of each of the sliced samples and the 2 bomb samples were then split using a rock splitter into small pieces of ~2 cm. Using the TEMA chromium steel rock crusher, each of the samples was crushed to several grain sizes and then sieved to separate the sample into >355 μm, >180 μm, >106 μm and <106 μm grain sizes.

The grain sizes of interest are >180 μm and >106 μm as they contain the largest proportion of olivine single grains. The samples were then cleaned, first with ~10% HCl to eliminate any carbonate and then ultrasonically washed with milli-Q water. The samples were dried in the oven at 80°C for ~12.
The process above described was performed three times for samples LL3, PY-8 and PY-9, twice for sample PY-7 and once for sample PY-4 as the amount of desired mineral produced in one individual step was not always sufficient. The amount of material processed during each of the crushing stages was recorded.

3.4.2 Magnetic Separation

The separation was undertaken using the Frantz Isodynamic Magnetic Separator (Fig 3.4). This apparatus generates a magnetic field, which is controlled in strength by varying the current to the electromagnet. The separation method is based on the magnetic susceptibilities of minerals and thus separates the highly magnetic minerals from the less magnetic ones.
Crushed samples were introduced in the upper end though a funnel, then into a chute with a partition in the centre and then the sample slide toward the lower end (Eby, 2010). The separator is mounted so that it can be rotated both in the direction of grain movement (slope) and in a direction normal to the direction of the grain movement (tilt) (Eby, 2010).

At a particular magnetic strength, the minerals with higher magnetic susceptibility move to the side of the chute with the greatest magnetic field and the non-magnetic minerals fall to the other side due to gravity. The two portions are collected at the end of the chute into separate containers.

The magnetic separator was first set at low amperage to separate all the highly magnetic minerals such as magnetite (Fe_3O_4). The magnesium-rich minerals such as olivine were separated using a current of 0.4 amps to 0.45 amps. Then, the non-magnetic minerals such as plagioclase were separated using higher amperage.

Figure 3.4: Frantz Isodynamic Magnetic Separator

3.4.3 Density Separation

The density separation method uses the density differences between minerals to separate them. The sample is introduced to a glass separation funnel filled with a liquid of known density. Here, the heavier minerals sink to the bottom by gravity and the lighter ones float on the surface of the liquid. The liquids used were sodium polytungstate (at UoW) and methylene iodide (at ANU) with a maximum density of 3.00 g/cm^3 and >3.33 g/cm^3 respectively.

For olivine separation the sodium polytungstate was set to a density of >2.95 g/cm^3. However olivine has a density of 3.32 g/cm^3. Minerals such as pyroxene and hornblende (3.24 g/cm^3) were not separated using sodium polytungstate heavy liquid, as the density difference between the three minerals (olivine, hornblende and pyroxene) is minimal. Therefore methylene iodide was used in a second step in order to separate the heavy minerals.

The final separated olivine samples contain minor impurities of pyroxene, hornblende, and spinel mainly from small inclusions in the olivine crystals or as composite grains. Each olivine sample was carefully examined under the microscope and residual impurities were removed by handpicking. To quantify the purity of each olivine sample, additional XRF analysis was done on each separated sample.

The final olivine product (~95% purity) was cleaned after the XRF analysis, by first placing the samples in a 50:50 ethanol/acetone mixture, in an ultrasonic bath for 15, min three times. Then, the samples were ultrasonically washed with pure ethanol three times for 15 min. Finally the samples were dried in an oven overnight at 70°C.

3.4.4 Isotopic Analysis

The He and Ne isotopic analysis was done at the Research School of Earth Sciences (RSES) at the Australian National University. Approximately 1.0 g of each olivine sample was wrapped in tin foil and loaded into an all-metal sample holder above a resistively heated, double vacuum tantalum furnace connected to a VG5400 noble gas mass spectrometer (Fig 3.5). The noble gas analysis requires three main steps.

1) Gas Extraction

The noble gases of interest (Ne and He) were extracted by increasing the temperature in a furnace to 1750°C using 3 steps (900°C, 1400°C and 1750°C). The gas extraction section consists of a tantalum (Ta) crucible with a molybdenum (Mo) liner to protect the Ta crucible from reaction with the samples. Prior to sample analysis the Ta crucible and Mo liner were degassed at 1850°C for at least 30 min, the same procedure was also used before each blank measurement. After the blank measurement, the samples were dropped into the Ta crucible to be analysed. The same analysis procedure was used for blanks and for each of the samples, increasing the temperature from room temperature to 1750°C and measuring Ne and He concentration and isotopic ratios at 900°C, 1400°C and 1750°C.

2) Gas purification and noble gas separation

Once the samples were extracted they were purified. The purification section consists of two bulk getters (containing titanium (Ti)-zirconium (Zr) alloy foils), two SAES(R) getters (St 707; Milan, Italy), a cryogenic charcoal trap, and an activated charcoal trap (Fujioka, 2006).

Active gases such as CO_2, H_2O, H_2, CO, and CH_4 were extracted by exposing the gases to the bulk getters and then to the SAES(R) getters at ~300°C. The bulk getters were then brought to room temperature.

The noble gases (He, Ne, Ar, Kr, and Xe), were separated using a cryogenic charcoal trap which desorbs the gases utilizing the noble gases different separation temperatures. The last charcoal trap located next to the ion source of the mass spectrometer was held at 77 K (-196°C) to reduce isobaric interferences during helium and neon analysis (Fujioka, 2006).

3) Mass Spectrometer gas analysis

Each of the noble gases was ionized with a Nier-type electron bombardment source and the gases were measured using two types of ion collectors: a Faraday collector (amplifier feedback resistors of 10^{10}, 10^{11}, and 10^{12} Ω) with a mass resolution of 230; and a Daly multiplier collector (amplifier feedback resistors of 10^7, 10^8, and 10^9 Ω) with a mass resolution of 600. The mass spectrometer operating conditions used throughout the analysis were 4500V for acceleration voltage, 75V for electron ionization potential, 200μA for Ne and He trap current. The Faraday collector was used to measure ^{4}He while the Daly detector was used to measure ^{3}He and the isotopes of neon.

3.4.5 Vacuum crushing analysis

Vacuum crushing analysis provides information in relation to the mantle He components, hence when the amount of mantle ^{3}He is determined it can be subtracted from the total ^{3}He measured by the Daly detector. For this procedure, approximately 100 mg of each sample were crushed under vacuum to extract gases trapped in fluid inclusions. The air-actuated vacuum crusher has three sample holders. The olivine samples were loaded into the holders. The blank experiment involves operating the vacuum crusher under the same conditions as for the samples but with an empty holder. Each sample was crushed by pressure as a screw was turned therefore increasing the pressure, and crushing the sample. The procedure for gas purification is the same as for the noble gas analysis purification described above.

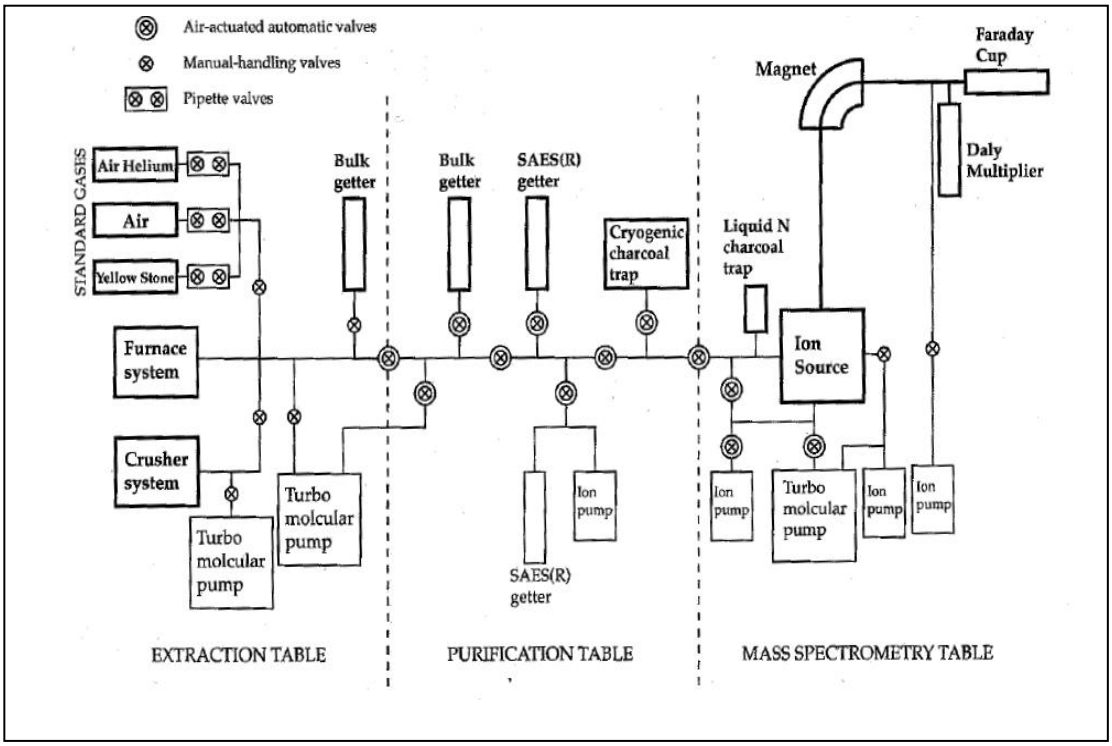

Figure 3.5: VG5400 noble gas ultra-high vacuum system at RSES, ANU. (Fujioka, 2006)

3.4.6 Sensitivity and mass discrimination

Sensitivity and mass discrimination correction were conducted every time the vacuum was vented to the air to change the sample at the end of each sample analysis. The calibration was performed by analysing samples of known volume and isotopic composition. The standard used is HESJ (Helium standard of Japan; Matsuda et al. (2002), which is used to standardize helium, whereas air was used to standardize the heavy noble gases. The mass discrimination factor is defined as the isotopic ratio of the standard divided by the measured isotopic ratio of the standard (Gillen, 2001).

3.4.7 Interference correction

Corrections have to be made in relation to some ions that contain the same *m/e* as neon isotopes, ^{20}Ne, ^{21}Ne and ^{22}Ne. The interfering ions include $^{40}Ar^{++}$, $H_2{}^{18}O^{+}$, and HF^{+} on *m/e* =20, CH_2CO^{++}, $C_3H_6{}^{++}$ and $H_3{}^{18}O^{+}$, on *m/e* = 21 and $CO_2{}^{++}$ and $C_3H_8{}^{++}$ on *m/e* = 22. In these $H_2{}^{18}O^{+}$ and HF^{+} on *m/e* = 20, $C_3H_6{}^{++}$ and $H_3{}^{18}O^{+}$, on *m/e* = 21 and $CO_2{}^{++}$ and C_3H^{8++} on *m/e* = 22 are resolved by carefully adjusting the peak centring position (Fujioka, 2006).

Corrections, by adjusting the peaks are essential to correct interferences generated by other ions that require higher resolution detection for separation.

3.4.8 Blanks

Sample blanks were measured before each olivine sample analysis. The sample blanks were treated and analysed using the same procedure used to analyse the olivine samples. The furnace and crucibles were outgassed at 1850°C, for at least 30 min prior to blank measurement. The three extraction steps heating (900°C, 1400°C and 1750°C) were also used for the blanks. The values detected from the blanks were similar to, or, lower than the atmospheric value ($^{3}He/^{4}He$ = 1.4E-06) in the case of helium and neon, hence assumed to be atmospheric. In addition two blanks were measured, namely a hot blank (described above) which is used for noble gas analysis during fusion and a cold blank which is used for the vacuum crushing experiment.

3.5 Ar-Ar dating

3.5.1 Sample preparation

Sample preparation for Ar-Ar dating was carried out at the School of Earth and Environmental Sciences at the University of Wollongong. The sample preparation involved crushing polycrystalline basalt to 0.5 – 1.0 mm chips, with hand picking to remove altered fragments and phenocrysts. Then the samples were washed with 5% nitric acid for 5 min, to remove any carbonates. Five samples were prepared for Ar/Ar dating: LL1, LL2, LL4, LL5 and PY-9. Samples of ~500 mg were sent to Melbourne to be analysed at the School of Earth Sciences at the University of Melbourne. These samples were chosen as they are considered the oldest ones based on field observations and the analysis becomes analytically complicated for younger samples. Furthermore, some of the older samples cannot be dated by cosmogenic He and Ne as the original lava surfaces are no longer intact.

3.5.2 Ar-Ar analysis

The Ar-Ar analysis involves converting all the ^{39}K to ^{39}Ar. This process was carried out in a nuclear reactor by irradiating the sample with fast neutrons.
The cleaned whole-rock aliquots were wrapped in aluminium foil packets and placed in a quartz glass vial, together with interspersed aliquots of the irradiation standard GA1550.
Samples were irradiated for 6 MWh in position 5c of the McMaster University reactor, Hamilton, Ontario (UM#39). After irradiation and cooling, the samples were loaded into tin foil packets and baked at ~120°C for 24 hours. Step-heating analyses were undertaken using a tantalum resistance furnace and gas purification was by means of two SAES NP10 getters, operated at 400°C and 20°C, respectively. Argon isotopic analyses were carried out on a VG3600 mass spectrometer, equipped with a Daly detector.

J-values were calculated relative to an age of 98.8 ± 0.5 Ma for GA1550 biotite (Renné et al., 1998) . Mass discrimination was monitored by analyses of standard air volumes from a Dorflinger pipette system. Typical line blanks were $<5 \times 10^{-16}$ moles for ^{40}Ar and $<5 \times 10^{-18}$ moles for ^{39}Ar, ^{38}Ar ^{37}Ar and ^{36}Ar. Extended line blanks (10 – 20 minutes) demonstrated atmospheric $^{40}Ar/^{36}Ar$ compositions. Correction factors for interfering reactions are as follows: $(^{39}Ar/^{37}Ar)_{Ca}$ = 0.000679 ± 0.000005; $(^{36}Ar/^{37}Ar)_{Ca}$ = 0.000270 ± 0.000005; $(^{40}Ar/^{39}Ar)_{K}$ = 0.0259 ± 0.0006; $(^{38}Ar/^{39}Ar)_{K}$ = 0.013 ± 0.001.

Reported argon isotopic data have been corrected for mass spectrometer backgrounds, mass discrimination, radioactive decay of ^{39}Ar and ^{37}Ar and reactor interferences. $^{40}Ar/^{39}Ar$ ages are additionally corrected for atmospheric contamination and fluence gradients. Unless otherwise stated, errors are two sigma (2σ) uncertainties and exclude uncertainties in the J-value estimates. The errors in the J-values exclude the uncertainty in the age of the GA1550 standard, the decay constant and potassium isotopic ratio uncertainties. Decay constants are those recommended in Steiger and Jäger (1977).

Chapter 4

Results

4.1 Petrography

The basalts analysed from the two volcanic fields are mainly composed of olivine, plagioclase and pyroxene phenocrysts in a crystal-rich groundmass. However the trachyte sample from PVF, contain abundance of K-feldspar phenocrysts.

LL1(Cerro Coral)

This basaltic rock has a hypocrystalline groundmass mainly composed of plagioclase and glass with some pyroxene (Fig 4.1). It has a porphyritic texture. The phenocrysts are predominantly plagioclase with some olivine and pyroxene. This sample has some veins of secondary minerals that traverse the groundmass and some of the phenocrysts. Some of the plagioclase phenocrysts show parallel or oscillatory zoning and twinning. In addition, some of the phenocrysts in the rock are arranged in clusters. Not many vesicles were observed in this rock.

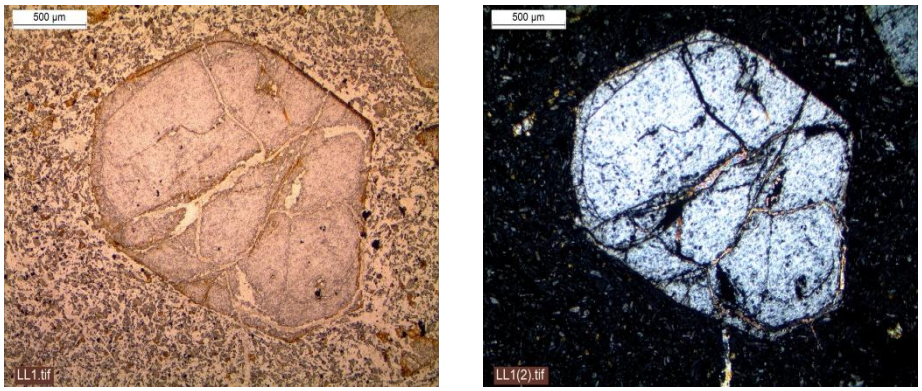

Figure 4.1: Olivine phenocrysts sample LL1. Plain polarized light image LL1 and in LL1 (2) under cross polarized light. In the two images a secondary mineral intergrowth may be pyroxene

LL2 (Cerro Trapal)

This sample is a porphyritic olivine basalt (Fig 4.2). The groundmass is mainly composed of equigranular plagioclase crystals, with a few olivine phenocrysts, and some glass, hence its crystallinity is hypocrystalline. The phenocrysts are mainly plagioclase sub-parallel to randomly oriented and almost all similar in size. There are some olivine and pyroxene phenocrysts. Some of the olivine phenocrysts display alteration and an euhedral shape.

The rock has an interstitial texture, because glass or hypocrystalline material wholly or partly occupies the wedge-shaped interstices between plagioclase laths.

Figure 4.2: Alkali Basalt sample LL2. Plain polarized light imageLL2, euhedral olivine phenocrysts surrounded by crystal-rich groundmass, largely composed of plagioclase. LL2 (2); cross polarized light, olivine phenocrysts, and olivine micro-crystals form the groundmass.

LL3 (basaltic flow side of road 186 top)

This sample is an inter-granular olivine basalt (Fig 4.3). The rock is hypocrystalline with approximately 75% crystals and 25% glass. The majority of the crystals in the groundmass are plagioclase. The phenocrysts are mainly plagioclase some of which are intergrown with olivine and plagioclase. There are also some pyroxene and olivine phenocrysts. The plagioclase phenocrysts show parallel and oscillatory zoning and twinning. The interstitial texture is intergranular, and the material that occupies the spaces between the plagioclase laths is mainly pyroxene or olivine. The rock is also vesicular and there are some carbonate minerals on the walls of the vesicles.

Figure 4.3: Inter-granular olivine basalt sample LL3. Plain polarized light image LL3, long plagioclase phenocrysts with intergrowth olivine crystals. Note the euhedral shape of the olivine crystals. LL3 (2) cross polarized light. Note the parallel twinning of the plagioclase phenocrysts

LL4 (basaltic flow side of road 186 bottom)

This sample is an inter-granular olivine basalt (Fig 4.4), and it constitutes the lower part of the same outcrop as sample LL3. This rock is hypocrystalline, the majority of the crystals within the groundmass are randomly oriented plagioclase and some of them intergrown with parallel twinning. The groundmass is 75% crystals and only a small portion of glass. The phenocrysts are mainly plagioclase with some olivine and pyroxene. The texture of the rock is inter-granular which means that the spaces between plagioclase laths are occupied by one or more grains of pyroxene (± olivine and opaque minerals). The rock shows some vesicles containing carbonate minerals. In comparison with LL3 (top part of the flow), LL4 has a lower olivine content.

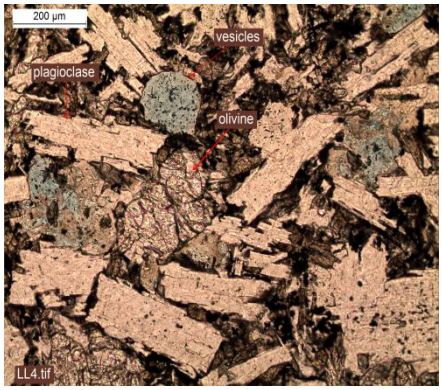

Figure 4.4: Inter-granular olivine basalt sample LL4. Plain polarized light image, olivine phenocryst with conchoidal fracture of olivine, and euhedral shape.

LL5 (scoria cone, Cerro Divisadero)

The rock is hypocrystalline; and the majority of the groundmass is composed of plagioclase and some pyroxene (Fig 4.5). It has a trachytic texture, which is defined by the sub-parallel orientation of the plagioclase phenocrysts. The phenocrysts are mainly plagioclase, however, there are some euhedral olivine phenocrysts. The rock contains some vesicles.

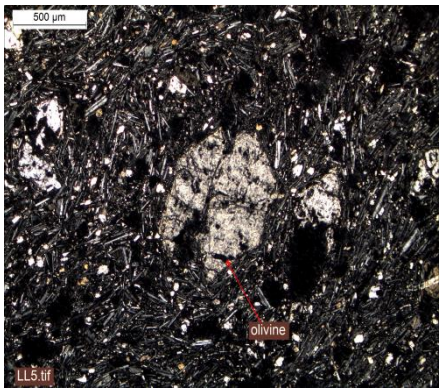

Figure 4.5: Hypocrystallyne scoria sample LL5. Euhedral olivine phenocrysts surrounded by trachytic textured groundmass composed mainly of plagioclase.

PY-1 (Scoria, East side of Morado Volcano)

This sample is a highly vesicular scoria. The groundmass is mainly composed of glass, and therefore its crystallinity is holohyaline. The phenocrysts are mainly plagioclase, but there is another mineral which may be olivine or another ferro-magnesian mineral.

PY-3 (Pampas Negras scoria)

This scoria sample shows high porosity and vesicles occupy the majority of the rock therefore it has a low density (Fig 4.6). The groundmass is holohyaline as the rock is mainly composed of glass. The phenocrysts are mainly plagioclase and some of them show oscillatory zoning and parallel twinning. Other phenocrysts are olivine with euhedral shape, and there are also pyroxene phenocrysts. In this sample there are a few K-feldspars (supported by its higher K_2O and Na_2O contents). There are some ferro-magnesian minerals such as olivine, pyroxene and hornblende.

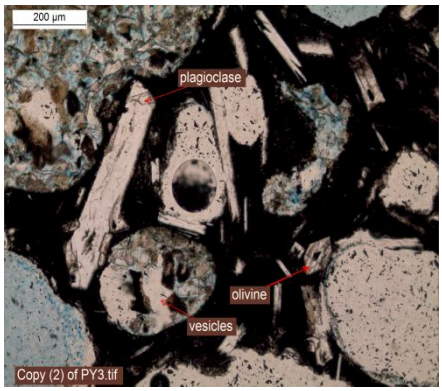

Figure 4.6: Pampas Negras scoria sample PY-3. Scoria plane polarized light. Note: the large vesicles and the glassy groundmass.

PY-4 (basaltic bombs close to Pampas Negras)

The groundmass is composed partly by plagioclase crystals and by glass, and is therefore hypocrystaline (Fig 4.7). The rock is highly vesicular with abundant olivine phenocrysts. The texture is trachytic as the plagioclase crystals in the groundmass show a sub-parallel arrangement, but this rock has a hyalopilitic texture as the material between the crystals is glassy.

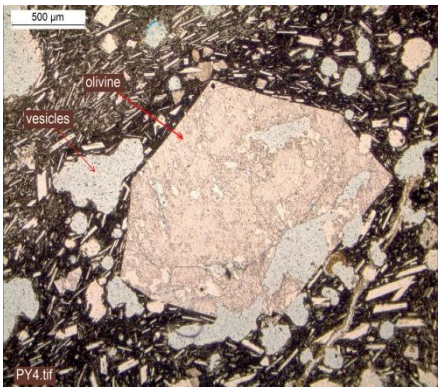

Figure 4.7: Basaltic Bomb sample PY-4 . Plain polarized light image. The olivine phenocryst is surrounded by vesicles and by a hypocrystalline trachytic groundmass.

PY-5 (trachyte flow)

The groundmass is holocrystalline and the majority of the crystals within the groundmass are K-feldspars (Fig 4.8). There are some plagioclase and K-feldspar phenocrysts, and there are other less abundant opaque minerals. The texture of the rock is trachytic, as the crystals are in sub-parallel alignment and the interstices between plagioclase grains are occupied by glass or cryptocrystalline material. The rock shows low porosity and only a little glass. Sample PY-5 shows abundant K-feldspar phenocrysts, which is also related to its high concentration of total alkalis.

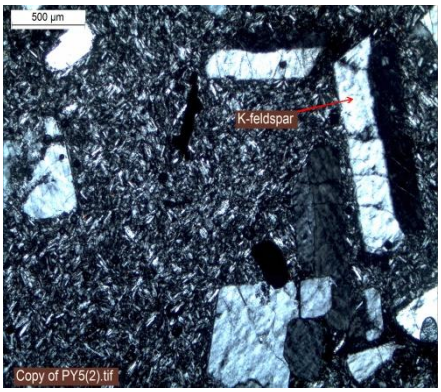

Figure 4.8: Cross polarized light sample PY-5. The K-feldspars are distinguished by simple twinning. Note opaque minerals and trachytic texture in the groundmass.

PY-6 (basaltic flow adjacent to trachyte flow)

The rock is a holocrystalline porphyritic basalt (Fig 4.9). The groundmass consists mainly of plagioclase micro-crystals. A few of the phenocrysts are K-feldspars, such as sanidine. However there is some plagioclase present such as labradorite or bytownite and some pyroxene phenocrysts. The rock shows a trachytic texture with a sub-parallel arrangement of tabular, bladed or prismatic crystals which is visible to the naked eye. This rock is porous as it has high amount of vesicles. There are also some euhedral olivine phenocrysts.

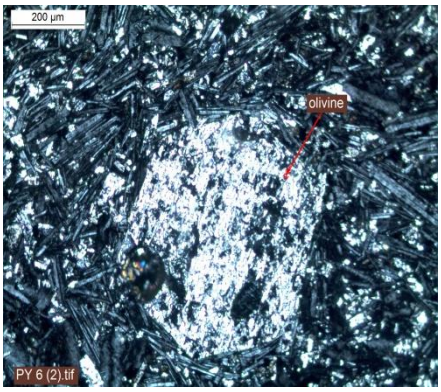

Figure 4.9: Holocrystalline porphyritic basalt sample PY-6. Cross polarized light image.

PY-7 (basaltic bombs from Santa Maria Volcano)

The groundmass of this alkali olivine basalt is hypocrystalline (Fig 4.10). It is composed of glass and crystals, and the majority of the crystals are plagioclase and olivine. The phenocrysts are mainly plagioclase and olivine. The olivine phenocrysts are euhedral and subhedral. The unusual shape of the olivine may be the result of remelting of a silica-rich groundmass, which is reacting with a silica under saturated olivine, therefore producing its current rounded shape.

There are also some clinopyroxene phenocrysts, which are possibly augite. Some of the plagioclase phenocrysts show oscillatory zoning and twinning. The rock has a high porosity, and the concentration of vesicles increases towards the outer part of the basaltic bomb.

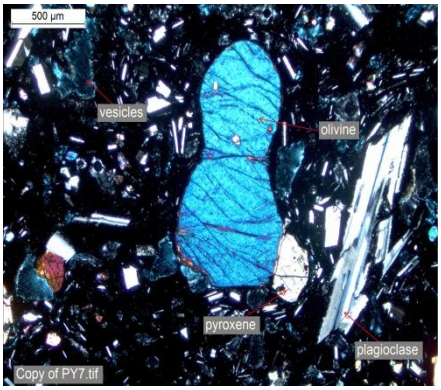

Figure 4.10: Alkali olivine basalt sample PY-7. Cross polarized light image. The olivine phenocryst has a conchoidal fracture and a subhedral shape.

PY-8 (lava flow from the N side of Santa Maria Volcano)

The rock is a hypocrystalline alkaline basalt (Fig 4.11). The groundmass is mainly composed of glass and plagioclase crystals, with some olivine microcrystals. The phenocrysts are mainly plagioclase with parallel twinning; however, some of them show oscillatory zoning. There are also some pyroxene phenocrysts. The sample has vesicles of various sizes; some of them are very large while others are much smaller. The olivine and pyroxene (augite) phenocrysts are euhedral. There are some clustered arrangements of minerals especially of olivine and plagioclase. In addition some of the olivine has secondary mineralization on the margins of some phenocrysts, which is probably iddingsite.

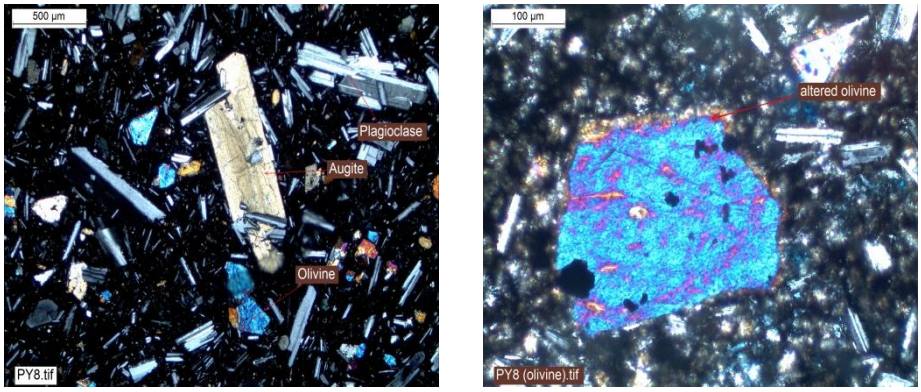

Figure 4.11: PY-8; Hypocrystalline alkaline basalt sample PY-8. cross polarized light image. The image to the left shows a large pyroxene phenocryst with some inclusions. The image to the right shows an euhedral olivine with secondary mineralization.

PY-9 (side of the track near Santa Maria)

The groundmass is crystal rich, but it has some glass, therefore it is holocrystalline (Fig 4.12). The crystals in the groundmass are mainly plagioclase with some olivine and pyroxene. The phenocrysts are plagioclase with parallel twinning. However some of them show oscillatory zoning. There are also very few K-feldspars. The rock is highly vesicular, with some carbonate minerals within the vesicles.

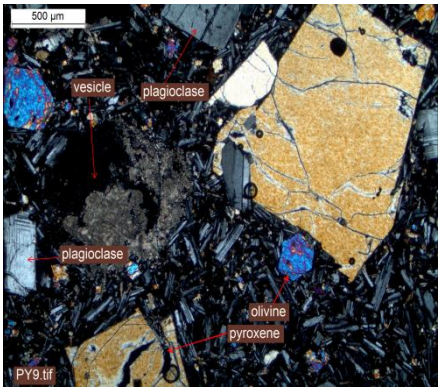

Figure 4.12: Olivine basalt sample PY-9. Cross polarized light image, with two euhedral olivine phenocrysts. Note the cleavage in the pyroxene phenocrysts

4.2 Geochemistry

4.2.1 Major Elements

Major element data for whole-rock samples show a clear differentiation between the basaltic flows and the intermediate flow. In the total alkalis vs silica diagram, several types of igneous rocks (nephelinite, basanite-picrite, basalt, hawaiite and trachyte), can be defined (Fig 4.13). Also by plotting total alkalis ($Na_2O + K_2O$), vs SiO_2, all the basalts were described as alkaline, however, samples LL2 and LL3 fall on the line separating alkaline from sub-alkaline basalts, while the trachyte sample falls on the alkaline classification but close to the boundary with the subalkaline series (Fig 4.14). The total alkali content is higher in the rocks from Payunia Volcanic Field than in the rocks from Llancanelo Volcanic Field.

The silica content varies from 43.8% in a basalt flow from Llancanelo Volcanic Field (LLVF) to 66.9% for the trachyte sample from Payunia Volcanic Field (PVF). However, calculating the mean silica content on the basaltic rocks from the two volcanic fields, it was found that PVF has about 2% higher SiO_2.

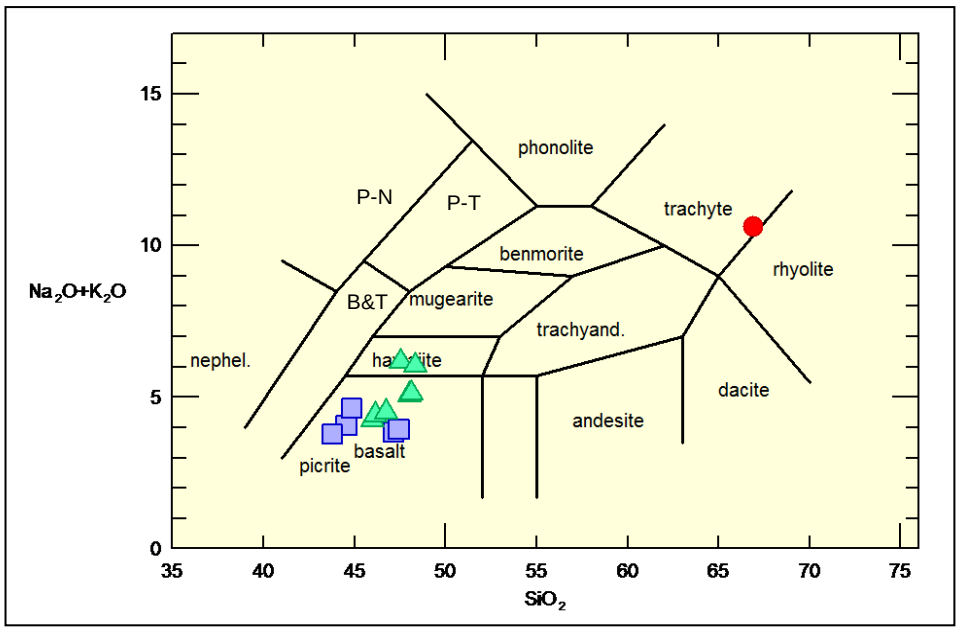

Figure 4.13: Alkali vs silica diagram of (Cox et al., 1979)(squares: basalts Llancanelo, triangles: basalts Payunia, circle: trachyte Payunia). Field P-N, refers to phonolitic nephelinite, P-T refers to phonolitic tephrite, and B&T refers to basanite and tephrite

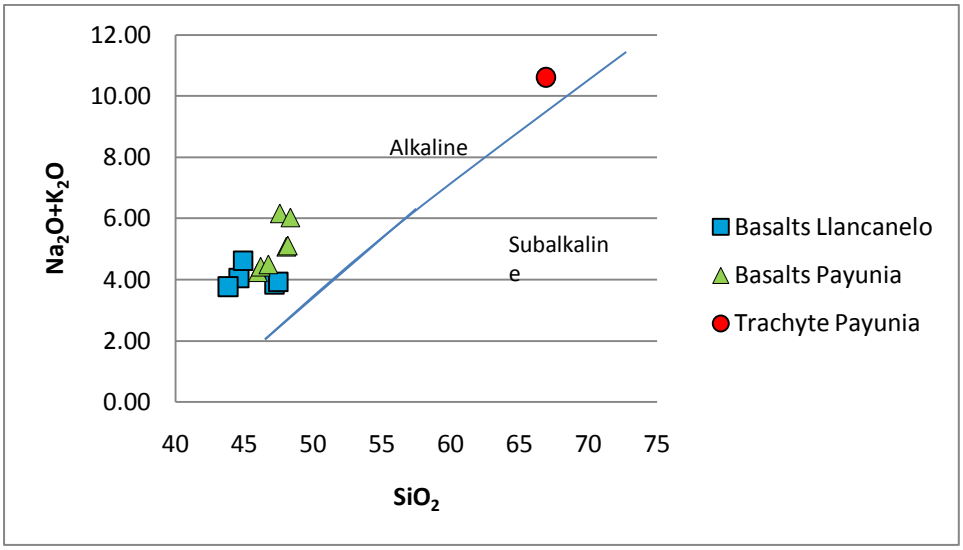

Figure 4.14: Total alkali vs silica diagram

Total alkalis range from 4.0% for LLVF to 5.1% for PVF, excluding the trachyte sample PY-5, which contains 10.6% alkalis. Furthermore the scoria samples PY-1 and PY-3 show the highest concentration in total alkalis among the basalts. The K_2O vs SiO_2 graph (Fig 4.15a) shows that the trachyte flow is within the shoshonitic series while the samples from PVF show a higher content of K_2O as these basalts are mainly located within the high-K calc-alkaline series. Samples PY-1 and PY-3 (scoria samples) fall within the shoshonitic series but close to the limit with high-K calc-alkaline series.

All the samples from LLVF show lower concentration of K_2O and fall close to the calc-alkaline series. The trend observed for K_2O vs SiO_2 is also similar to the one observed from Na_2O (Fig 4.15b) as the concentration of SiO_2 increases the concentration of total alkalis (K_2O and Na_2O) also increases. The ΣFeO vs SiO_2 graph (Fig 4.15c) indicates that the mean concentration of the ΣFeO is nearly constant within the basalts in the two volcanic fields. However, PVF samples show a slightly higher concentration. The trachyte sample has a low ΣFeO concentration of 2.99% as is expected from intermediate igneous rocks.

The Al_2O_3 vs. SiO_2 (Fig 4.15, f) plot indicates that the average concentration of Al_2O_3 is higher for the basalts of PVF than for LLVF, but also it indicates that the basalts from LLVF show a higher variability in Al_2O_3 ranging from 14.57% to 17.27%. The variability of the basalts from LLVF is also evident from MnO (Table 4.1) and from the P_2O_5 vs. SiO_2 plot (Fig 4.15e). The mean MnO concentration between PVF and LLVF are almost the same, however the MnO concentration within the LLVF show a greater variability ranging from 0.14% to 0.18% while for PVF the MnO values show small variations. In relation to P_2O_5, LLVF shows a higher variability ranging from 0.33% to 0.71%. The PVF presents higher average P_2O_5 concentrations than LLVF with relatively small variations. The trachyte sample shows a marked decrease in the concentration of MnO and P_2O_5 which is also related to an increase in SiO_2

When plotting Al_2O_3 vs. MgO (Fig 4.16, a) a negative correlation can be observed in basaltic rocks from both volcanic fields. The concentration of Al_2O_3 decreases with increasing MgO content. On the contrary, MnO plotted against MgO (Fig 4.16b) displays a positive correlation for the rocks from the LLVF. However, the rocks from the PVF range from 0.15% to 0.16%, except the trachyte flow (0.12%) at a MgO interval 5% to 8%. In addition for a plot of CaO, K_2O and Ti_2O vs MgO a constant trend is observed as the MgO content increases especially in LLVF rocks. While the basalt samples from PVF can be grouped with higher concentration of K_2O and Ti_2O above the LLVF. Nevertheless, the CaO values from PVF show a constant trend in the same range as the rocks from LLFV with increasing MgO content.

Sample	LL1	LL2	LL3	LL4	LL5	PY-1	PY-3	PY-4	PY-5	PY-6	PY-7	PY-8	PY-9
SiO_2	44.59	47.17	47.45	44.88	43.8	47.56	48.33	45.97	66.93	46.17	48.03	48.14	46.73
TiO_2	1.44	1.47	1.65	1.55	1.35	2.28	2.19	1.98	0.40	2.15	1.81	1.77	2.06
Al_2O_3	15.86	16.81	17.27	16.29	14.57	18.24	18.08	16.07	15.17	17	16.93	16.84	17.88
ΣFeO	10.25	11.14	10.89	10.13	10.39	11.07	10.59	11.17	2.995	11.21	10.42	10.42	10.2
MnO	0.18	0.17	0.15	0.14	0.16	0.16	0.16	0.16	0.12	0.16	0.15	0.16	0.15
MgO	8.29	7.20	5.73	5.70	10.73	4.61	4.43	8.13	0.21	6.57	6.17	6.17	4.62
CaO	11.44	10.43	10.20	10.56	10.07	8.17	7.64	10.16	0.74	10.87	8.97	8.97	9.85
Na_2O	3.48	3.06	3.25	3.93	2.86	4.41	4.24	3.06	5.20	3.23	3.58	3.65	3.31
K_2O	0.58	0.78	0.68	0.69	0.91	1.75	1.79	1.18	5.42	1.18	1.49	1.46	1.18
P_2O_5	0.71	0.36	0.36	0.34	0.33	0.74	0.69	0.42	0.08	0.43	0.52	0.47	0.60
LOI	2.19	-0.15	0.47	1.96	0.39	-0.19	0.12	-0.22	-0.06	-0.37	-0.14	-0.38	1.24
Total	99.05	98.46	98.13	98.35	96.40	98.95	98.31	98.17	97.23	98.76	97.96	97.68	97.84
Mg#(%)	59	54	48	48	65	43	43	56	11	51	51	51	45

Table 4.1: Major element composition. Major element analysis determined using X-ray fluorescence, and loss on ignition (LOI) determined at the School of Earth and Environmental Sciences, University of Wollongong.

LL1: Basalt sample from Cerro Coral
LL2: Basalt sample from Cerro Trapal
LL3:Upper part of Basalt from side of road 186
LL4: Lower part of Basalt from side of road 186
LL5:Basalt sample from Cerro Divisadero
PY-1: Scoria sample from Pampas Negras, east side of Morado Volcano
PY-3: Scoria sample from Pampas Negras
PY-4: Basaltic bomb from Pampas Negras
PY-5: Trachyte flow from western side of Payún Matrú
PY-6: Basalt flow sample adjacent to PY-5 from western side of Payún Matrú
PY-7: Basaltic bomb from Santa Maria volcano
PY-8: Basaltic flow from Santa Maria volcano
PY-9: Basaltic flow side of the road, south of Santa Maria Volcano.

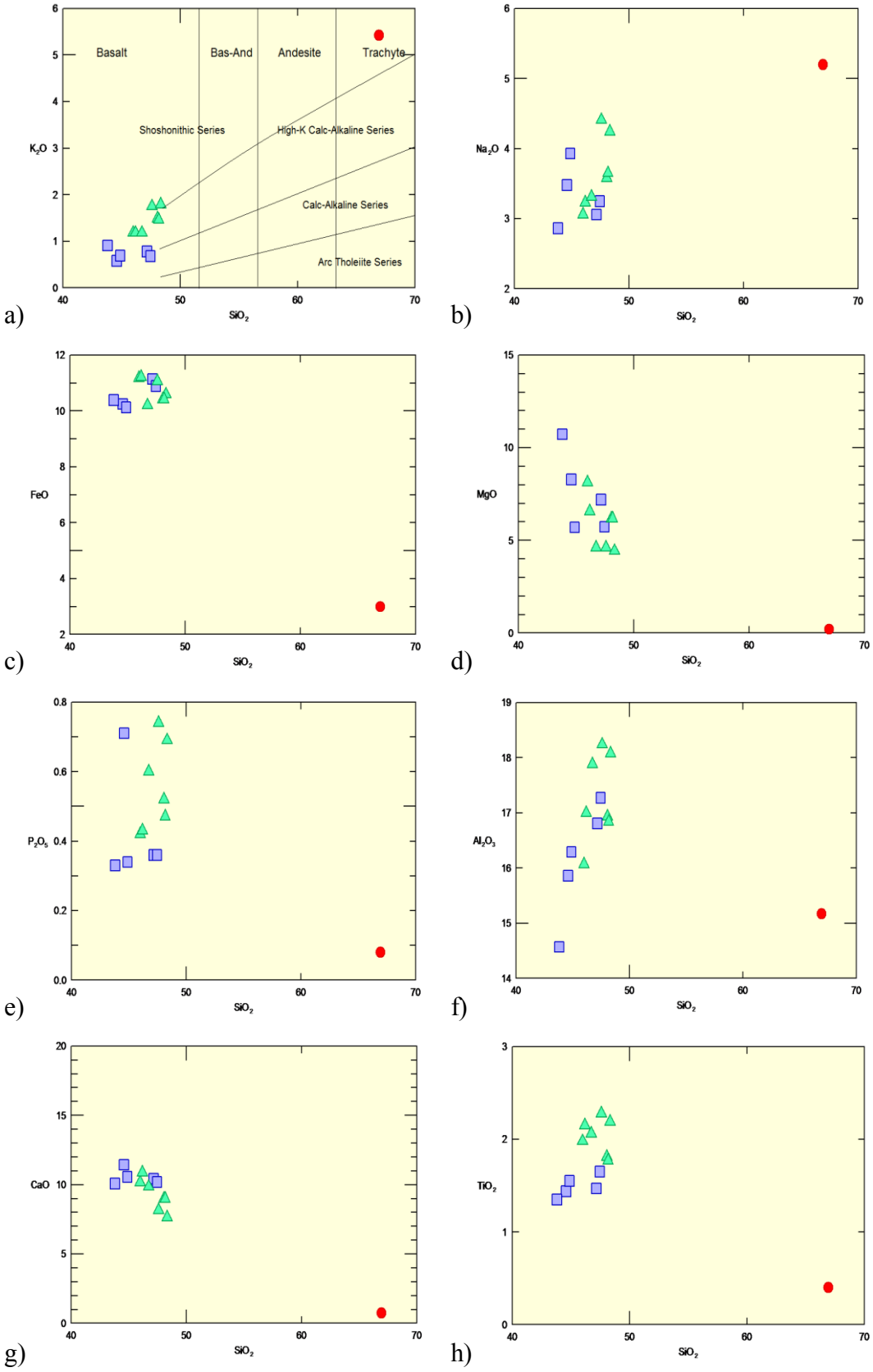

Figure 4.15: Diagrams of SiO_2 plotted against K_2O (a), Na_2O (b),ΣFeO(c), MgO(d), P_2O_5(e), Al_2O_3 (f), CaO(g), TiO_2(h) for rocks of LLVF and PVF. (Symbols as on Fig 4.13).

The Mg number (Mg# = molar Mg/(molar Mg + molar Fe)) was calculated for all of the samples and shows that the rocks from LLVF range between 48 (LL4) to 65 (LL5) while the rocks from PVF (except PY-5) oscillates between 43 and 56, indicating that none of the rocks has a primary mantle influence. Sample LL5 presents the highest Mg# and also it has the highest concentration of Ni (205 ppm) and Cr (505 ppm) which may indicate that this sample could have some influence from the primitive mantle. A plot of Ni against MgO shows a positive correlation. (Fig 4.17)

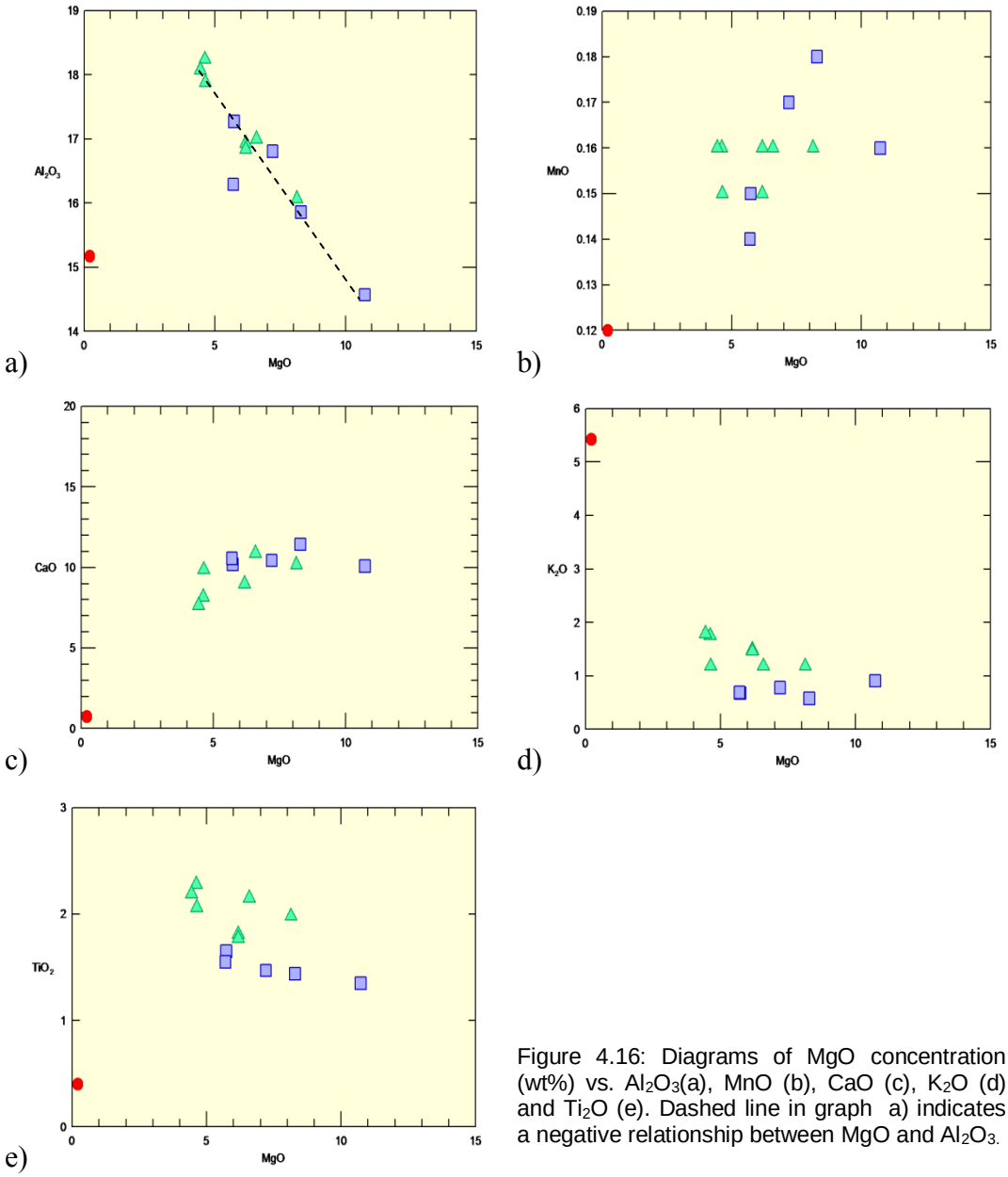

Figure 4.16: Diagrams of MgO concentration (wt%) vs. Al_2O_3(a), MnO (b), CaO (c), K_2O (d) and Ti_2O (e). Dashed line in graph a) indicates a negative relationship between MgO and Al_2O_3.

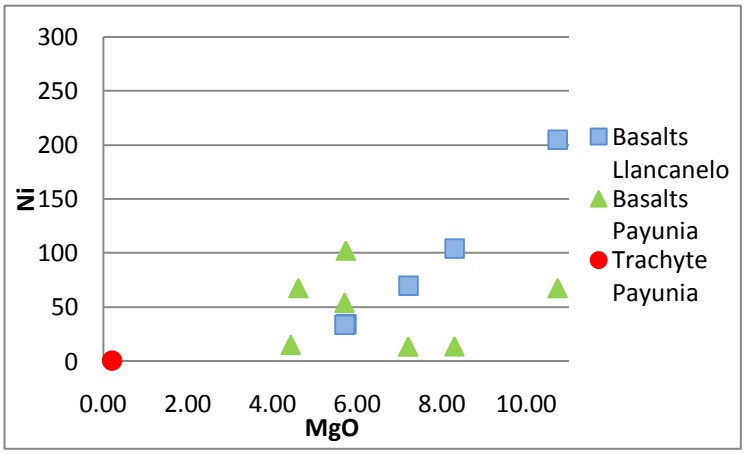

Figure 4.17: Ni vs MgO

4.2.2 Trace Elements

The results from trace-element analysis (Table 4.2) show that the basalts from LLVF contain higher concentrations of La than the rocks from PVF. However the trachyte flow from PVF has a very high content of La (~10x higher than the ones from PVF). Ba shows slightly higher concentrations in the rocks from LLVF while the trachyte flow shows a depletion of Ba (Fig 4.18 and 4.19). Ta concentrations are markedly higher in the trachyte than in the basalts, and LLVF samples have higher concentrations than the basalts from PVF.

High field strength elements (HFSE) such as Zr, Ta, Nb, Th, and U are enriched in total content in the trachyte sample. However, when comparing the basaltic rocks from the two volcanic fields; the rocks from the PVF show higher HFSE concentrations than the basalts from the LLVF. The large-ion lithophile elements (LILE) such as K, Rb, Cs, Sr, and Ba do not show great variability between basaltic rocks from the two volcanic fields. Only the trachyte sample it is enriched in K and in Rb.

The PVF basaltic samples are characterized by slightly higher concentration of incompatible elements such as Sn, Rb, Sr than the basalts from LLVF. Nevertheless the trachyte sample from PVF shows enrichment of incompatible elements (Sn, Rb, La, Sm, Nd). Compatible elements, which are the elements that do not partition from the crust into the melt and therefore do not modify the original basalt pattern such as Ti, Tb, Y, Tm, Yb, Ni, Cr and Co, are more concentrated in the rocks from LLVF.

The trachyte flow is highly depleted in compatible elements particularly, Ni, Co and Cr, compared with basaltic rocks from PVF and LLVF.

Furthermore, when analysing elements such as Ba, Nd, Cd, Sn, Sb, Te, La, Sm, Th, Rb, and K, which are indictors of contaminated magma; it is noted that the trachyte flow shows enrichment in almost of these elements therefore suggesting that the magma may be contaminated by crustal material. However, it is possible that the trachyte flow was not contaminated by crustal components as the Ba content does not show enrichment while the Rb concentration is highly enriched.

The basaltic rocks from the two volcanic fields show very similar values of Ba/Sr; 0.48 for LLVF and 0.45 for PVF. The trachyte flow shows a very high value of 3.08.

The trace-element spider diagrams normalized to primitive mantle (McDonough 1992) (Fig 4.18 and 4.19), indicate that the basaltic rocks from LLVF and PVF show relatively similar trace element distributions. The Andean volcanic arc trace elements have also been plotted for comparison (Hickey et. al., 1986). The basalts from PVF present no similarities with the volcanic arc. However the basalts from LLVF tend to be more related with the volcanic arc in elements such as in Nb, Ba, La, Zr and Y.

There are some particular trends, especially in the case of the sample from Cerro Coral (LL1), which indicates enrichment of incompatible elements such as Rb, Ba, Th, Sr, Zr and Ta. Furthermore, the incompatible elements can be sub-divided into low ionic potential elements (Rb, Ba, and Sr), which show higher concentrations in sample LL1 than in the rest of the samples in relation to high ionic potential elements (Nb, Ta, Zr, Ti, and Y) which are characteristic of ocean island basalts. All the basaltic samples from LLVF display negative K anomalies, when compared with PVF, the trachyte sample and the volcanic arc. However, all the basaltic rocks, except sample LL2 tend to show negative La anomalies. Moreover, the basaltic rocks from the two volcanic fields show positive anomalies of Ta and Sr, whereas the trachyte flow displays negative anomalies for both elements and also for Ba.

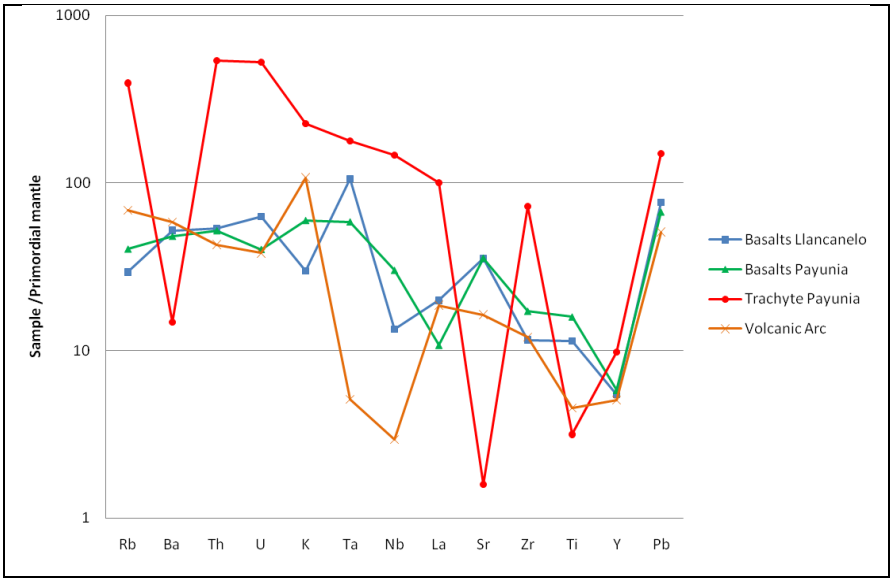

Figure 4.18: Primitive mantle normalized trace element diagram. Simplified by the different areas and the rock types. Note the similarities between the two basaltic areas. Normalizing values from (McDonough W.F. et al., 1991)

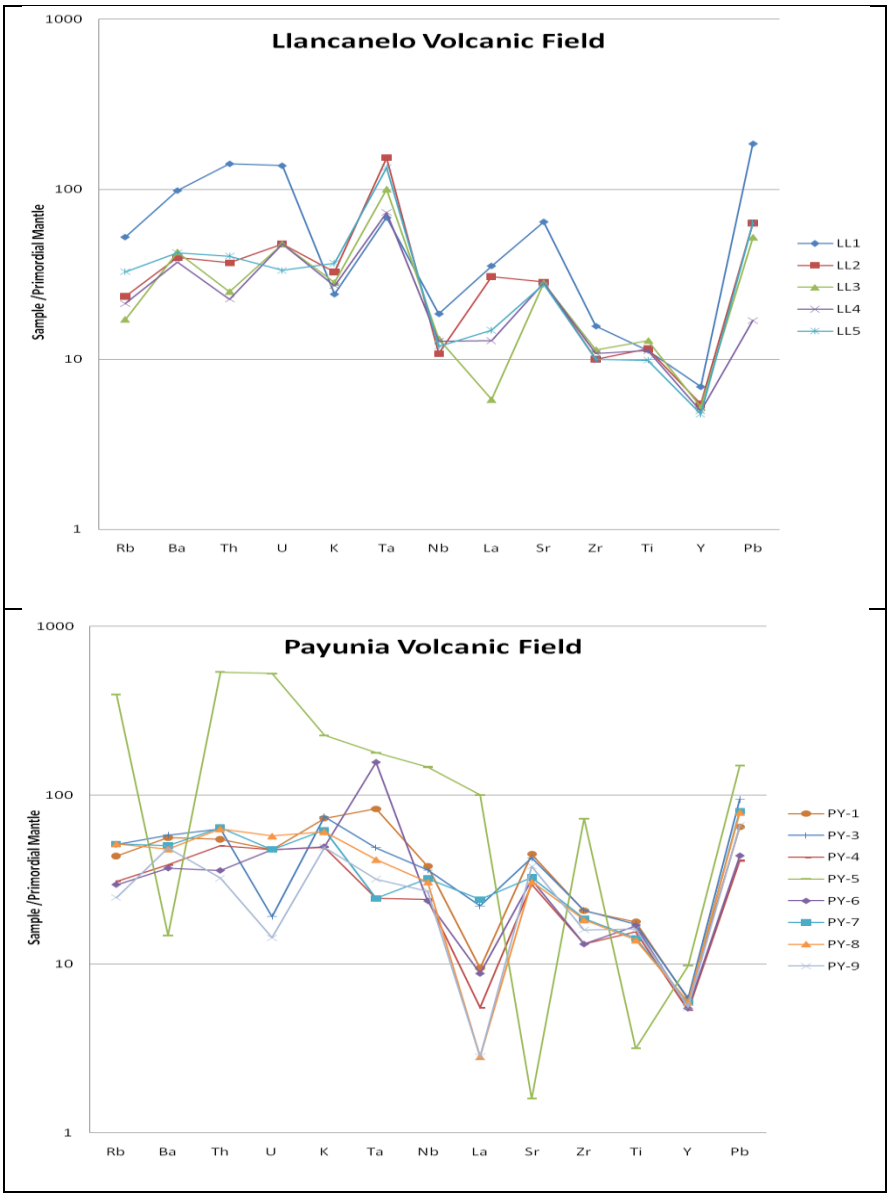

Figure 4.19: Primitive mantle normalized trace element diagram for LLVF and PVF. Normalizing values from (McDonough W.F. et al., 1991)

	LL1	LL2	LL3	LL4	LL5
location	Cerro Coral	Cerro Trapal	Upper part of flow side of road 186	Lower part of flow side of road 186	Cerro Divisadero
Rock type	Basalt	Basalt	Basalt	Basalt	Basalt
S	71	43.9	48.1	6836	2192
Cl	272.2	203.5	2	42.7	269.2
V	292.9	245.3	197.7	185.9	249.6
Cr	215.2	229.2	81.8	112.7	504.9
Co	45.8	15.5	22.8	25.5	56
Ni	104.1	69.7	34	33.4	204.7
Cu	64	63.3	38.6	38.1	60.4
Zn	81.3	79.4	85.8	84.3	71.6
Ga	19.7	19.5	20.9	20.4	16.1
Ge	1	1	1	1	1
As	1	1	1	1	1
Br	0.7	1	1	0.7	0.7
Rb	33.3	14.9	10.9	13.5	20.8
Sr	1360	601.3	594.4	592	581.4
Y	31.3	24.8	23.8	22.6	21.7
Zr	175.3	112.1	127.5	121.5	112
Nb	13.2	7.7	9.4	9.1	8.5
Cd	1	2	2	3	2
Sn	3	3	3	3	3
Sb	2.5	3	3	3	1.5
Te	3	3	3	3	3
Ba	689.8	278.2	298.8	260.7	296.7
La	25.1	21.7	4.1	9.1	10.5
Ta	2.8	6.3	4.1	3	5.5
W	1.7	1.7	1	1	0.8
Hg	0.6	1	0.8	1	0.4
Pb	13.2	4.5	3.7	1.2	4.5
Th	11.9	3.1	2.1	1.9	3.4
U	2.9	1	1	1	0.7
Ba/Ta	246.36	44.16	72.88	86.90	53.95
La/Ta	8.96	3.44	1.00	3.03	1.91
Ba/La	27.48	12.82	72.88	28.65	28.26
La/Nb	1.90	2.82	0.44	1.00	1.24

	PY-1	PY-3	PY-4	PY-5	PY-6	PY-7	PY-8	PY-9
locality	E side of Morado V.	Pampas Negras	Pampas Negras	W side of Payún Matrú	W side of Payún Matrú	Santa Maria	Santa Maria	South of Santa. Maria
Rock type	Scoria	Scoria	Basaltic bomb	Trachyte	Basaltic flow	Basaltic bomb	Basaltic flow	Basaltic flow
S	524.3	71.9	258.2	23.7	290.6	42.3	29	653.7
Cl	146.4	162.1	162.3	2	24.3	200.9	187.7	29.3
V	215.7	223.3	261.6	1	255.3	211.8	213.9	200.9
Cr	0.6	3.2	295.5	1	109.1	157.5	164.7	19.5
Co	11	11	52.5	3	36.8	29.9	25.1	11.6
Ni	13.6	13.4	102.2	0.6	53.9	67.5	67.5	14.9
Cu	28.5	33.2	49.4	2.6	59	45.7	48.1	28.3
Zn	83.1	87.8	87.6	59.1	81.2	90.3	91.5	79.8
Ga	19.6	20.8	20.8	26.3	19.7	21.4	20.7	20.5
Ge	1	1	1	1	1	1	1	1
As	1	1	1	7.6	1	1	1	1
Br	1	0.6	1	0.6	1	0.8	0.6	1
Rb	27.6	32.3	19.6	250.5	18.7	32.5	32.7	15.7
Sr	943.4	896.6	625.9	33.5	665.8	687.4	647.1	799.1
Y	28.1	28.5	24.2	44.4	24.8	26.9	27	25.2
Zr	231	232.3	147.5	810.6	146.5	207.6	204.1	178.1
Nb	27	25.6	17.2	104.5	16.8	22.8	21.8	19.2
Cd	2	2	2	2	2	2	1	2
Sn	3	3	3	6.5	3	3	3	3
Sb	3	3	3	3	3	1.2	2.5	3
Te	3	3	3	3	3	3	3	3
Ba	391.9	405.8	269.8	103.3	257.8	350.6	334.9	340.9
La	6.7	15.6	3.9	70.9	6.2	17	2	2
Ta	3.4	2	1	7.3	6.4	1	1.7	1.3
W	0.8	1	1	7.8	1	0.8	0.8	1.1
Hg	0.7	1	1	1	0.6	0.4	0.9	1
Pb	4.6	6.7	2.9	10.6	3.1	5.7	5.6	4.7
Th	4.6	5.3	4.2	45	3	5.4	5.3	2.7
U	1	0.4	1	11	1	1	1.2	0.3
Ba/Ta	115.26	202.90	269.80	14.15	40.28	350.60	197.00	262.23
La/Ta	1.97	7.80	3.90	9.71	0.97	17.00	1.00	2.00
Ba/La	58.49	26.01	69.18	1.46	41.58	20.62	167.45	170.45
La/Nb	0.25	0.61	0.23	0.68	0.37	0.75	0.09	0.10

Table 4.2: Trace elements composition. All the values are in ppm. LL = samples from Llancanelo Volcanic Field, PY = samples from Payunia Volcanic Field

When comparing ratios of different incompatible elements such as Th/Ta, it was found that the trachyte flow shows a higher value (6.16) than the samples from LLVF (1.30) and from PVF (2.75). The Th/Ta ratio is used in Patagonian basalts as an indicator of subduction-enriched mantle source (Bertotto et. al., 2009); indicating that the trachyte flow may have some influence from the subduction enriched mantle. However, samples LL1 (basalt from Cerro Coral, LLVF), PY-4 (basaltic bomb from Pampas Negras, PVF) and PY-7 (basaltic bomb from the Santa Maria Volcano, PVF) show remarkably high Th/Ta values of 4.25, 4.20 and 5.40 respectively, which may also indicate that these samples have received some influence from a subduction-enriched mantle.

Furthermore, the Ba/Nb ratios of the rocks from LLVF have the highest mean value (36.75), which is twice the value from PVF (15.70). In contrast the trachyte sample shows a very low value as the result of Ba depletion, which corresponds to intermediate and more evolved rocks. This pattern is also observed with the La/Nb ratio, in which the average values from LLVF are higher (1.48) than those from PVF (0.34).

The ratios of Ba/Nb and La/Nb in the rocks from LLVF are similar to the Andean volcanic arc basalts (Bertotto et.al., 2009), especially the ones from LL1. However the ratios between these incompatible elements show similarities with the transitional basalts in rocks from PVF.

An increase in Ba/Ta ratio indicates increasing fluids and crustal components, whereas increasing La/Ta ratios indicate increasing arc-like signatures (Kay, et al., 2005). The basaltic rocks from PVF show an increase in the Ba/Ta (205.4) ratio in relation to LLVF (100.8), and it is also important to note that the two basaltic bomb samples show the highest Ba/Ta ratio. In relation to the La/Ta ratio, the rocks from PVF show higher average values (4.95) than the ones from LLVF (3.67). The trachyte sample displays the highest value (9.71) indicting that it has some arc signatures. Nevertheless, sample PY-7 (basaltic bomb from Santa Maria Volcano) shows the highest La/Ta ratio, suggesting arc-like signatures.

4.2.3 Isotopes

Isotope ratios in a magma are used to characterise the source region from which the magma was extracted (Rollinson, 1993), therefore providing valuable information in relation to the chemical composition of the original mantle. Three samples were analysed for strontium, neodymium and samarium isotopes (Table 4.3).

The results show that the trachyte sample has slightly higher $^{87}Sr/^{86}Sr$ ratios than the basalts. Among the $^{87}Sr/^{86}Sr$ ratio the basalts, is slightly lower in sample PY-6 and is concordant with transitional basalts from the Patagonian plateau described by Stern et.al., 1990 with a value of 0.7039 (Stern et al., 1990) . The $^{147}Nd/^{144}Nd$ ratio is lower in the trachyte sample than in the basalts. The Sr and Nd isotopic compositions of the basalts are similar to the mantle-derived arc magmas (0.7038 and 0.7040), which is also supported by the high Sr/Nd ratio indicating arc signatures.

Sample	**PY-9**	**PY-6**	**PY-5**
	basalt	basalt	trachyte
$^{87}Sr/^{86}Sr$	0.703987	0.703798	0.704207
$^{143}Nd/^{144}Nd$	0.512781	0.51283	0.512769
$^{147}Sm/^{144}Nd$	0.13409305	0.14191634	0.10685038
Sr ppm	687.296864	580.910303	36.803447
Nd ppm	24.459147	21.104053	49.845369
Sm ppm	5.424039	4.953	8.07997
Rb/Nd	0.71016377	0.78705261	4.87507676
Sm/Nd	0.22175912	0.23469426	0.16210072
Sr/Nd	28.0997888	27.5260066	0.73835238
Rb/Sr	0.02527292	0.02859305	6.60264241

Table 4.3: Isotope ratios and REE ratios of the rocks.

The concentrations of Nd and Sm are higher in the trachyte sample than in the basalts, which support the statement above in the trace elements section, that the intermediate sample is enriched in incompatible elements. In addition, when Ba/Nb and $^{87}Sr/^{86}Sr$ ratios are considered the transitional trend of the basalts is further reinforced.

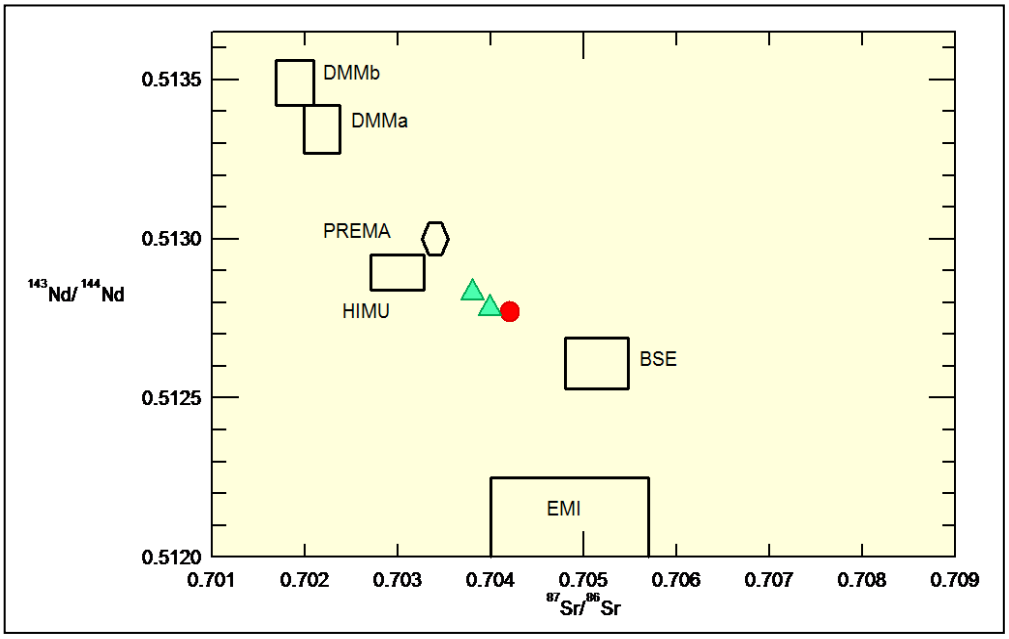

Figure 4.20: Sr – Nd isotopic ratios. Triangles correspond to PVF basalts and the circle corresponds to PVF trachyte. DMM a and b corresponds to depleted MORB mantle, PREMA prevalent mantle, HIMU corresponds to high μ , BSE corresponds to bulk silicate earth, EMI corresponds to enriched mantle I.

4.3 Cosmogenic ^{21}Ne and ^{3}He

Tables 4.4 and 4.5 present concentrations of ^{20}Ne, ^{4}He and also the relative ratios at the different extraction temperatures. Approximately 2 of each of the samples were used for the He and Ne analyses by a noble gas mass spectrometer, during the first pilot study, and ~1 was used for the second batch of analyses.

Detectable amounts of ^{4}He and ^{20}Ne were found in each of the temperature fractions of the step-heating experiments. The amounts of ^{3}He and ^{21}Ne were calculated using the ^{4}He and ^{3}He/^{4}He ratio concentration and the ^{20}Ne and ^{21}Ne/^{20}Ne ratio respectively. Cosmogenic ^{3}He (^{3}He*) and ^{21}Ne (^{21}Ne*) were calculated using the following formulae and using error propagation formulae to calculate the error corresponding to each of the measurements and calculations (See Appendix C for detailed explanation of ^{21}Ne* and ^{3}He* calculation).

$$^{3}He^{*} = {}^{4}He \times \{(^{3}He/^{4}He)_{meas} - (^{3}He/^{4}He)_{trapped}\} \quad \textbf{(1)}$$

$$^{21}Ne^{*} = {}^{20}Ne \times \{(^{21}Ne/^{20}Ne)_{meas} - (^{21}Ne/^{20}Ne)_{air}\} \quad \textbf{(2)}$$

The formula used to calculate cosmogenic ^{3}He (1) utilises the standard value of $^{3}He/^{4}He$ for MORB (mid ocean ridge basalt) which is $1.2x10^{-5}$. The formula to calculate cosmogenic ^{21}Ne (2), subtracts atmospheric Ne from the observed $^{21}Ne/^{20}Ne$ ratio, using the standard air value of 0.00296.

All the samples show detectable amounts of cosmogenic ^{3}He. Furthermore, cosmogenic ^{21}Ne shows a lower abundance than $^{3}He^*$, especially on samples PY-8, and PY-7, which were expected to be the youngest (based on field observation), of the five samples analysed for cosmogenic dating. The $^{21}Ne/^{20}Ne$ ratios from samples PY-8 and PY-7 are close to the air value. This indicates that the sample size analysed was small and that the sample is particularly young as with the amount analysed it was not enough to detect measurable amounts of cosmogenic ^{21}Ne, because atmospheric Ne overwhelms small amounts of cosmogenic Ne. Nevertheless $^{21}Ne^*$ was calculated for all the samples at the various extraction temperatures (Table 4.4). Sample PY-4 has detectable and measurable amounts of both isotopes at the two extraction temperatures (900°C and 1750°C), therefore total $^{3}He^*$ and $^{21}Ne^*$ extracted at both temperatures were used to calculate the ages.

In addition, the $^{22}Ne/^{20}Ne$ ratios of the samples are closely related to the atmospheric value of 0.102 and, as expected, the cosmogenic ^{20}Ne and ^{22}Ne is negligible in comparison to atmospheric Ne.

The cosmogenic ^{3}He ($^{3}He^*$) value of sample LL3 from the two aliquots, seems to be high (Table 4.5) and when the value is used to calculate the age of the lava flow, it provides an older apparent age in comparison with cosmogenic ^{21}Ne ($^{21}Ne^*$). This may be the result of mantle ^{3}He trapped in fluid inclusions from olivine phenocrysts. To detect and quantify mantle ^{3}He, a vacuum crushing experiment is necessary. Once the mantle ^{3}He concentration has been determined then it can be subtracted from the total ^{3}He detected. In relation to ^{21}Ne, the vacuum crushing experiment was not necessary as mantle-derived ^{21}Ne is found in very low concentrations close to the limit of detection. In addition, unavoidable adsorption of atmospheric gases onto the high surface area of the crushed sample during transfer from the vacuum crusher to the vacuum furnace may produce high concentrations of atmospheric Ne, compared to the subsequent fusion experiment (this is not considered when doing vacuum crushing experiment of helium as it is near zero in the atmosphere) (Gillen et al., 2010).

The attempted vacuum crushing experiments were not successful, for sample LL3, PY-9 and PY-4 as the samples were not crushed properly; hence no mantle helium was released. Furthermore, another approach taken to explain the anomalously high concentration of helium, especially in sample LL3 was to assume that the age found from cosmogenic ^{21}Ne was correct and that the age from the two cosmogenic isotopes ^{3}He and ^{21}Ne should be the same. Accordingly, using the age provided from ^{21}Ne*; the expected trapped component was calculated for ^{3}He for the first and the second aliquot (see Appendix D, for detailed explanation of the calculation). Accordingly, it was found that the trapped helium for the first and the second aliquot of sample LL3 was anomalously high. This introduced another question to explain why the ^{3}He/^{4}He ratio is anomalously high especially for sample LL3 in comparison with the samples from the Payunia Volcanic Field.

The calculated ^{3}He trapped from the first aliquot was lower than the trapped ^{3}He calculated from the second aliquot, despite the sample size from the first aliquot being 2.5 times larger than sample size from the second aliquot. These differences can be further interpreted as a function of the grain size. For the first aliquot, the grain size used was ~106 μm whereas for the second aliquot the grain size was >180 μm. This may indicate that mantle helium from the finer grain size was previously released during sample preparation as the sample was crushed.

However, in the case of the coarser grain size, the fluid inclusions have not been broken, as the phenocrysts have not been further crushed hence the gases held inside them were not released until the sample was fused during gas extraction and analysis. This is also true for sample PY-9, as the grain size used during the first aliquot was larger than the one used for the second aliquot analysis. Hence, in the first aliquot the amount of total helium detected is in excess, and it may contain trapped mantle helium.

The results indicate that the olivine separates do not contain mantle-derived Ne, as the measurement of the ^{20}Ne/^{22}Ne ratio is characteristic of the air value of about 9.8. The values obtained range from 7.77 to 9.78 while the value of mantle-derived ^{20}Ne/^{22}Ne is close to 13. If the ^{20}Ne/^{22}Ne ratio is close to 13 in the sample then it would produce an increase in the ^{21}Ne/^{20}Ne ratio which corresponds to the air neon component which has to be subtracted from the total ^{21}Ne* detected.

Sample LL3, shows an excess of non-atmospheric $^{21}Ne/^{20}Ne$ ratio, while sample PY-8, a basaltic flow from Santa Maria volcano, has values similar to the atmospheric values (Fig 4.21). The reason for sample PY-8 having an isotopic composition close to the atmospheric value is that the sample is significantly young and that the sample size analysed was small. Accordingly the $^{22}Ne/^{20}Ne$ and $^{21}Ne/^{20}Ne$ ratios of all the sample seems to have an excess of atmospheric neon.

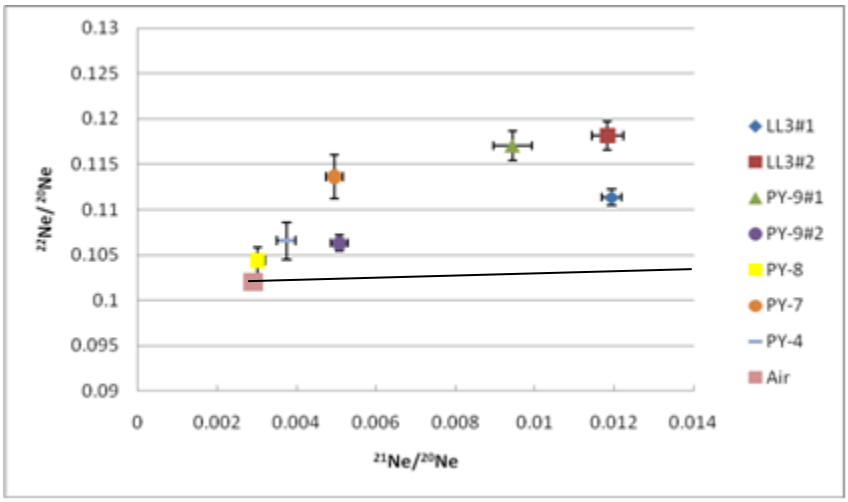

Figure 4.21: Three-isotope plot for neon extracted from olivine separates. Note that the atmospheric value is shown as air and mixing line between cosmogenic and atmospheric neon is from Gillen et al. (2010). #1 and #2 refers to first and second aliquots respectively

Sample	Weight	temp	^{20}Ne	Error	^{21}Ne/^{20}Ne	Error	^{20}Ne/^{22}Ne	Error	^{22}Ne/^{20}Ne	Error	^{21}Ne*	^{21}Ne* error
	aliquot	900°C	4.68E-11	1.22E-12	3.60E-03	7.94E-05	9.74	5.71E-02	1.03E-01	6.02E-04	3.00E-14	3.80E-15
LL3	#1	1400°C	7.26E-12	1.96E-13	2.78E-02	5.90E-04	7.77	8.52E-02	1.29E-01	1.41E-03	1.80E-13	6.48E-15
	3.275g	1750°C	6.35E-12	5.66E-13	4.40E-03	4.18E-04	9.74	2.10E-01	1.03E-01	2.22E-03	9.14E-15	2.78E-15
	aliquot #2	900°C	4.47E-11	3.40E-12	3.26E-03	1.89E-04	9.13	9.43E-02	1.10E-01	1.13E-03	1.30E-14	8.50E-15
LL3	0.953g	1750°C	1.59E-11	7.38E-13	2.04E-02	7.69E-04	7.90	1.82E-01	1.27E-01	2.92E-03	2.80E-13	1.80E-14
	aliquot	900°C	2.29E-10	2.78E-12	3.01E-03	2.94E-05	9.78	5.21E-02	1.02E-01	5.24E-04	1.15E-14	6.73E-15
PY-9	#1	1400°C	1.05E-11	3.21E-13	1.83E-02	4.12E-04	8.08	9.05E-02	1.24E-01	1.39E-03	1.61E-13	6.55E-15
	3.026g	1750°C	2.53E-12	5.20E-13	7.00E-03	1.39E-03	7.99	2.97E-01	1.25E-01	4.65E-03	1.02E-14	4.10E-15
PY-9	aliquot #2	900°C	1.13E-10	4.05E-12	3.05E-03	7.97E-05	9.48	6.14E-02	1.05E-01	6.84E-04	1.02E-14	9.01E-15
	1.091g	1750°C	4.15E-11	3.26E-12	7.10E-03	4.14E-04	9.34	1.42E-01	1.07E-01	1.63E-03	1.72E-13	2.18E-14
PY-8	aliquot #1	1750°C	1.55E-10	9.45E-12	3.02E-03	1.70E-04	9.58	1.39E-01	1.04E-01	1.52E-03	9.95E-15	2.60E-14
	0.264g											
PY-7	aliquot #1	900°C	9.17E-11	3.08E-12	2.81E-03	7.21E-05	9.72	6.69E-02	1.03E-01	7.08E-04	-1.4E-14	-6.6E-15
	1.01g	1750°C	4.15E-11	3.26E-12	7.10E-03	4.14E-04	9.34	1.42E-01	1.07E-01	1.63E-03	4.83E-15	4.91E-15
PY-4	aliquot #1	900°C	1.11E-10	2.14E-12	3.10E-03	4.37E-05	9.62	6.75E-02	1.04E-01	7.30E-04	1.55E-14	4.86E-15
	1.54g	1750°C	1.36E-11	1.75E-12	4.39E-03	4.69E-04	9.16	3.39E-01	1.09E-01	4.05E-03	1.94E-14	6.85E-15

Table 4.4: Elemental and isotopic composition of neon. Concentration obtained at the several step-heating temperatures.

LL3:Upper part of Basalt from side of road 186
PY-9: Basaltic flow side of the road, south of Santa Maria Volcano.
PY-8: Basaltic flow from Santa Maria volcano
PY-7: Basaltic bomb from Santa Maria volcano
PY-4: Basaltic bomb from Pampas Negras

Sample	Weight	temp	^{4}He	error	^{3}He/^{4}He	error	^{3}He*	^{3}He* error
	aliquot #1	900°C	9.88E-09	4.29E-11	1.06E-04	1.17E-06	6.05E-13	1.20E-14
LL3	3.275g	1400°C	4.59E-09	2.32E-11	3.28E-05	2.23E-06	-5.48E-14	-1E-14
LL3	aliquot #2	900°C	2.20E-09	3.18E-11	3.93E-04	9.77E-06	6.15E-13	2.32E-14
	0.953g	1750°C	2.31E-09	3.00E-11	1.49E-04	1.16E-05	8.18E-14	2.68E-14
PY-9	aliquot #1	900°C	1.22E-08	5.46E-11	6.81E-05	1.04E-06	6.84E-13	1.31E-14
	3.03g	1400°C	1.93E-08	8.44E-11	1.88E-05	5.50E-07	1.31E-13	1.06E-14
		1750°C	2.87E-09	1.83E-11	1.78E-05	2.89E-06	1.66E-14	8.29E-15
PY-9	aliquot #2	900°C	1.93E-08	7.40E-11	3.90E-05	1.18E-06	5.21E-13	2.29E-14
	1.09g	1750°C	1.93E-08	8.44E-11	1.88E-05	5.50E-07	-2.32E-14	-1.75E-14
PY-8	aliquot #1	1750°C	2.59E-08	2.30E-10	1.65E-05	2.09E-06	1.16E-13	5.4E-14
	0.264g							
PY-7	aliquot #1	900°C	8.76E-09	4.14E-11	1.41E-05	2.47E-06	1.84E-14	2.16E-14
	1.01g	1750°C	1.51E-08	6.28E-11	1.07E-05	1.89E-06	-2.0E-14	-2.9E-14
PY-4	aliquot #1	900°C	6.66E-09	2.93E-11	1.73E-05	1.45E-06	3.53E-14	9.66E-15
	1.54g	1750°C	3.25E-08	1.20E-10	1.36E-05	5.91E-07	5.20E-14	1.92E-14

Table 4.5: Elemental and isotopic composition of helium. Concentrations obtained at the several step-heating temperatures.

LL3:Upper part of Basalt from side of road 186
PY-9: Basaltic flow side of the road, south of Santa Maria Volcano.
PY-8: Basaltic flow from Santa Maria volcano
PY-7: Basaltic bomb from Santa Maria volcano
PY-4: Basaltic bomb from Pampas Negras

The ages were calculated in relation to the total cosmogenic ^{21}Ne and ^{3}He content, released at several temperatures, applying the following formula with its corresponding production rate at the sampling site.

$$Age = {}^{21}Ne^{*} \text{ or } {}^{3}He^{*}/P \quad \textbf{(3)}$$

In formula (3) P corresponds to the production rate of cosmogenic ^{21}Ne or ^{3}He according to the cosmogenic isotope used. The production rate of cosmogenic ^{21}Ne was calculated for each of the samples individually based on the latitude, elevation and magnesium content. The scaling factor used is the one described by Lal (1991), in which a relationship between the latitude and the elevation is established and according to the latitude and the differences in altitude among the samples, a different scaling factor was determined for each of the samples.
Furthermore, using formula (4), and replacing the different terms; scaling factor ($N(\lambda_{m,}h)$) and production rate at sea level and high latitudes (P_n), the production rate of each of the samples at their particular latitude and elevation can be calculated.

$$P = N(\lambda_{m,}h) \times P_n \quad \textbf{(4)}$$

The production rate for ^{21}Ne and ^{3}He is calculated using the same formula by changing the production rate value according to the cosmogenic isotope used. However, the production rate determined is characteristic of Fo_{81}, which has to be adjusted to the particular Fo (forsterite) content of each of the samples (for explanation on the Fo content calculation see Appendix A). The final production rate for each of the olivine-separate samples, in relation to their particular location and magnesium content, were used to calculate the age of the samples (refer to Appendix B for detailed explanation of production rate calculations).
The magnesium content of the olivine separates was measured twice, to validate the purity and to calculate the Fo content of each sample. After the second olivine purification using methylene iodide and handpicking, the samples were re-analysed using XRF. This analysis indicated that the olivine samples were >90% pure (see Appendix E, major-element analysis of olivine samples).

Sample	Site location	Forsterite cont.	$P^{21}Ne^*$ (atoms/g/a)	P^3He^* (atoms/g/a)	$^{21}Ne^*/^3He^*$	$P^{21}Ne^*/P^3He^*$ (expected)
LL3 (aliquot #1)	Upper part of basaltic flow	74	115.81	290.811	0.398	0.3982
LL3 (aliquot #2)	side of road 186	76	118.94	298.67	0.454	0.398
PY-9 (aliquot #1)	Track south of	73	160.32	402.47	0.220	0.398
PY-9 (aliquot #2)	Santa Maria	74	162.47	407.98	0.330	0.398
PY-8	Santa Maria flow	79	162.32	407.33	0.085	0.3985
PY-4	Pampas Negras	80	229.51	576.32	0.401	0.3982
PY-7	Santa Maria bomb	80	164.26	412.49	0.266	0.3982

Table 4.6: Forsterite content of olivine separates and cosmogenic ^{21}Ne and ^3He production rates.

The ratio between $P^{21}Ne^*/P^3He^*$ (production rate) is mainly the same for all of the samples (Table 4.6), and is also related to the $^{21}Ne^*/^3He^*$ratio described by Fenton et al. (2009) of 0.400 and Gillen et al. (2010) of 0.37 to 0.40 respectively; thereby suggesting that the production rate calculated is correct. In addition, when the $^{21}Ne^*/^3He^*$ ratio for the first aliquot of sample PY-9 was calculated using total $^3He^*$ and total $^{21}Ne^*$ measured, it was found that the value was lower than the expected value from the $^{21}Ne^*/^3He^*$ ratio, which indicates an excess of ^3He, which further reinforces the presence of excess helium, which may be derived from the mantle. Furthermore, when the expected trapped ^3He was calculated from $^{21}Ne^*$ age, and subtracted from the total ^3He measured, such as in aliquot #1 from sample LL3, it was found that the $^{21}Ne^*/^3He^*$ ratio was the same as the expected value. In the case of sample PY-9, the first aliquot showed a lower $^{21}Ne^*/^3He^*$ ratio than expected, thereby suggesting an excess of helium which is also related to the grain size used as it was coarser than in the second aliquot, hence reinforcing the importance of grain size and fluid inclusions when analysing noble gases.

During the second aliquot analysis, of sample LL3 and PY-9, reasonable agreement between measured and expected cosmogenic $^{21}Ne/^3He$ ratio was noted, thereby providing reliability and robustness to the measurements and ages calculated.

The exposure ages were calculated using the total cosmogenic ^{3}He and ^{21}Ne, measured at the three step heating temperatures; in the case of the first aliquot, for sample LL3 and PY-9. However, a great discrepancy between $^{3}He^{*}$ and $^{21}Ne^{*}$ ages was noted, especially for the first and second aliquots of sample LL3. To calculate the age and the cosmogenic ^{3}He of sample LL3, the expected trapped helium component in fluid inclusions calculated from $^{21}Ne^{*}$ ages was subtracted from the total ^{3}He measured. This indicates that sample LL3 from Llancanelo Volcanic Field has a total $^{21}Ne^{*}$ and total $^{3}He^{*}$ content higher than the samples from Payunia Volcanic Field, which is also consistent with the ages (Table 4.7). Cosmogenic ^{3}He concentrations for samples LL3, PY-9, PY-8 and PY-4 show higher values than those presented by Gillen et al. (2010) for the Newer Volcanic Province, Australia; and very similar values to the ones described by Fenton et al. (2010) from the Bar Ten lava flows, USA.

This may indicate the importance of the altitude from which each sample was taken, as the samples from USA were taken from similar altitudes and latitudes to the Mendoza sites; however, the samples from Australia were taken at similar latitudes but much lower altitude.

In addition, when comparing $^{21}Ne^{*}$, a similar trend is observed in relation to the Newer Volcanic Province. However, compared with the results from the Bar Ten Lava Flows, the values from Llancanelo and Payunia Volcanic Fields are lower. This may reflect the importance of the magnesium content in each sample as a direct relationship was observed between $^{21}Ne^{*}$ and the Fo (magnesium content). At lower Fo contents the concentration of $^{21}Ne^{*}$ also decreases independently of altitude and latitude.

The ages calculated using cosmogenic exposure (Table 4.7) are broadly within the expected range, as in the area there are no other dates, the only reference is the geological map of the area.

In the case of sample LL3, the basaltic flow sampled according to the geological map corresponds to the mid-late Pleistocene Puente Formation. A cosmogenic ^{3}He date from the same formation but located 70 km to the SW of sample LL3 has an ^{3}He age of 41±1 ka (Marchetti et al., 2006) which is close to the $^{21}Ne^{*}$ age found by the present study.

There are no other dates at the location of sample PY-9; however, the geological map of the area shows that the basaltic flow is from the late Pleistocene. Additionally, Germa et al. (2010) produced a date using K-Ar of 28 ± 5 ka from a basalt flow located 6km to the east of PY-9 which is likely to correspond to the same formation. This is very similar to the cosmogenic ages found from ^{21}Ne* from the first and second aliquot and the second aliquot ^{3}He* date. Is likely that ^{3}He* age from the first aliquot of PY-9, contains excess ^{3}He as the grain size used was coarser (>180 μm) and therefore it is likely to contain some helium from fluid inclusions. In addition, special consideration has to be taken when analysing total cosmogenic ^{3}He, as it may show a much higher value than ^{21}Ne*. This may be the result of interferences in the total cosmogenic ^{3}He from mantle helium, which increases the total cosmogenic ^{3}He yield; however, mantle ^{3}He is not produced by cosmic rays, it is primordial component which had been acquired during formation of the Earth and stored in the mantle, and introduced into the magma and then brought to the surface within the lava flow. Hence it is essential to determine the concentration of trapped ^{3}He in order to obtain reliable and accurate dates.

The younger samples from Payunia Volcanic Field (PY-7, PY-8 and PY-4), indicate that is likely that volcanism was active in historical times. However, it cannot be proved as the youngest dates from Santa Maria volcano have large errors and may be also have excess mantle helium; therefore the ages are not particularly reliable. However they provide an older possible age of eruption. In the case of sample PY-4, the age is reliable as ^{21}Ne* and ^{3}He* date are in strong agreement (at about 4.1 ka).

The isotopic concentrations at the various extraction temperatures was carefully examined in order to produce accurate dates; as a result some extraction temperatures were not included within the total cosmogenic ^{21}Ne and ^{3}He calculation and age calculation as some of the values detected were close to the air value in the case of ^{21}Ne and close to MORB value in the case of ^{3}He (Table 4.7). To calculate cosmogenic ^{3}He, the lower temperature of extraction was commonly used, whereas for cosmogenic ^{21}Ne, the higher extraction temperatures were used.

Sample	Temp (°C)	^{21}Ne* (atoms/g)x10^{+5}	^{3}He* (atoms/g)x10^{+6}	^{21}Ne age (ka)	^{3}He age (ka)
LL3 (aliquot #1)	900,1400, 1750	59.0 ± 2.1	14.8 ± 0.4	50.9 ± 1.86	(50.87 ± 1.45)
LL3 (aliquot #2)	^{21}Ne=1750 ^{3}He=900	74.5 ± 4.7	16.5 ± 0.6	62.7 ± 4.01	(55.31 ±2.09)
PY-9 (aliquot #1)	900,1450, 1750	49.1 ± 2.7	22.4 ± 0.5	30.6 ± 1.72	55.58 ± 1.25
PY-9 (aliquot #2)	^{21}Ne=1750 ^{3}He=900	46.2 ± 5.8	14.0 ± 0.06	28.4 ± 3.61	34.33 ± 1.5
PY-8	1750	2.67 ± 7.1	3.13 ± 1.45	1.65 ± 4.37	7.69 ± 3.57
PY-4	900, 1750	9.40 ± 2.3	2.3 ± 0.5	4.10 ± 0.98	4.07 ± 1.00
PY-7	^{21}Ne=1750 ^{3}He=900	1.30 ± 1.3	4.94 ± 0.6	0.79 ± 0.80	1.20 ± 1.41

Table 4.7: Cosmogenic ^{21}Ne (^{21}Ne*) and ^{3}He (^{3}He*) concentrations. Ages determined from both cosmogenic isotopes according to the production rates and temperatures. (Note the concentration of ^{3}He* and ^{3}He* age in sample LL3 are calibrated according to the trapped ^{3}He component calculated from the ^{21}Ne ages, accordingly these dates are given in parenthesis).

LL3:Upper part of Basalt from side of road 186
PY-9: Basaltic flow side of the road, south of Santa Maria Volcano.
PY-8: Basaltic flow from Santa Maria volcano
PY-7: Basaltic bomb from Santa Maria volcano
PY-4: Basaltic bomb from Pampas Negras

4.4 Ar-Ar dating

Five samples were analysed for Ar-Ar dating; however, due to technical problems only three samples were fully analysed (LL1, LL2, and LL4), while sample LL5 was analysed for only one aliquot, and PY-9 was not analysed (Table 4.8). The ages found especially for LL1 are in strong agreement with the previous dates determined by K-Ar method for Cerro Nevado (Fig 2.2, east of Llancanelo Lake) which indicates ages ranging from 1.878±0.028 Ma to 0.944±0.016 Ma (Quidelleur et al., 2009). The ages correspond to the late Pliocene to early Pleistocene Chapua Formation. Sample LL1 yielded the most concordant results, with two aliquots giving the same age of 1.69 Ma (Ar-Ar spectrum, Appendix F).

Sample LL2 shows two similar ages from the two aliquots; however, according to the geological map of the area the basaltic flow from Cerro Trapal corresponds to the same Chapua Formation as sample LL1.

In addition, the first aliquot of sample LL2 produced a saddle-shaped age spectrum, which is characteristic of samples with excess argon which indicates that these are maximum ages (Appendix F, Ar-Ar age spectra). Sample LL4 has a low potassium content and is clearly very young and at the limits of the Ar-Ar technique. The

average age for both aliquots is 120 ± 130 ka (2s). It may be possible to improve this result by analysing multiple aliquots (>5) of finer groundmass material that has been through the magnetic separator to remove all phenocrystic material. However the age obtained is not reliable as it is close to the detection limit and the uncertainty is larger than the age value, therefore it is neither accurate nor reliable. In relation to sample LL5, only one aliquot of this sample has been analysed to date. The sample gives a statistical plateau age of 613 ± 192 ka (2s), but additional aliquots need to be analysed to evaluate the robustness of this result. These ages from LLVF corresponds to the first radiometric dates from the three volcanoes (LL1, LL2 and LL5) on the edges of Llancanelo Lake. Sample LL4 corresponds to the same basaltic flow as sample LL3 (analysed by cosmogenic ^{21}Ne and ^{3}He) but was collected from ~ 1 m below the original lava flow surface.

Sample	**^{39}Ar ($x10^{-13}$mol)**	**^{40}Ar ($x10^{-13}$mol)**	**^{40}Ar (%)**	**^{40}Ar*/Ar^{39}**	**Age ± 1σ (Ma)**	**Mean (Ma)**
LL1	0.4601	1.6818	10.0	4.33	1.69±0.22	1.69±0.29
	0.4207	1.3006	8.8	3.52	1.69±0.20	
LL2	1.0355	0.2751	25.1	0.90	0.354±0.081 (2σ)	0.395±0.068
	0.8836	0.4009	12.7	0.78	0.436±0.055	
LL4	0.5056	1.2362	3.4	0.96	0.03±0.11	0.12±0.13
	0.3233	0.7048	1.9	0.26	0.172±0.083	
LL5	0.8502	1.7275	4.8	2.08	0.613±0.096	0.613±0.096

Table 4.8: Ar-Ar ages from Llancanelo Volcanic Field.

LL1: Basalt sample from Cerro Coral
LL2: Basalt sample from Cerro Trapal
LL3:Upper part of Basalt from side of road 186
LL4: Lower part of Basalt from side of road 186
LL5:Basalt sample from Cerro Divisadero

Chapter 5

Discussion

5.1 Magmatic origin and evolution

The chemical analysis of the basaltic rocks indicates that they are olivine-rich alkaline basalts, with some differences between Llancanelo and Payunia Volcanic Fields. The rocks from LLVF indicate trends similar to the ones observed in the volcanic arc, while the rocks from PVF show intermediate trends, with similarities to the samples described by Stern et, al. (1990).

According to Bertotto et al. (2009), the source of subduction-related magma is a subcontinental lithosphere that has been enriched in Sr, K, Rb, Ba, and Th by subduction-related fluids. Enrichment of these elements has been clearly evident especially in sample LL1 from Cerro Coral. This sample also presents enrichment of Pb, U, Th, alkali ($Na_2O + K_2O$) and alkaline earth elements (MgO, CaO, Sr, Ba) which may further denote the subduction-related origin of this particular alkaline basalt. In addition, Bertotto et al. (2009) detected an increase in Th/Ta, Ba/Nb and La/Nb, in a volcanic area located ~40km to the south-east of Cerro Coral. These trace element ratios show enrichment also in sample LL1, which according to Bertotto et. al., 2009, may be explained as the result of the elements supplied by the Nazca Plate. Furthermore, and in relation to their major elements, sample LL1 shows a clear affinity with arc-like magmas, in comparison with the other samples from the Llancanelo Volcanic Field and from the Payunia Volcanic Field. Geochemical evidence from sample LL1 (located on the eastern edge of Llancanelo Lake), indicates that it has been influenced by slab-related metasomatism, and that the lake was not there at the time of the Cerro Coral eruption, as it does not show hydromagmatic or phreatomagmatic influence. Additionally, the Cl (chlorine) content of the three samples, LL1, LL2 and LL5, situated on the edges of the lake, show very high Cl concentrations of 272 ppm, 204 ppm and 269 ppm, respectively, which may be the result of the high salinity levels (75 g/l) of the lake. Deflation from highly saline sediments and aerosols from the lake could be a post-eruption contamination of lava outcrops.

However, Rivalenty et al., 2004, have proposed that high Cl values are typical of subducted slab-derived components because of hydrothermal alteration of the ocean floor before subduction (Rivalenti et al., 2004). Nevertheless the LILE (large ion lithophile elements) enrichment and the abundance of Cl and H_2O may be only a weak signature of a slab component (Laurora et al., 2001). According to the different subduction-related parameters analysed, is proposed that sample LL1 has a strong association with enrichment of elements derived by the subducting Nazca plate. Furthermore, it is appropriate to relate other samples that may also indicate subduction-related influence such as sample PY-7 and PY-8. Both samples show very similar geochemical signatures as both derive from the Santa Maria volcano; however, PY-7 is a basaltic bomb whereas PY-8 is a basaltic flow. The two samples show enrichment of LILE, Pb, U, Th and alkalis, as well as other trace elements ratios such as Ba/Ta, La/Ta and Th/Ta which are typical of subduction-related magmas. The same trend is evident in the results from the two scoria samples (PY-1 and PY-3), which also indicate influence from the subducting slab.

The results show that the basalts from LLVF tend to be more fractionated than the basalts from PVF, especially of olivine. In relation to the trachyte flow (PY-5) it shows an intermediate, and more evolved geochemistry, hence its fractional crystallization is mainly characterized by plagioclases, as shown by negative anomalies in by Ba, Sr, and Ti. The Ba/Sr ratio tends to be enriched in the first products of partial melting or the residual liquids following fractional crystallization. This ratio is very high for in the trachyte sample.

In addition, plagioclase fractionation in the trachyte is evident from the low concentration of Sr and the low Sr/Nd ratio. Germa et al. (2010), suggested that evolved samples from Payún Matrú Volcano show positive Th and negative Nb anomalies, associated with Ba depletion (<200ppm), this is also valid for the trachyte flow sampled from the western part of the Payún Matrú caldera.

The data provided by the $^{87}Sr/^{86}Sr$ ratio (0.703987 to 0.704207) indicate that the samples analysed are within the range described by Stern et al., (1990), who stated that the plateau basalts from Patagonia show a range in Sr isotope composition that is larger than in the lavas from the Andean orogenic arc. The Sr and Nd isotopic composition of the two basaltic samples analysed (PY-9 and PY-6) indicate mantle-derived arc magmas.

This information is also consistent with the previously described fractional crystallization of mafic magmas like the basalts to produce the trachyte with relatively minor addition of more evolved crustal components. The high Sr/Nd ratios of the basalts are also indicative of arc signatures, as the ratio of the primitive mantle is 16, and the two basalts show values >27.5.

In addition, the low Sm/Nd ratios of the three samples indicate enrichment of LREE (light rare earth elements), although a full suite of REEs were not analysed to validate this.

Furthermore, by relating different areas to the west and to the east of ACBP (Andino-Cuyana Basaltic Province) and observing their basaltic geochemical signatures in comparison with ACBP, it was found that, elements such as La and Ba tend to decrease eastwards from the volcanic arc, while the concentration of Ta tends to increase. This was observed analysing geochemical information from the Tromen Region (Kay et al., 2004), Lancoupe back-arc basalts (Varekamp et al., 2010), and Payunia and Llancanelo Volcanic Fields (this study). The three areas analysed here are from the same geological period, approximately from the latest Pliocene to Holocene and from the same latitudinal range ~38°S to ~36°S. Furthermore, when comparing rocks of the late Miocene from the area east of PVF (Bertotto et al., 2009) it was found that the geochemistry was different to that of the Pleistocene-Holocene basalts from PVF. This indicates that the rocks from the eastern part of the PVF have geochemical signatures typical of the volcanic arc, further emphasising the eastern migration of the volcanic arc ~5Ma, as the result of flat subduction.

The basalts analysed within this study fall into the transitional basalts described by Stern et al., 1990. However, the two volcanic fields analysed present differences. Overall the basalts from LLVF tend to show arc-like signatures (especially sample LL1), while the basalts from PVF are more associated with intra-plate like chemistry. Germa et al. (2010) and Kay et al. (2004) have attributed the intraplate signatures of the back arc basalts to a thinned continental lithosphere, emphasized by the influx of asthenosphere during and after the steepening of the subducting slab. The basalts erupted from the Payunia Volcanic Field show strong association with extensional processes that facilitated the extrusion of magmas.

As extensional processes occur the continental lithosphere tends to thin, and fractures tend to occur such as the Carbonilla Fault, which is strongly associated with extensive lava flows and the development of scoria and cinder cones along this major fault. The basalts from LLVF clearly show a different geochemistry with much more influence from the subducting slab.

The present study provides the first comprehensive analysis of basalts of the LLVF, indicating that sample LL1 shows strong association with the volcanic arc magmatism and with the general geochemistry from the Nevado Volcanic Field, while in general the samples from the LLVF show slab-derived metasomatism.

The information from PVF adds to the current geochemical data and it corroborates some of the previous findings. However this investigation constitutes the first one in analysing basaltic bombs and also in relating a basaltic flow and basaltic bomb from the same volcano, indicating that bombs are slightly more influenced from fluids derived from the subducting slab, compared with the basaltic flow. This investigation also indicates that the processes of formation from the two volcanic fields are different, although heavily influenced by the subduction of the Nazca plate. The back-arc part of the Andean volcanic arc is mainly dominated by extensional processes, evident especially from PVF.

5.2 Cosmogenic ^{21}Ne and ^{3}He

The ages obtained from cosmogenic dating indicate that the basaltic flows from LLVF and from PVF are of late Pleistocene and Holocene age. The cosmogenic surface ^{21}Ne exposure age obtained from the original lava flow surface of sample LL3 from LLVF, indicates that the alkaline basalt was extruded 54.9 ± 1.3 ka. This age seems to be in agreement with the age range from the geological map of the area (Nullo et al., 2005). However there are no dates from the basalts of nearby areas. Furthermore, it is hypothesized that sample LL3 corresponds to a basaltic flow from the Malacara volcano and the late Pleistocene Puente Formation. In addition, and according to Marchetti et al. (2006), an age from a different basaltic flow located ~70 km to the SW of LL3 but corresponding to the same Puente Formation was obtained using cosmogenic ^{3}He. The age of this olivine basalt flow is 41±1ka (37 ± 3 to 44 ± 2 ka) (Marchetti et al., 2006) and is in broad agreement with the cosmogenic ^{21}Ne age obtained from the current work.

The ages produced from cosmogenic ^{3}He in this study seem to be older than the ages obtained from cosmogenic ^{21}Ne. The discrepancy between cosmogenic ^{3}He and ^{21}Ne ages, may be the high $^{3}He^{*}$ content and which may indicate a component of mantle ^{3}He. These sources can be differentiated by performing a vacuum crushing experiment. Unfortunately, the vacuum crushing experiment in this study was not successful. Therefore the mantle helium was not experimentally differentiated from cosmogenic helium-3; hence the expected trapped mantle helium component was calculated from the $^{21}Ne^{*}$ age assuming that the two isotopes should indicate the same age. Accordingly, the ages calculated and presented for sample LL3 in this study correspond to the total $^{3}He^{*}$ calculated after the expected ^{3}He component was subtracted from the total ^{3}He detected.

The results from $^{20}Ne/^{22}Ne$ ratios indicate that the olivine separate samples do not contain mantle-derived Ne. Nevertheless, the samples are a mixture of cosmogenic and atmospheric Ne. Therefore it was not necessary to undertake a vacuum crushing experiment to characterize the Ne isotope composition trapped in fluid inclusions.

The results from cosmogenic ^{21}Ne and ^{3}He from sample LL3 and the Ar-Ar date from sample LL4 which corresponds to the same basaltic flow are discrepant. The cosmogenic dating indicates an age of 54.94 ± 1.3 ka, whereas the Ar-Ar date of the flow is 120 ± 130 ka. The two aliquots analysed from LL4 using Ar-Ar indicate that the results are discordant and inaccurate as the uncertainty is larger than the age.

It is possible that a portion of the argon detected corresponds to mantle argon and there are parallels with possible mantle helium affecting the ^{3}He ages.

Sample PY-9, has a mean age of 31.1 ± 1.4 ka from cosmogenic ^{21}Ne and ^{3}He (calculated from first and second aliquot $^{21}Ne^{*}$ and second aliquot $^{3}He^{*}$). This sample corresponds to the area of Los Volcanes. Germa et al. (2010) produced some ages along PVF using K-Ar dating, finding that the basalts from the area close to PY-9 show an age of 28 ± 5 ka (sample 94AF from Germa et al., 2010). The geochemistry of the Germa et al. (2010) sample and the one from sample PY-9, are very similar. It is possible that the two samples (94AF and PY-9) correspond to the same basaltic flow. In addition, this age is also in agreement with the age range from the geologic map as it indicates that the basalts correspond to the late Pleistocene to the early Holocene.

The age from $^{3}He^{*}$ in the first aliquot of sample PY-9 is much older 55.6 ± 1.2 ka and does not correlate with the $^{21}Ne^{*}$ date, hence, it was not included in the mean age calculation or discussion. As it was discussed before it may be related to an excess of helium derived from mantle helium and not from cosmogenic helium.

Sample PY-7 (basaltic bomb) and PY-8 (basaltic flow) are from the Santa Maria volcano. Both samples indicate that the volcano was possibly active until quite recent times. However, the ages calculated are not reliable as the measurements show very low $^{3}He^{*}$ and almost no $^{21}Ne^{*}$ was detected, therefore the uncertainty is larger than the age calculated, nevertheless it is suggested that the volcanic eruptions that formed the basaltic flow and the basaltic bomb are younger than 7ka. The ages indicate the oldest possible eruption, and thereby provide some numerical indication regarding how young the volcano is likely to be. However further samples and of a larger sample size needed to be analysed in order to produce reliable results. At the moment the results from this volcano are only used as an age indicator.

Sample PY-4 (a basaltic bomb from Pampas Negras) shows consistent and reliable results as the two isotopic systems show consistent ages, 4.07±1.00 ka from $^{3}He^{*}$ and 4.10±0.98 ka from $^{21}Ne^{*}$. These provides the first accurate age for Pampas Negras. This age indicates that the area was active 4.09± 0.7 ka.

The chronological results demonstrate that the ages are in agreement with the K-Ar, the single cosmogenic ^{3}He age, from previous investigations and from the geological map of the area. The results also demonstrate that cosmogenic ^{21}Ne and ^{3}He dating can be used to date young basaltic flows. Furthermore, is important to use the two cosmogenic isotopes, ^{3}He and ^{21}Ne, to assess the reliability and accuracy of the results. In this sense, the method has shown a strong correlation between the two isotopes for sample PY-4, and it demonstrates that with further improvements, the methods could be applied to other areas and geological problems.

Chapter 6

Conclusions and Recommendations

6.1 Conclusions

This study demonstrates that the geochemistry of the back-arc basaltic rocks from ACBP has been influenced by the subducting Nazca plate. Sample LL1 from Cerro Coral seems to have a strong influence from the subducting slab. This sample corresponds to the late Pliocene to early Pleistocene Chapúa Formation. Sample LL1 is the oldest (1.7 Ma) from this current research and has affinities with the Cerro Nevado volcanic field located to the east of Cerro Coral, and which corresponds to an older volcanic period highly influenced by slab-related metasomatism. The other samples dated by Ar-Ar from Llancanelo Volcanic Field, indicate that they are younger than LL1, but older than the Payunia Volcanic Field. The origin of Payunia is multiple as some rocks indicate a geochemistry influenced by the subducting slab, while others are typical of a transitional intraplate basaltic source. The basaltic bombs, scoria and the basaltic flow from Santa Maria indicate influence from fluids of the subducting slab. The geochronology of the basaltic bombs and the basaltic flow from Santa Maria volcano indicate eruption is quite young (<7 ka).

The ages obtained from paired cosmogenic ^{21}Ne and ^{3}He analyses show agreement among them, especially in sample PY-4 from the Pampas Negras scoria field, in which the young ages (4.1 ka) calculated by the two isotope systems are identical. However the ages from the two samples from the Santa Maria volcano are not accurate, and have to be further analysed with larger sample sizes to produce reliable dates.

The samples contain measurable amounts of ^{21}Ne and ^{3}He, indicating that they are appropriate for $^{21}Ne^{*}$ and $^{3}He^{*}$ exposure age calculations despite the youthfulness of the samples.

The concentration of $^{3}He^{*}$ measured was elevated in some samples and therefore it is suggested that there is a component of mantle helium. Accordingly a vacuum crushing experiment is important to determine this component and thereby avoid producing older apparent ages.

The study provides new dates and data from this basaltic province, and also indicates that $^{21}Ne^*$ and $^{3}He^*$ can provide reliable young ages. However, more studies are needed to further develop and test this new dating method, and to provide more geochemical information in relation to the Andino-Cuyana Basaltic Province.

6.2 Recommendations

6.2.1 Areas for further geochemical analysis

This study constitutes the first comprehensive geochemical analysis in the Llancanelo Volcanic Field, and provides additional new data for the Payunia Volcanic Field. Nevertheless, many questions remain unanswered which need future investigation to better understand the processes responsible for the formation of this extensive volcanic province.

Further Sr and Nd isotope analyses are needed especially in the LLVF to confirm the geochemical signatures, as well as REE analysis in both fields. Reliable dates from the two volcanic fields could provide an explanation for the geochemical differences observed between PVF and LLVF. Tectonic processes occurring at different periods in the subducting slab can potentially have a major influence on the rock chemistry erupted in the back arc. Furthermore, future studies should focus on the origin of the subduction-related metasomatism, and investigate, whether it is derived from (i) fluids from the subducting slab or from older rocks with an arc-like geochemistry, or (ii) from the arc when the volcanic arc was located further east. In addition, geochemically evolved rocks from the Payún Matrú caldera, such as trachytes, rhyolites and ignimbrites, should also be analysed and dated to further interpret how mafic and felsic rocks can coexist within the same limited area. The degree of crustal contamination and assimilation in the more evolved rock remains a key question.

6.2.2 Areas for further cosmogenic ^{3}He and ^{21}Ne analysis

The method of cosmogenic ^{3}He and ^{21}Ne analysis is still under development. Each of the previous three studies (two published and this thesis) has used different parameters, minerals and scaling factors. This will eventually assist in the goal of establishing cosmogenic ^{3}He and ^{21}Ne dating as a reliable and accurate dating method that will contribute to understand a variety of geologic process.

This study has been based on analysis of olivine separates in order to calculate the age of the basalts. However, other minerals such as pyroxenes (especially clinopyroxene) and plagioclases have also been tested by other authors (Fenton et al., 2010; Poreda and Cerling, 1992). Different mineral separates should be analysed from individual samples, to determine the accuracy and also the variability of the method. Measurable concentrations of cosmogenic ^{3}He and ^{21}Ne from different minerals will expand the range of possible applications of the method. In addition, analysing the production rate and using the most appropriate production rate has become one of the major challenges of the method, as different scaling factors and production rates will produce different ages. In the current research, Lal's scaling factor (Lal, 1991) was used. Furthermore, it is essential to correlate the dates from $^{3}He^{*}$ and $^{21}Ne^{*}$ using different methods as well as testing the method at different age intervals, to demonstrate its feasibility. In theory, this method could be used to accurately date events as young as 1000 years, but this remains to be practically and analytically developed. Sample collection and preparation specifications have to be established, simplified and standardised in order to obtain reliable and comparable dates. In relation to sample preparation, it is accepted that the higher the purity of the mineral separate, the more accurate will likely be the derived age. Nevertheless, upper and lower limits of acceptable mineral purity and levels of contamination from minerals other than olivine have not been established. Another important question raised from this research which remains unanswered is to understand why sample LL3 from the Llancanelo Volcanic Field has an anomalously high $^{3}He/^{4}He$ ratio ($8.28x10^{-5}$ for aliquot#1 and $2.68x10^{-4}$ for aliquot #2) in comparison with samples from the Payunia Volcanic Field. One possibility could be the presence of a mantle plume; however, further analysis involving additional samples is required to test this assumption.

REFERENCES

Bermúdez, A. & Delpino, D. 1989. La Provincia Basaltica Andino Cuyana (35-37°L.S.). *Revista de la Asociación Geológica Argentina,* 40**,** 35-55.

Bertotto, G., Cingolani, C. & Bjerg, E. 2009. Geochemical variations in Cenozoic back-arc basalts at the border of La Pampa and Mendoza provinces, Argentina. *Journal of South American Earth Sciences,* 28**,** 360-373.

Clapperton, C. 1993. *Quaternary Geology and Geomorphology of South America.* Elsevier, Amsterdam, The Netherlands.

Cox, K., Bell, J. D. & Pankhurst, R. J. 1979. *The Interpretation of Igneous Rocks* London, Allen & Unwin.

Dickin, A. 2005. *Radiogenic Isotope Geology*. Cambridge University Press,UK.

Duran, V. and Mikkan, R. 2009. Impacto del volcanismo hologenico sobre el poblamiento humano del sur de Mendoza (Argentina). *Intersecciones en Antropologia,* 10**,** 295-310.

Eby, N. G. 2010. *Using mineralogy to identify the source of a sample* [Online]. Massachusetts: http://faculty.uml.edu/nelson.eby/ [Accessed 25/05 2010].

Fenton, C. R., Niedermann, S., Goethals, M. M., Schneider, B. & Wijbrans, J. 2009. Evaluation of cosmogenic ^{3}He and ^{21}Ne production rates in olivine and pyroxene from two Pleistocene basalt flows, western Grand Canyon, AZ, USA. *Quaternary Geochronology*, 4**,** 475–492.

Folguera, A., Naranjo, J. A., Orihashi, Y., Sumino, H., Nagao, K., Polanco, E. & Ramos, V. A. 2009. Retroarc volcanism in the northern San Rafael Block (34°–35°30′S), southern Central Andes: Occurrence, age, and tectonic setting. *Journal of Volcanology and Geothermal Research,* 186**,** 169–185.

Fujioka, T. 2006. *Development of in situ cosmogenic ^{21}Ne exposure dating, and dating of Australian arid landforms by combined stable and radioactive in situ cosmogenic nuclides.* PhD thesis, Australian National University.

Germa, A., Quidelleur, X., Gillot, P. Y. & Tchilinguirian, P. 2010. Volcanic evolution of the back-arc Pleistocene Payun Matru volcanic field (Argentina). *Journal of South American Earth Sciences,* 29**,** 717-730.

Gillen, D. 2001. *Exposure dating of young basaltic lava flows using cosmogenic neon-21.* BSc Honours thesis, University of Wollongong.

Gillen, D., Honda, M., Chivas, A. R., Yatsevich, I., Patterson, D. B. & Carr, P. F. 2010. Cosmogenic ^{21}Ne exposure dating of young basaltic lava flows from the Newer Volcanic Province, Western Victoria, Australia. *Quaternary Geochronology,* 5**,** 1-9.

Hickey, R.L., Frey, F.A., Gerlach, D.C., Lopez-Escobar, L., 1986. Multiple sources for basaltic arc rocks from the southern volcanic zone of the Andes (34_–41_S): trace element and isotopic evidence for contributions from subducted oceanic crust, mantle, and continental crust. *Journal of Geophysical Research,*91 (B6), 5963–5983.

Inbar, M. & Risso, C. 2001a. Holocene yardangs in volcanic terrains in the southern Andes, Argentina. *Earth Surface Processes and Landforms,* 26**,** 657–666.

Inbar, M. & Risso, C. 2001b. A morphological and morphometric analysis of high density cinder cone volcanic field - Payun Matru, south-central Andes, Argentina. *Z. Geomorph. N. F.,* 45**,** 321-343.

Kay, S. M., Gorring, M. & Ramos, V. A. 2004. Magmatic sources, setting and causes of Eocene to Recent Patagonian plateau magmatism (36°S to 52°S latitude). *Revista de la Asociación Geológica Argentina,* 59**,** 556-568.

Lal, D. 1991. Cosmic ray labelling of erosion surfaces: in situ nuclide production rates and erosion models. . *Earth and Planetary Science Letters,* 104**,** 424-439.

Lamb, S. & Hoke, L. 1997. Origin of the high plateau in the Central Andes, Bolivia, South America *Tectonics,* 16**,** 632-649.

Laurora, A., Rivalenti, G., Vannucci, R., Zanetti, A., Barbieri, M. A. & Cingolani, C. A. 2001. Metasomatism and melting in carbonated peridotite xenoliths from the mantle wedge: the Gobernador Gregores case (Southern Patagonia). *Journal of Petrology,* 42**,** 69-87.

Llambías, E. J., Quenardelle, S. & Montenegro, T. 2003. The Choiyoi Group from central Argentina: a subalkaline transitional to alkaline association in the craton adjacent to the active margin of the Gondwana continent. *Journal of South American Earth Sciences,* 16**,** 243–257.

MacKenzie, W. S., Donaldson, C. H. & Guilford, C. 1982. *Atlas of Igneous Rocks and their Textures.* Longman, London.

MacKenzie, W. S. & Guilford, C. 1980. *Atlas of rock-forming minerals in thin section.* Logman, London.

Marchetti, D., Cerling, T., Evenson, E., Gosse, K. J. & Martinez, O. 2006. Cosmogenic exposure ages of lava flows that temporarily dammed the Rio Grande and Rio Salado, Mendoza Province, Argentina. *Backbone of the Americas. Patagonia to Alaska.* Mendoza: Geological Society of America-Asociación Geológica Argentina (Conference abstract only).

Matsuda, J., Matsumoto, T., Sumino, H., Nagao, K., Yamamoto, J., Miura, Y., Kaneoka, I., Takahata, N. & Sano, Y. 2002. The $^{3}He/^{4}He$ ratio of the new internal He Standard of Japan (HESJ). *Geochemical Journal,* 36**,** 191-195.

McDonough W.F., Sun S., Ringwood A.E., Jagoutz E. & Hofmann A. 1991. K, Rb, and Cs in the earth and moon and the evolution of the earth's mantle. *Geochimica et Cosmochimica Acta,* Ross Taylor Symposium volume
.

McKeever, S. 1985. *Thermoluminescence of Solids.* Cambridge University Press.

Mendoza on line. 2010. *Laguna de Llancanelo* [Online]. http://www.mendozaonline.us/2010/04/30/laguna-de-llancanelo/). [Accessed 24/05 2010].

Nesse, W. 1991. *Introduction to Optical Mineralogy*, New York, Oxford University Press.

Niedermann, S. 2002. *Noble Gases in Geochemistry an Cosmochemistry,*in Reviews in Mineralogy and Geochemistry vol 47. Mineralogical Society of America, Washington.

Nullo, F., Stephens, G., Combina, A. M., Dimieri, L., Baldauf, P. & Bouza, P. 2005. *Hoja Geológica 3569-III/3572-IV Malargüe*, 1:250000. Buenos Aires: SEGEMAR (Servicio Geologico y Minero Argentino)

Pasquare, G., Bistacchi, A., Francalanci, L., Bertotto, G., Boari, E., Massironi, M. & Rossotti, A. 2008. Very long pahoehoe inflated basaltic lava flows in the Payenia Volcanic Province (Mendoza and La Pampa, Argentina). *Revista de la Asociación Geológica Argentina,* 63**,** 131-149.

Poreda, R. & Cerling, T. 1992. Cosmogenic neon in recent lavas from the western United States. *Geophysical Research Letters,* 19**,** 1863-1866.

Quidelleur, X., Carlut, J., Tchilinguirian, P., Germa, A. & Gillot, P. Y. 2009. Paleomagnetic directions from mid-latitude sites in the southern hemisphere (Argentina): Contribution to time averaged field models. *Physics of the Earth and Planetary Interiors,* 172**,** 199-209.

Renné, P. R., Swisher, C., Deino, A., Karner, D., Owens, T. L. & DePaolo, D. J. 1998. Intercalibration of standards, absolute ages and uncertainties in $^{40}Ar/^{39}Ar$ dating *Chemical Geology,* 145**,** 117-152.

Rivalenti, G., Mazzucchelli, M., Laurora, A., Ciuffi, S. I. A., Zanetti, A., Vannucci, R. & Cingolani, C. 2004. The backarc mantle lithosphere in Patagonia, South America. *Journal of South American Earth Sciences,* 17**,** 121–152.

Rollinson, H. 1993. *Using Geochemical Data: Evaluation, Presentation, Interpretaion.* Longman, Essex, England.

Royden, L. 1993. The tectonic expression of slab pull at continental convergent boundaries. *Tectonics,* 12**,** 303-325.

Rutter, N. & Catto, N. (eds.) 1996. *Dating Methods for Quaternary Deposits.* Geological Association of Canada, Newfoundland, Canada.

Steriger, R.H. & Jäger, E. 1977. Subcommision on geochronoly: Convention on the use of decay constants in geo- and cosmochronology. *Earth and Planetary Science Letters,* 36, 3, 359-362.

Stern, C. R. 2004. Active Andean volcanism: its geologic and tectonic setting *Revista Geológica de Chile*, 31**,** 161-206.

Stern, C. R., Frey, F. A., Futa, K., Zartman, R. E., Peng, Z. & Kyser, T. K. 1990. Trace-elements and Sr, Nd, Pb and O isotopic composition of Pliocene and Quaternary alkali basalts of the Patagonian Plateau lavas of southernmost South America. *Contributions to Mineralogy and Petrology*, 104**,** 294-308.

Tuniz, C., Bird, J. R., Fink, D. & Herzog, G. 1998. *Accelerator Mass Spectrometry*, CRC Press, United States of America.

Van Der Pluijm, B. & Marshak, S. 2004. *Earth Structure.* W.W. Norton & Company, New York.

Varekamp, J., Hesse, A. & Mandeville, C. 2010. Back-arc basalts from the Loncoupe graben (Province of Neuquén, Argentina). *Journal of Volcanology and Geothermal Research***,** doi: 10.1016/j.jvolgeores.2010.04.003.

Violante, R., Osella, A., De la Vega, M., Rovere, E. & Osterrieth, M. 2010. Paleoenvironmental reconstruction in the western lacustrine plain of Llancanelo Lake, Mendoza, Argentina. *Journal of South American Earth Sciences,* 29**,** 650–664.

Wirth K. & Barth A. *Geochemical Instrumentation and Analysis* [Online]. Indianapolis:http://serc.carleton.edu/research_education/geochemsheets/techniques/XRF.html. [Accessed 28/05 2010].

APPENDIX A

Forsterite content calculation $(Mg,Fe)_2 SiO_4$ for sample LL3

Major-element composition of olivine separates

Sample	Molecular Weight (g/mol)	LL3	PY-4	PY-7	PY-8	PY-9
SiO_2	60.09	38.48	40.25	39.33	40.53	40.05
TiO_2	79.9	0.11	0.40	0.19	0.51	0.53
Al_2O_3	101.96	1.74	1.95	1.27	2.48	2.13
Fe_2O_3	71.85	22.44	16.25	17.92	16.65	19.88
MnO	70.94	0.30	0.22	0.23	0.22	0.29
MgO	40.3	36.15	36.60	39.22	34.41	30.86
CaO	56.08	1.17	4.31	1.80	4.45	5.25
K_2O	55.1	0.03	0.03	0.06	0.14	0.08
P_2O_5	141.94	0.02	0.00	0.03	0.06	0.07
Total		100.45	100.01	100.04	99.44	99.14

Molecular proportion of oxides

SiO_2 = 38.48/60.09 = 0.6319
TiO_2 = 0.11/79.9 = 0.0013
Al_2O_3 = 1.79/101.96 = 0.0171
FeO = 22.44/71.85 = 0.3123
MnO = 0.30/70.94 = 0.0042
MgO = 36.15/40.3 = 0.8970
CaO = 1.17/56.08 = 0.0209
K_2O = 0.03/55.1 = 0.0006
P_2O_5 = 0.02/141.94 = 0.0002

Atomic proportion of oxygen from each molecule

SiO_2 = 0.6319 x 2 = 1.2637
TiO_2 = 0.0013 x 2 =0.0027
Al_2O_3 = 0.0171 x 3 = 0.0513
FeO = 0.3123 x 1= 0.3123
MnO = 0.0042 x 1 = 0.0042
MgO = 0.8970 x 1 = 0.8970
CaO = 0.0209 x 1 = 0.0209
K_2O = 0.0006 x 1= 0.0006
P_2O_5 = 0.0002 x 5 = 0.0008

} 2.5535

4 oxygen ions in the basic olivine

4/2.5535 = 1.5665

Number of anions on basis of O_4 (olivine)

SiO_2 = 1.2637 x 1.5665 = 1.9796
TiO_2 = 0.0027 x 1.5665 = 0.042
Al_2O_3 = 0.0513 x 1.5665 = 0.0803
FeO = 0.3123 x 1.5665 = 0.4892
MnO = 0.0042 x 1.5665 = 0.0066
MgO = 0.8970 x 1.5665 = 1.4052
CaO = 0.0209 x 1.5665 = 0.0328
K_2O = 0.0006 x 1.5665 = 0.0009
P_2O_5 = 0.0008 x 1.5665 = 0.0013
End Member % = 100 x Mg molar fraction/ (Mg + Fe molar fraction)

End Member % = 100 x 1.4052 / (1.4052 + 0.4892) = 74.2 %
The magnesium content was calculated in the same way for all other samples.

APPENDIX B

Production rate calculation

P ^{3}He at sea level and high altitude 113 ± 10 atoms/g/a
P ^{21}Ne at sea level and high altitude 45 ± 4 atoms/g/a (Fo_{81})

Scaling factor values according to Lal (using Lal's scaling spreadsheet)

LL3 : (35.7°S, altitude 1449 m)
nucleogenic component of cosmic rays : 2.817
muon component of cosmic ray : 1.7376

PY-9 : (36.3°S, altitude 1907 m)
nucleogenic component of cosmic rays : 3.952
muon component of cosmic ray : 2.1211

PY-8 & PY-7 (same site; one sample is a flow the other is a bomb): (36.3°S, altitude 1811m)
nucleogenic component of cosmic rays : 3.696
muon component of cosmic ray : 2.0384

PY-4 : (36.4°S, altitude 2301 m)
nucleogenic component of cosmic rays : 5.164
muon component of cosmic ray : 2.4885

^{3}He production rate (formula from Niedermann 2002, page 737)

$P\ ^{3}He = N(\lambda_{m,}h) \times P_n$

For LL3 P ^{3}He= 2.817 x 113 atoms/g/a = 318.321 atoms/g/a

For PY-9 P ^{3}He= 3.952 x 113 atoms/g/a = 446.576 atoms/g/a

For PY-8 & PY-7 P ^{3}He= 3.696 x 113 atoms/g/a = 417.648 atoms/g/a

For PY-4 P ^{3}He= 5.164 x 113 atoms/g/a = 583.532 atoms/g/a

^{21}Ne production rate (formula from Niedermann 2002, page 737)

$P\ ^{21}Ne = N(\lambda_{m,}h) \times P_n$

For LL3 P ^{21}Ne= 2.817 x 45 atoms/g/a = 126.765 atoms/g/a

For PY-9 P ^{21}Ne= 3.952 x 45 atoms/g/a = 177.84 atoms/g/a

For PY-8 & PY-7 P ^{21}Ne= 3.696 x 45 atoms/g/a = 166.32 atoms/g/a

For PY-4 P ^{21}Ne= 5.164 x 45 atoms/g/a = 232.38 atoms/g/a

The values above correspond to Fo_{81} (at site calculation)
LL3
P ^{21}Ne Fo_{74} = 115.81 atoms/g/a
P ^{3}He Fo_{74} = 290.811 atoms/g/a

PY-9
P ^{21}Ne Fo_{73} = 160.27 atoms/g/a
P ^{3}He Fo_{73} = 402.47 atoms/g/a

PY-8
P ^{21}Ne Fo_{79} = 162.32 atoms/g/a
P ^{3}He Fo_{79} = 407.33 atoms/g/a

PY-4
P ^{21}Ne Fo_{80} = 229.51 atoms/g/a
P ^{3}He Fo_{80} = 576.32 atoms/g/a

PY-7
P ^{21}Ne Fo_{80} = 164.26 atoms/g/a
P ^{3}He Fo_{80} = 412.49 atoms/g/a

Estimated age =10000
Exposure age =cosmogenic abundance /production rate

LL3 ^{3}He (10000a = χ / 290.811atoms/g/a) χ= 2908100 atoms /g
^{21}Ne = 1558100 atoms /g

PY -9 ^{3}He = 4024700atoms/g
^{21} Ne = 1602700atoms/g

PY -8 ^{3}He = 4073300atoms/g
^{21} Ne = 1623200atoms/g

PY -4 ^{3}He = 5763200atoms/g
^{21} Ne = 2295100atoms/g

PY -7 ^{3}He = 4124900atoms/g
^{21} Ne = 1642600atoms/g

APPENDIX C

Cosmogenic ^{21}Ne, ^{3}He and age calculation (sample PY-9 (3))

Reference isotope = ^{20}Ne

Cosmogenic ^{21}Ne calculation at 900°C

$$^{21}Ne^* = {}^{20}Ne \times \{\underbrace{(^{21}Ne/^{20}Ne)\ meas - (^{21}Ne/^{20}Ne)air}_{R}\}$$

$^{21}Ne^* = 2.29E\text{-}10 \times \{(3.01E\text{-}3) - (0.00296)\}$

$^{21}Ne^* = 2.29E\text{-}10 \times 0.00005$

$^{21}Ne^* = 1.145E\text{-}14$

Error calculation

$(\sigma^{21}Ne^* / ^{21}Ne^*)^2 = (\sigma^{20}Ne/^{20}Ne)^2 + (\sigma R/R)^2$

$(\sigma^{21}Ne^*/ 1.145E\text{-}14)^2 = (2.78E\text{-}12 / 2.29E\text{-}10)^2 + (2.94E\text{-}5/0.00005)^2$

$(\sigma^{21}Ne^*/ 1.145E\text{-}14)^2 = (0.0121397)^2 + (0.588)^2$

$(\sigma^{21}Ne^*/ 1.145E\text{-}14) = \sqrt{(0.0001474) + (0.3457)}$

$(\sigma^{21}Ne^*/ 1.145E\text{-}14) = \sqrt{0.3458914}$

$\sigma^{21}Ne^* = 0.588125 \times 1.145E\text{-}14$

$\sigma^{21}Ne^* = 6.7340E\text{-}15$

at 900°C $^{21}Ne^* = 1.145E\text{-}14 \pm 6.734E\text{-}15$

The same procedure was used to calculate cosmogenic ^{21}Ne at 1400°C and 1750°C
Then all the cosmogenic ^{21}Ne was added =

Total $^{21}Ne^* = 1.8274E\text{-}13 \pm 1.0251E\text{-}14$

Exposure Age (PY-9) = $^{21}Ne^*$ / production rate

Age= (1.8274E-13±1.0251E-14 / 22400 x 6.02E+23) / 160.27 at/g/a

^{21}Ne age of PY-9 = 30642.899 ± 1718.95

^{21}Ne age of PY-9 = 30643 ±1719

The same procedure was used for LL3 finding that the age is

^{21}Ne age of LL3 = 50922.1958 ± 1859.07

^{21}Ne age of LL3 = 50922 ± 1859

- The same procedure was used to calculate the concentration of total cosmogenic ^{3}He in both samples and its corresponding age.

APPENDIX D

Estimated ^{3}He trapped in fluid inclusions calculated from ^{21}Ne* dates
(sample LL3, from first aliquot)

Assuming age ^{3}He* = ^{21}Ne*
^{21}Ne* age = 50922 years
^{3}He* age = 50922years
P^{3}He* (production rate) = 290.811atoms/g/yr

Age = ^{3}He*/ P^{3}He*
50922yr = ^{3}He*/ 290.811atoms/g/yr
^{3}He* = 50922yr x 290.811atoms/g/yr
^{3}He* = 14808677.74 atoms/g

The total ^{3}He* has to be converted to ccSTP/g

^{3}He* = (14808677.74/6.02 E+23) x 22400

^{3}He* = 5.51 E-13

Using the formula to calculate ^{3}He*, the estimated trapped component can be calculated

$^{3}He^{*} = {}^{4}He_{meas}\{(^{3}He/^{4}He)_{meas} - (^{3}He/^{4}He)_{trapped}\}$

5.51 E-13 = 1.46 E-8 $\{(8.2839\ E\text{-}5) - (^{3}He/^{4}He)_{trapped}\}$

$\{(8.2839\ E\text{-}5) - (^{3}He/^{4}He)_{trapped}\} = 5.51\ E\text{-}13 / 1.46\ E+8$

$(^{3}He/^{4}He)_{trapped} = 8.2839\ E\text{-}5 - 3.7739\ E\text{-}5$

$(^{3}He/^{4}He)_{trapped} = 4.4739\ E\text{-}5$

The same calculation was used to estimate the trapped component from the second aliquot

$(^{3}He/^{4}He)_{trapped} = 1.136\ E\text{-}4$

APPENDIX E

Mayor-element analysis of olivine samples (by XRF)

Major-element results from the first analysis after sodium polytungastate separation

	LL3	PY-4	PY-7	PY-8	PY-9
SiO_2	38.48	40.25	39.33	40.53	40.05
TiO_2	0.11	0.40	0.19	0.51	0.53
Al_2O_3	1.74	1.95	1.27	2.48	2.13
FeO	22.44	16.25	17.92	16.65	19.88
MnO	0.30	0.22	0.23	0.22	0.29
MgO	36.15	36.60	39.22	34.41	30.86
CaO	1.17	4.31	1.80	4.45	5.25
K_2O	0.03	0.03	0.06	0.14	0.08
P_2O_5	0.02	0.00	0.03	0.06	0.07
Total	100.45	100.01	100.04	99.44	99.14

Note, the high content of CaO especially in sample PY-9, which may indicate that the sample is contaminated by pyroxene.

Major-element results from the second analysis, after methylene iodide separation

	LL3	PY-4	PY-7	PY-8	PY-9
SiO_2	38	38.31	39.06	38.44	37.95
TiO_2	0.06912	0.1134	0.1215	0.1576	0.1659
Al_2O_3	0.6709	0.787	0.7117	0.907	0.6736
FeO	21.75	17.98	18.39	18.47	22.96
MnO	0.281	0.2302	0.2388	0.2372	0.3186
MgO	38.96	40.68	40.99	40.11	36.69
CaO	0.4961	0.7771	0.8221	0.7052	1.021
K_2O	0.01902	0.0327	0.0442	0.0742	0.0407
P_2O_5	0.01922	0.02464	0.02752	0.03624	0.0448
Na_2O	0.077	0.02	0.02	0.1269	0.076
Total	100.34	98.95	100.42	99.26	99.94

After methylene iodide density separation and hand picking the concentration of MgO is greater and the concentration of CaO is less, suggesting that the olivine samples are >90% pure. The majority of the pyroxene impurities have been removed.

APPENDIX F

Ar-Ar age spectra

Sample LL1 (Cerro Coral)

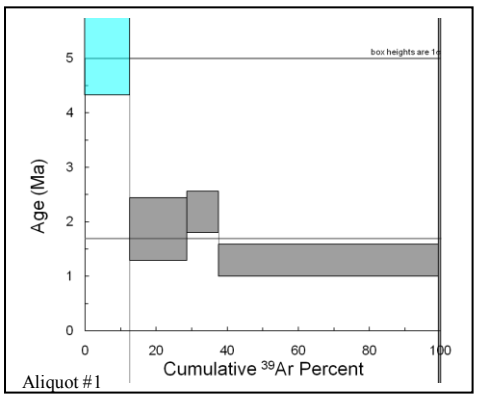

Plateau age = 1.69 ± 0.22 Ma
(1σ, including J-error of 0.24%)
MSWD = 1.9, probability = 0.12
Includes 87.4% of the ^{39}Ar

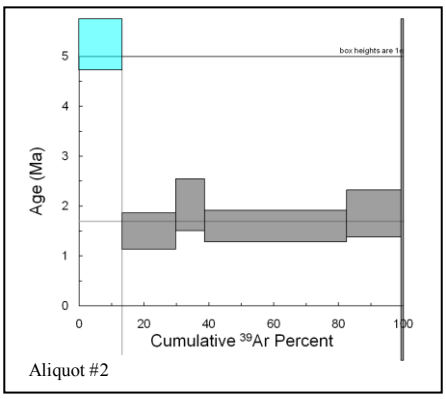

Plateau age = 1.69 ± 0.20 Ma
(1σ, including J-error of 0.24%)
MSWD = 0.72, probability = 0.58
Includes 86.8% of the ^{39}Ar

Sample LL2 (Cerro Trapal)

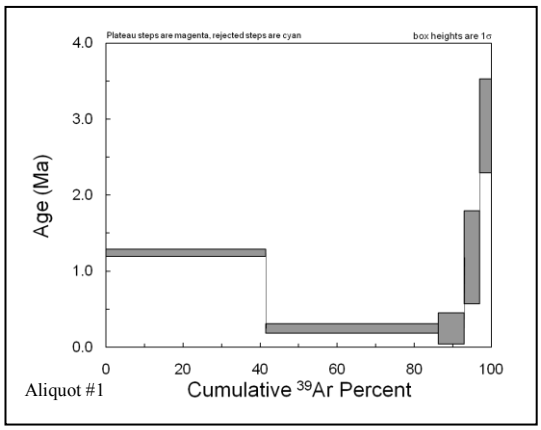

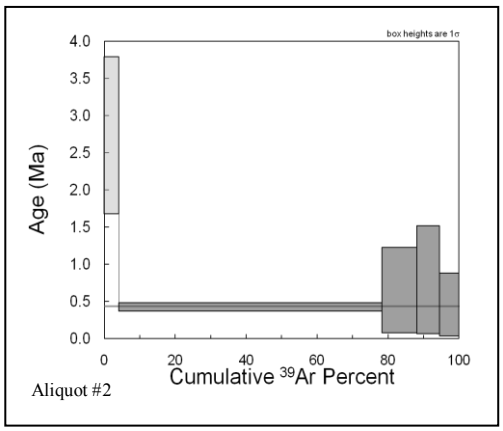

Plateau age = 0.436 ± 0.055 Ma
(1σ, including J-error of 0.26%)
MSWD = 0.13, probability = 0.94
Includes 95.9% of the ^{39}Ar

Sample LL4 (Lower part of basaltic flow, on the side of road 186)

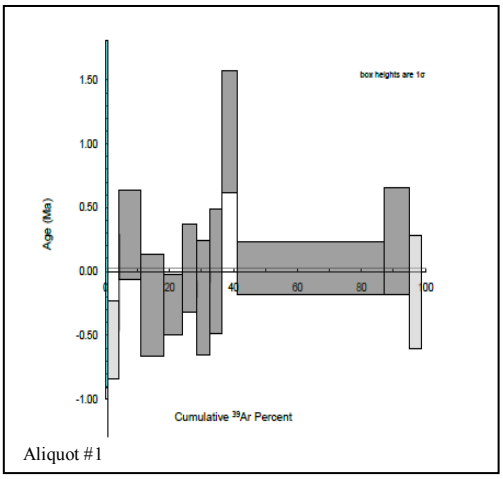

Plateau age = 0.03 ± 0.11 Ma
(1σ, including J-error of 0.28%)
MSWD = 1.00, probability=0.43
Includes 90.8% of the ^{39}Ar

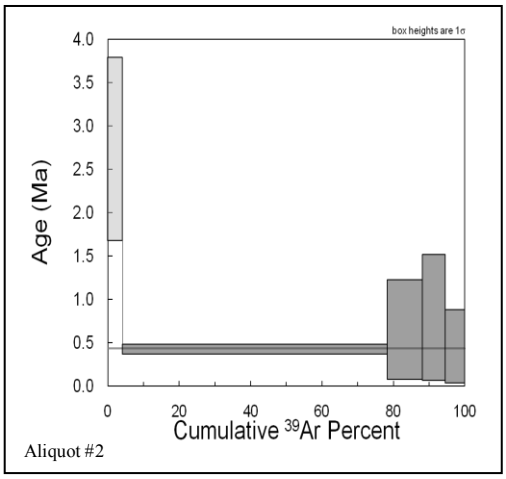

Plateau age = 0.172 ± 0.083 Ma
(1σ, including J-error of 0.28%)
MSWD = 1.2, probability = 0.27
Includes 81% of the ^{39}Ar

Sample LL5 (Cerro Divisadero)

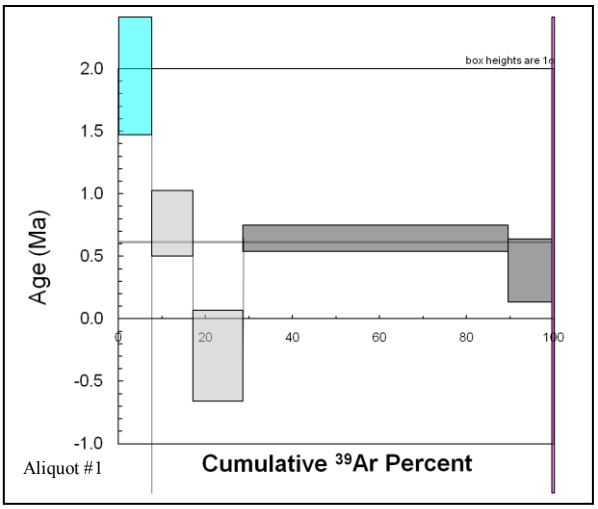

Plateau age = 0.613 ± 0.096 Ma
(1σ, including J-error of 0.28%)
MSWD = 1.4, probability = 0.23
Includes 71.5% of the ^{39}Ar